university of groningen

faculty of science and engineering

The Numerical Simulation of a Tank Model for the Lateral Line Canal in Fish

Bachelor Project Mathematics

February 2017

Student: E. Ooms

First supervisor: Dr. ir. R. Luppes

Second supervisor: Dr. A.E. Sterk

Abstract

Fish are able to picture moving and vibrating objects of their surroundings by using their mechanosensory lateral line organ. Water displacements and pressure fluctuations, present in the neighbourhoud of the fish can be detected by neuromasts located on their skin and in their lateral line canal. At the department of Artificial Intelligence of the RuG, reseachers are investigating if they are able to design a flow detection system based on this mechanosensory lateral line system in fish. In trying to build this, they want to know what the most suitable settings for their modelled canal should be. In this thesis, the effects of a canal on the flow produced by a moving object is simulated by using ComFLOW, a program that simulates fluid flow numerically based on the Navier-Stokes equations. We start with considering a very simplified two-dimensional case in which one sensor is placed at the bottom of a tank partially filled with water and an object is moving from one side to the other side. This simplified case is extended to more sophisticated cases that resemble the situation in fish better, e.g. by adding horizontal and vertical walls around a series of sensors. The effect of vortices, shedded by the moving object, on the measured signals of velocity and pressure near the sensors is studied in detail.

Contents

Chapter 1

Introduction

Fish are able to picture moving and vibrating objects of their surroundings by using their mechanosensory lateral line organ. The movement of for example an other animal through the water, will cause for water displacements and pressure fluctuations. These hydrodynamic stimuli can be detected by the sensory system of a fish, the mechanosensory lateral line organ [1]. The lateral line organ consists of several thousand mechanosensors, called neuromasts. These can be divided into two different types: the superficial neuromasts, distributed superficially over the fish's skin, and the canal neuromasts, located in the lateral line canals [2]. They are built up from a number of directionally sensitive haircells encapsulated by a gelatinous cupula that is sensitive to extremely small displacements (Figure 1.1) [3].

The fluid-filled canals are present under the skin on either side of the fish and have pore-like openings to the outside, as shown in Figure 1.1. When the water around the fish is set in motion by a moving object, via the openings of the lateral line canals the fluid inside the fish will also be set in motion, causing the cupula of the neuromast to detect a change in velocity and pressure. This information is passed on to the connecting haircells which generate graded potentials that are sent (via the sensory nerves) to the brain, where the fish is able to locate the moving object [3].

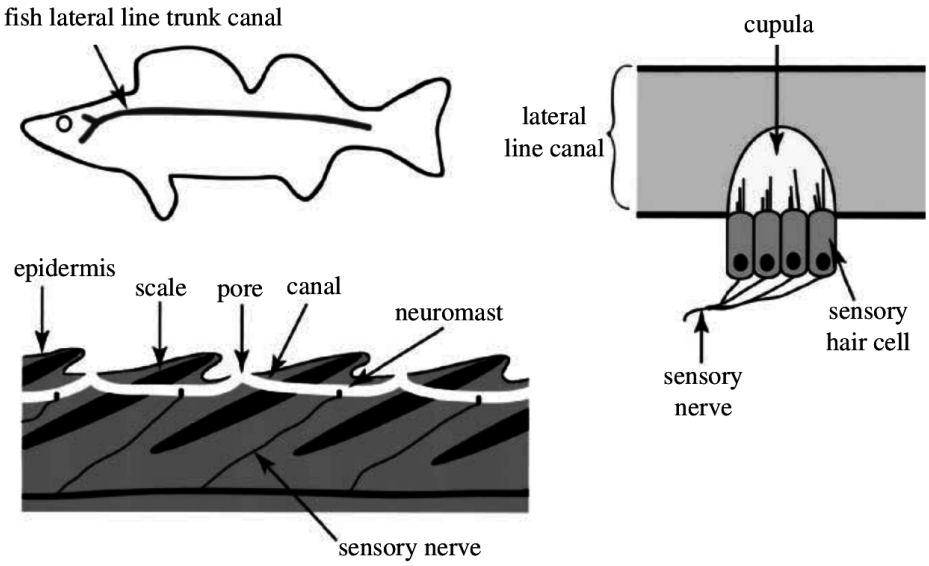

Figure 1.1: Schematics of a lateral line canal in fish.

At the department of Artificial Intelligence of the RuG, researchers are investigating if they are able to design a flow detection system based on this mechanosensory lateral line organ in fish. In trying to build this, they want to model the situation in fish as accurate as possible. The neuromasts in a lateral line canal receive a filtered version of the flow outside the fish. The characteristics of this filtering is expected to depend on dimensions, shape and wall properties of the canal. To find out what the best suitable settings for their modelled canal should be, they want to hydrodynamically simulate the effects of a canal on the flow produced by a moving object. In earlier research the fluid flow generated by a moving object already has been simulated, but without considering the housing structure.

In the present study, these simulations have been extended. The effects of a canal on the flow produced by a moving object have been simulated with the use of ComFLOW, a program that simulates fluid flow numerically based on the Navier-Stokes equations [4]. These equations describe the flow of a viscous fluid. Assuming that water is an incompressible and viscous fluid, the Navier-Stokes momentum equation is

$$\frac{\partial \mathbf{u}}{\partial t} + (\mathbf{u} \cdot \nabla)\mathbf{u} = -\frac{1}{\rho}\nabla p + \frac{\mu}{\rho}\nabla^2 \mathbf{u} + \mathbf{F},$$

where $\mathbf{u} = (u, v, w)$ is the velocity vector, t the time, ρ denotes the density, p the pressure, μ represents the dynamic viscosity and $\mathbf{F}$ the external forces. Then, for the conservation of mass, the continuity equation is applied. Because water is assumed to be an incompressible fluid, the mass continuity equation simplifies to

$$\nabla \cdot \mathbf{u} = 0.$$

In order to let the program ComFLOW describe the complete fluid flow, boundary conditions are needed for the domain boundary and the free water surface. At solid boundaries the no-slip condition is specified, which means that at these moments the fluid has zero velocity relative to the boundary for all velocity components. This is given by the formula $\mathbf{u} = 0$ [5] Considering a point $y = (y, t)$ of the free water surface, the displacement of the free water surface is described by the following Stokes equation

$$\frac{Dy}{Dt} = \frac{\partial y}{\partial t} + (\mathbf{u} \cdot \nabla)y = 0.$$

The other boundary conditions needed at the free water surface are for the velocities and pressure. These are obtained by the continuity of normal and tangential stresses

$$-p + 2\mu \frac{\partial u_n}{\partial n} = -p_0 = 2\sigma H$$

$$\mu(\frac{\partial u_n}{\partial t} + \frac{\partial u_t}{\partial n}) = 0,$$

where u_n denotes the normal component of the velocity, u_t the tangential component of the velocity, p_0 is the atmospheric pressure, σ the surface tension and $2H$ stands for the total curvature.

Normally, the force on an object caused by the flow of the fluid consists of two parts: the pressure force and the shear force. However, compared to the pressure force, the shear force is much smaller and is therefore negligible. That is also the reason why ComFLOW only considers the pressure force for its simulations. This force is being calculated with the integral of the pressure along the boundary of the object S, which is given by the following formula [4]

$$\mathbf{F_p} = \int_S p\mathbf{n}\, dS.$$

With this program ComFLOW, a tank filled with water will be simulated. We start with a simplified case, considered in the two-dimensional space, in which only one sensor is present at the bottom. Between the water surface and this sensor, a cube moves with a constant velocity from one side of the tank to the other side of the tank. After evaluating the results, the simplified case will be extended step by step, by inserting more sensors, giving the object an acceleration, inserting both horizontal and vertical walls and changing the shape of the moving object. The last and most sophisticated case that will be computed is considered in the three-dimensional

space. The effects on the velocities and pressure reported by the sensors will be evaluated after every change that have been made to the set-up.

In Chapter 2 is investigated what the most suitable grid should be for the experiment of this study. Grids of different sizes will be tested using the simplified case. The results are evaluated based on the accuracy of the measurements and the duration of the computing time. Once found the most suitable grid for the simulations of this study, in Chapter 3 the simplified case will be extended by giving the object an acceleration at the start. Chapter 4 shows what the effect is of inserting horizontal and vertical walls. Two different cases will be considered and compared to each other: the case in which only horizontal walls are present and the case in which both horizontal and vertical walls are placed. Another change to the case is made in Chapter 5, where the cube is replaced by a ball. In the last Chapter, Chapter 6, the cases are considered in the three-dimensional space. With this extra dimension, the sensor array and walls can be placed at different positions in the tank. Again, two cases will be compared to each other: the case in which the walls and sensors are located in the middle of the tank and the case in which the walls and sensors are located at the right side of the tank.

Chapter 2

Finding the most suitable grid

The first step to take, is trying to find the most suitable grid. With a coarse grid it takes shorter time to compute, but the computation also will be less accurate. With a finer grid you will get more accurate results, because the situation will be considered in more detail. However, that also means that it takes much more time to compute. Therefore, we want to find a grid that won't take too much time for ComFLOW to compute, but is still accurate enough. In searching for the optimal grid, we use a very simple set-up to begin with.

2.1 First try with different grids and one sensor

We start building a two-dimensional set-up in which we have a tank partially filled with water. As seen in Figure 2.1, this tank has a length of 0.515 m, a height of 0.280 m and the water surface is located at 0.250 m above the bottom of the tank. At a height of 0.085 m in the middle of the tank, a sensor is placed. This sensor will register the pressure and the velocities in the horizontal and vertical direction. Above this sensor a little cube will move from the left side of the tank to the right side of the tank, with a speed of 1 m/s. Its middlepoint starts at a height of 0.140 m of the bottom and 0.02 m from the left wall of the tank. All these dimensions are also applicable to all the set-ups described below, unless it is stated that something is different.

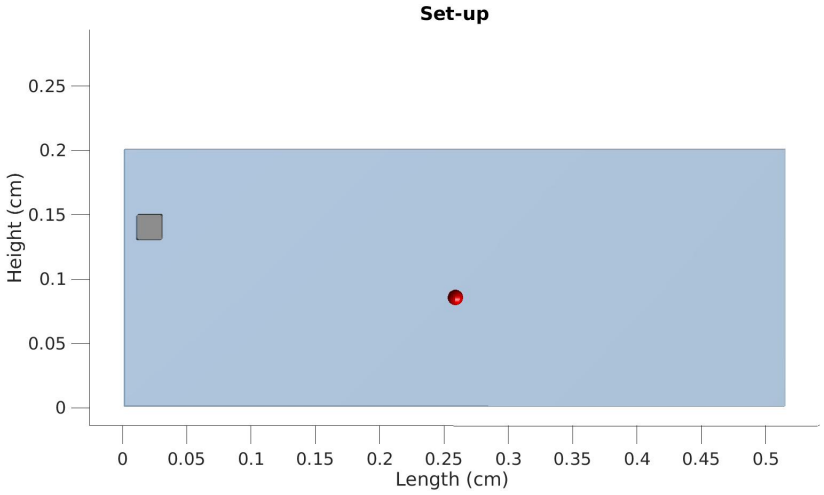

Figure 2.1: Set-up of a tank, partially filled with water, with a sensor placed at the bottom and an object that moves from the right side to the left side of the tank.

Different kinds of grids of different sizes will be tested in order to find the most suitable grid. For the first try we look at the grids with the following dimensions: 172x1x93, 258x1x140, 343x1x187 and 515x1x280. We evaluate how long every computation takes and how accurate the results obtained with a particular grid are. It is expected that at a certain grid size the measurements do not differ a lot from the reportments of the finer grid that was tested before. If that grid also has an acceptable computing time, we have found our optimal grid which, will be used during the rest of the study.

Results

When we evaluate the results of the computed grids, we look at the computation time and at the pressure, the horizontal velocity and the vertical velocity that is registered by the sensor in the tank. We compare these values from different grids with each other and look to what extent they differ.

Beginning with the computation time, we find that the computation of the coarsest grid, 172x1x93, lasted approximately 9 minutes. The computation of the finest grid, 515x1x280, took 7 hours to complete. These are acceptable computing times to work with.

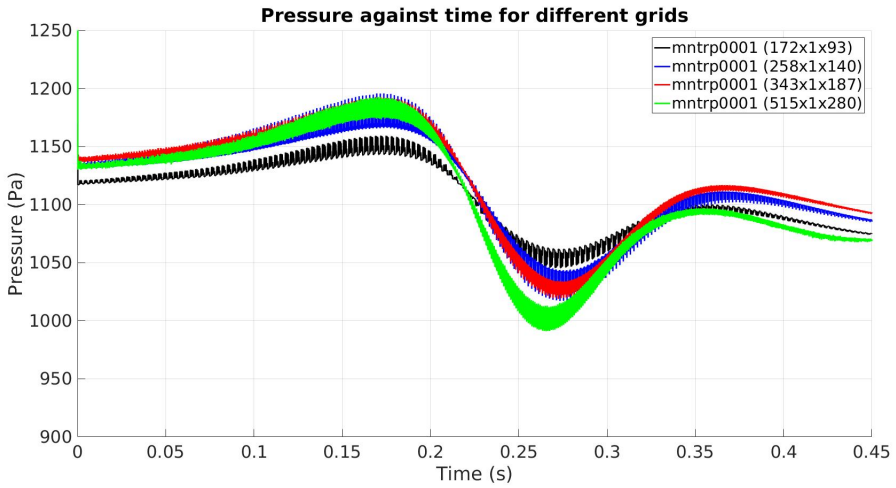

Figure 2.2: Pressure against time for the 172x1x93, 258x1x140, 343x1x187 and 515x1x280 grids.

Then, looking at the pressure in Figure 2.2, we see that with every grid the maximum value of the pressure is achieved around $t = 0.175$ s and the minimum around $t = 0.265$ s. At $t = 0.1750$ s, the moving object is approaching the sensor (Figure 2.3), pushing the water forwards. By doing so, a rise in pressure arises in the area right in front of the cube. But some water will be pushed in the direction of the sensor as well, causing a rise in pressure around the sensor. We see in Figure 2.4, that right after the moving object has passed the sensor, the pressure drops significantly causing the minimum around $t = 0.265$ s. Further, in the rest of the water of both situations, we observe a constant pressure in each horizontal layer. This indicates that there is a hydrostatic pressure present.

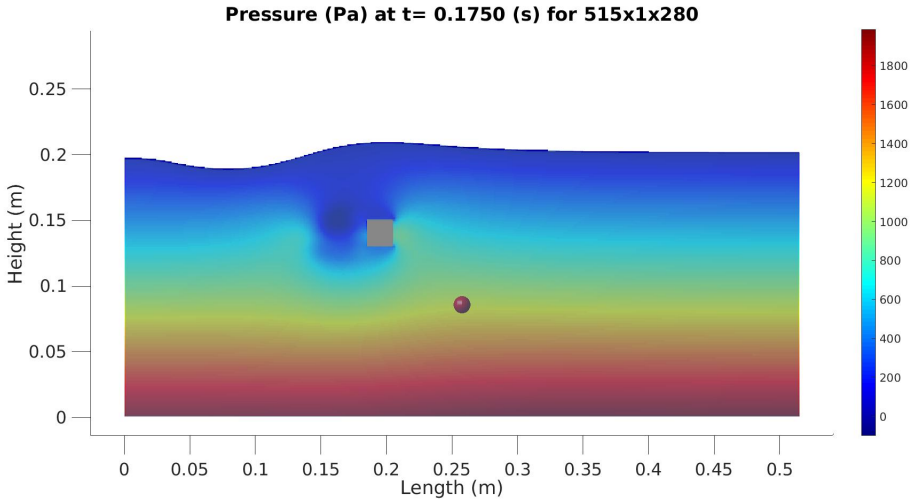

Figure 2.3: Pressure in Pa at $t = 0.1750$ s for the 515x1x280 grid.

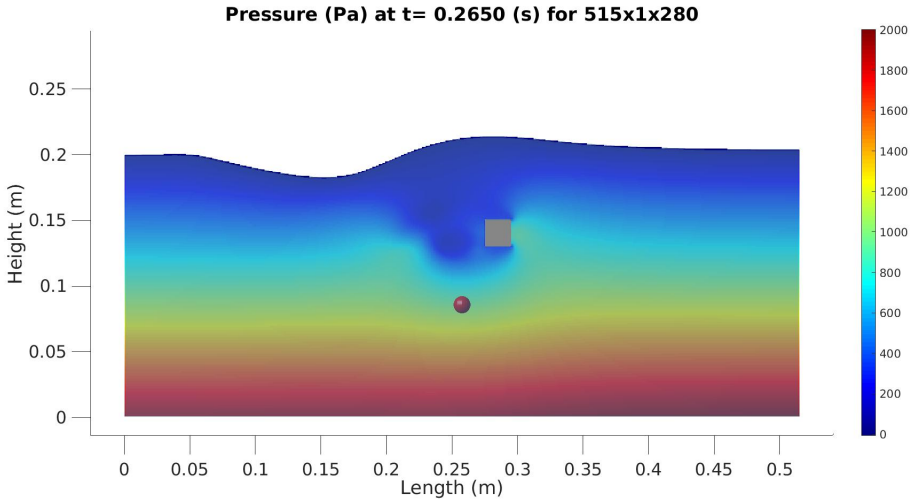

Figure 2.4: Pressure in Pa at $t = 0.2650$ s for the 515x1x280 grid.

Thus, the graphs of the different grids have their extrema around the same time. Although they differ somewhat in their values, this difference is not very significant. Therefore, we can assume that the measurements for the pressure are sufficiently accurate for every grid. So, only considering the pressure, for the accuracy it does not matter which size of grid you take. A finer grid does not mean that the accuracy of the measurements declines significantly. Since a course grid takes less time to compute compared to a fine grid, a finer one is preferred.

However, when we take a look at the horizontal velocity and vertical velocity for the different grids, we see a larger difference.

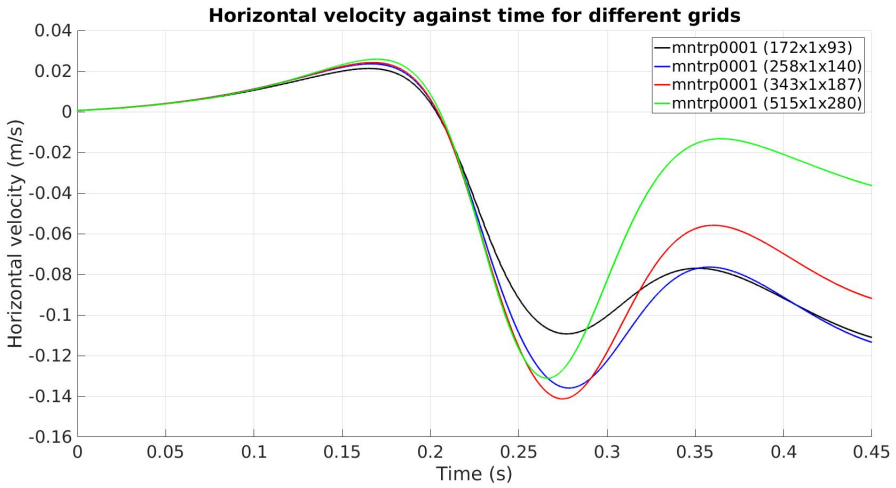

Figure 2.5: Horizontal velocity against time for the 172x1x93, 258x1x140, 343x1x187 and 515x1x280 grids.

In Figure 2.5, we observe that all grids start with having the same horizontal velocity during the first few hundreds of seconds. After approximately 0.17 seconds the sensor measures a maximum value of the horizontal velocity. We see in Figure 2.6 what happens at this moment in time. The moving object is approaching the sensor and while moving, it pushes the water forward causing a flow in the direction of the sensor.

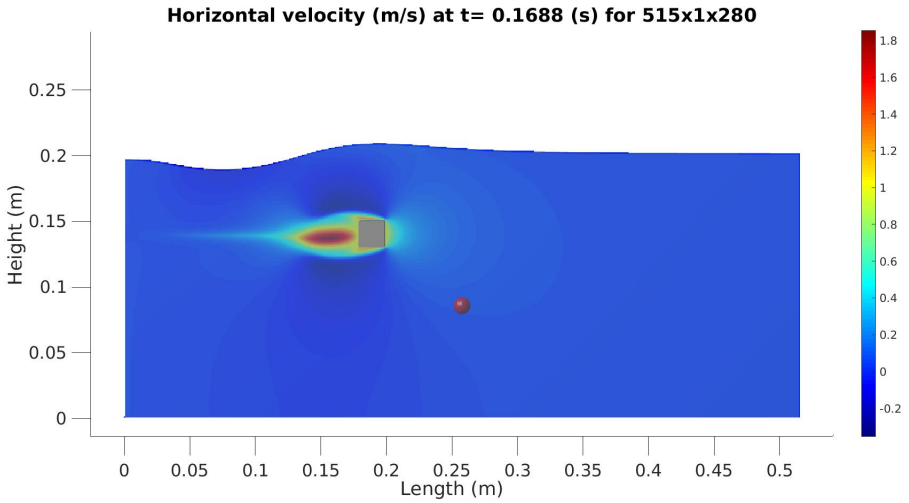

Figure 2.6: Horizontal velocity in m/s at $t = 0.1688$ s for the 515x1x280 grid.

Around $t = 0.27$ s, the sensor reports a minimum value of the horizontal velocity (Figure 2.5). We see in Figure 2.7 that at this moment the moving object has passed the sensor. The negative values are the result of the moving cube pushing the water backwards along its top and bottom. This action causes a flow in again the direction of the sensor, which is now behind the object. This means that in this case we have negative values of the horizontal velocity.

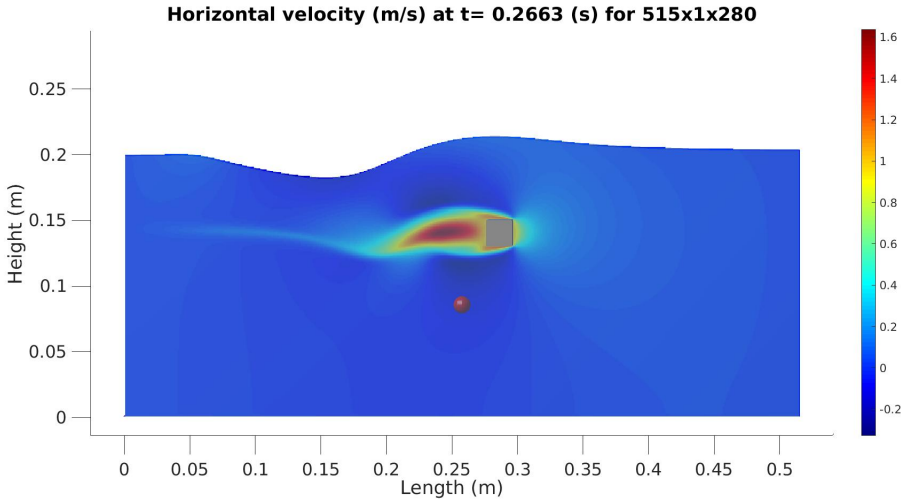

Figure 2.7: Horizontal velocity in m/s at $t = 0.2663$ s for the 515x1x280 grid.

When we again take a look at the graphs of the different grids at this minimum horizontal velocity in Figure 2.5, we observe that every grid has a different value and different moment in time to reach the minimum. And after this moment the graphs seem to deviate even further from each other.

Looking at the graph of the vertical velocity (Figure 2.8), we observe that around 0.22 s the minimum vertical velocity has been reached. This is the moment where the front of the cube is right above the sensor, as shown in Figure 2.9. With moving the cube through the water, there also arises a flow at the front of the cube that goes to the bottom. Therefore the sensor reports a negative value of the vertical velocity at that moment.

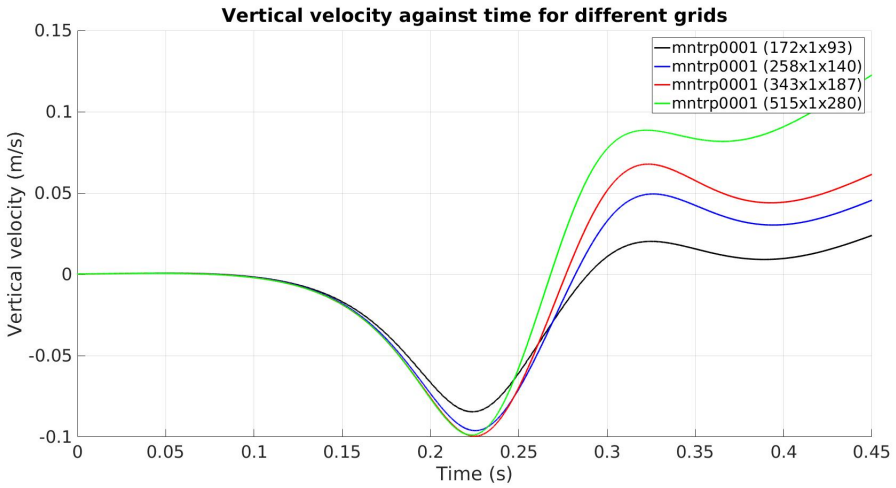

Figure 2.8: Vertical velocity against time for the 172x1x93, 258x1x140, 343x1x187 and 515x1x280 grids.

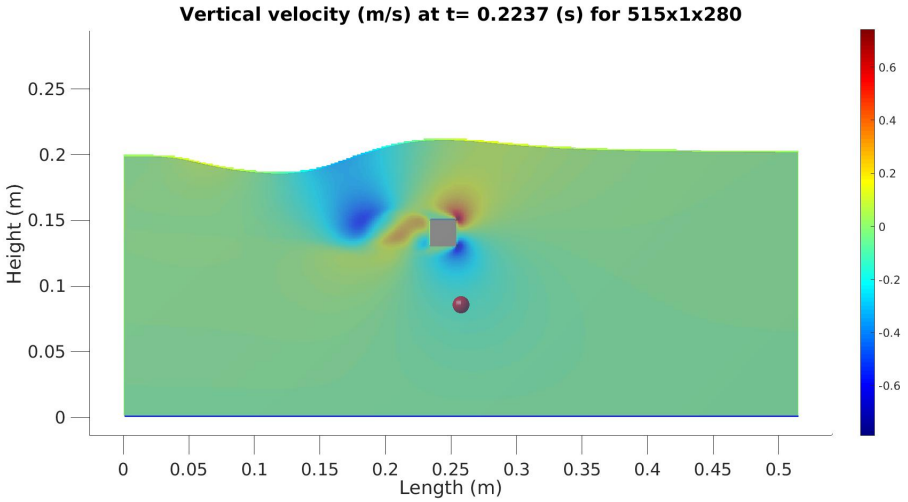

Figure 2.9: Vertical velocity in m/s at $t = 0.2237$ s for the 515x1x280 grid.

The movement of the object through the water not only causes flows directly around the object, it also creates bigger vortices in the rest of the water. After the cube left the sensor behind, the vertical velocity that is reported by the sensor will depend on the bigger vortices in the water. If the water surface is moving upwards, there will be registered a positive value of the vertical velocity (Figure 2.10), if it is moving downwards a negative value is given.

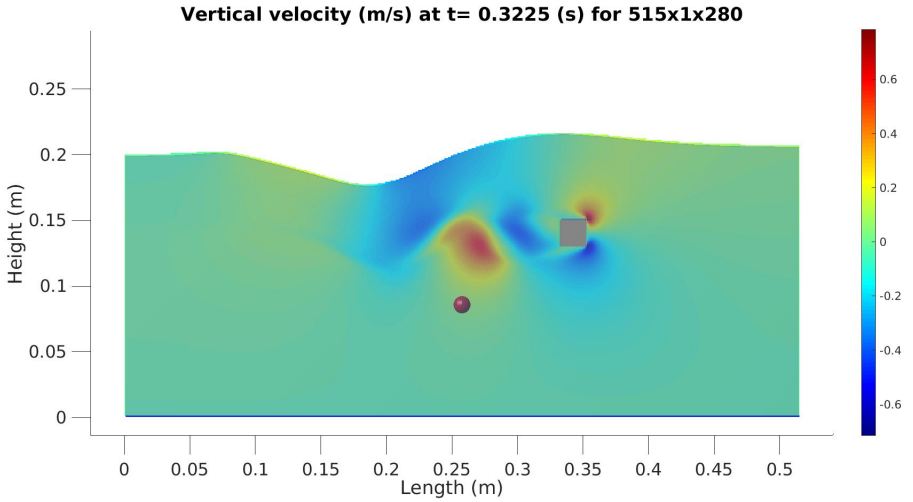

Figure 2.10: Vertical velocity in m/s at $t = 0.3225$ s for the 515x1x280 grid.

As with the horizontal velocity, also for the vertical velocity the different grids have the same value during the first hundreds of seconds. However, the graphs start to deviate from the moment where the cube has passed the sensor.

So, for both the horizontal velocity and the vertical velocity, we see that there are no two or more graphs that look like each other. For every grid there are different values of the velocities. This means that we have not yet found the most suitable grid.

2.2 Second try with finer grids and three sensors

Testing grids with the dimensions of 172x1x93, 258x1x140, 343x2x187 and 515x1x280 did not lead to finding a sufficiently accurate grid that could be used during the rest of the study. A possible explanation for the divergence is that the grids are just not fine enough for the measurements to be accurate. To test whether this is the case, with the next try also finer grids are being considered. So, also grids of the following dimensions will be investigated: 773x1x420, 1030x1x560 and 2060x1x1120.

In trying to make the results more accurate such that the graphs do converge, some changes will be made to the input files in the next part of the research. Firstly, the value of upwind will be set to 2. With the first computations in the previous section a value of 1 for upwind is used, which means that first-order upwind spatial discretization has been applied. This is a method that gives stable computations, but less accurate results than with the second-order upwind spatial discretization. Namely, while simulating with ComFLOW, an artificial numerical diffusion proportional to the grid size is applied to stabilize the computation.

The formula for this artificial numerical diffusion is given by

$$k_a = u\frac{\Delta x}{2}, v\frac{\Delta y}{2},$$

where k_a is the artificial diffusion, u and v are velocities in respectively the x- and y-direction, and Δx and Δy are mesh widths in these directions.

However, when this artificial diffusion dominates the real diffusion, it can lead to decreased usefulness of the upwind discretized solution [6]. To overcome this undesirable effect, we can take a finer grid such that the mesh widths, Δx and Δy, decrease, making the artificial numerical diffusion decrease as well. We can also use second-order upwind spatial discretization. With this method the mesh sizes, Δx and Δy, decrease with order 2, when taking a finer grid, making the artificial numerical diffusion to decrease faster.

So, using the second-order method might give us more accurate results. With changing the upwind scheme, you also have to change the time integration method. The parameters feab1 and feab2 firstly had the values of 1.0 and 0.0 respectively giving first-order Euler time integration and will from now on get the values of 1.5 and -0.5 for the second-order Adam-Bashforth scheme. The second-order method appears to work best with these values.

Another change that could make the results more accurate is adjusting the cflmin and cflmax. They were set to 0.2 and 0.5 respectively, but now will be given the values of 0.05 and 0.125. Choosing smaller values for cflmin and especially for cflmax, means that there will be more smaller time steps taken, which leads to more accuracy.

Testing the computations with these changes will be done with the same set-up as was used before, with the only adjustment that there are two more sensors inserted. One is placed at 0.029 m from the left wall of the tank and the other is placed at 0.029 m from the right wall. With three sensors we can gather more information about different points in the tank, which may help in getting clear of what exactly happens during the numerical experiment

Results

The first try gave us graphs of different grids for the velocity that diverged from each other at a certain moment. It was expected that with finer grids we would get more accurate results and thus graphs that will converge. However, when investigating this, the computations of these finer grids appeared to be too complex. The computations of the grids with the dimensions of 773x1x420 and 1030x1x560 needed several days to complete, while the one of 2060x1x1120 never even started. Also, Figure 2.11 tells us that using finer grids did not lead to grid convergence. So, considering finer grids did not help in finding the best fitting grid.

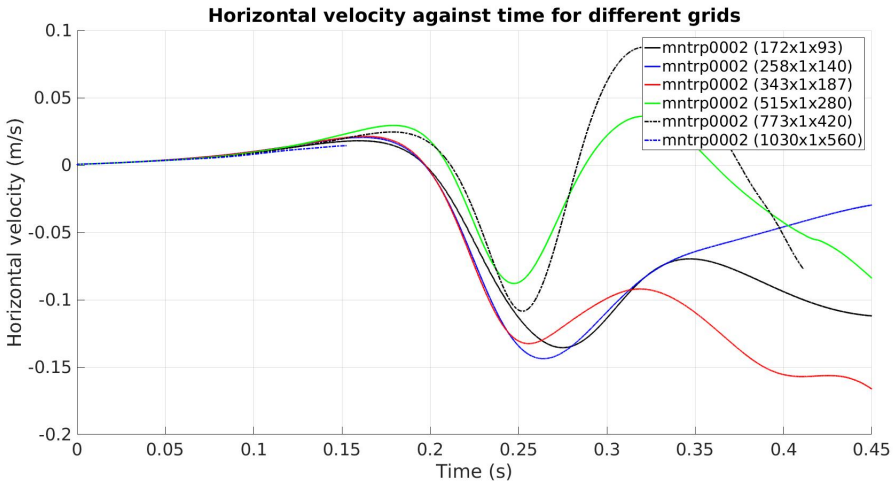

Figure 2.11: Horizontal velocity against time for the 172x1x93, 258x1x140, 343x2x187, 515x1x280, 773x1x420 and 1030x1x560 grids, reported by the middle sensor.

To find out what exactly is making the graphs diverge, we will make use of the information of the three sensors by comparing their information with each other and see what happens on the two other points in the tank during the experiment. In Figures 2.12 and 2.13 we observe that the graphs for the different grids at the first and third sensor don't differ that much as the graphs at the second sensor does. To find out why that is, we will investigate again what happens at the extrema registered by the second sensor for the 515x1x280 grid at the three sensors.

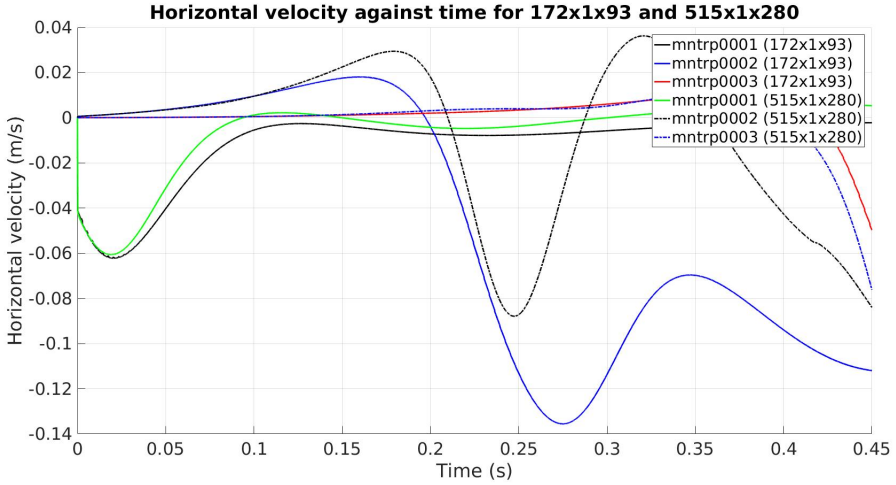

Figure 2.12: Horizontal velocity against time for the 172x1x93 and 515x1x280 grids, reported by three sensors.

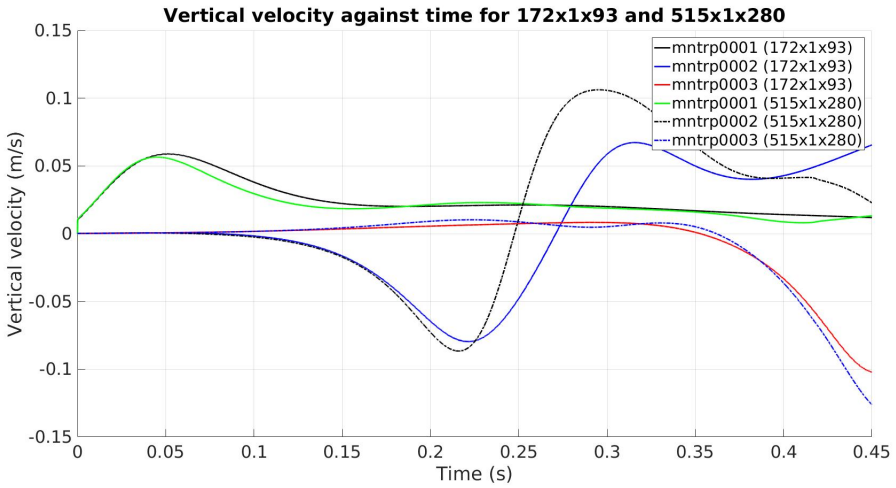

Figure 2.13: Vertical velocity against time for the 172x1x93 and 515x1x280 grids, reported by three sensors.

The first maximum for the horizontal velocity is attained around $t = 0.17$ s. At that moment we see that the moving object has passed the first sensor (Figure 2.14) and is approaching the second sensor. There is relatively little activity in the water. In front of the object the water is pushed forward such that in that area the horizontal velocity slightly increases. Behind the cube some more activity arose by the movement of the object through the water, but the area that is put in motion is restricted to only a small part right after the object.

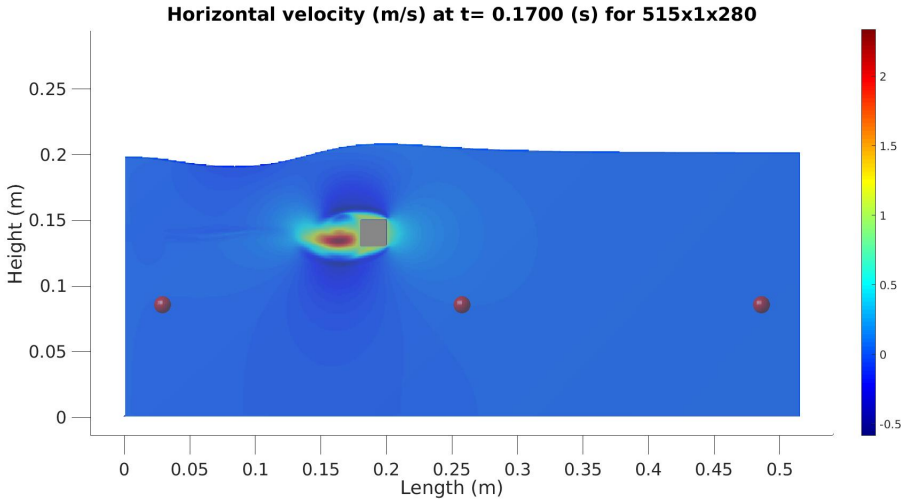

Figure 2.14: Horizontal velocity in m/s at $t = 0.1700$ s for the 515x1x280 grid.

If we look at the minimum of the 515x1x280 grid in Figure 2.15, we observe some more activity in the water already. The cube is now passing the second sensor and in his movement the water beneath has a negative horizontal velocity, which is also reported by the sensor. Though, the water after the cube has a positive horizontal velocity again. But this time the area in which there is activity has increased, it is not restricted to only a small part directly after the object anymore.

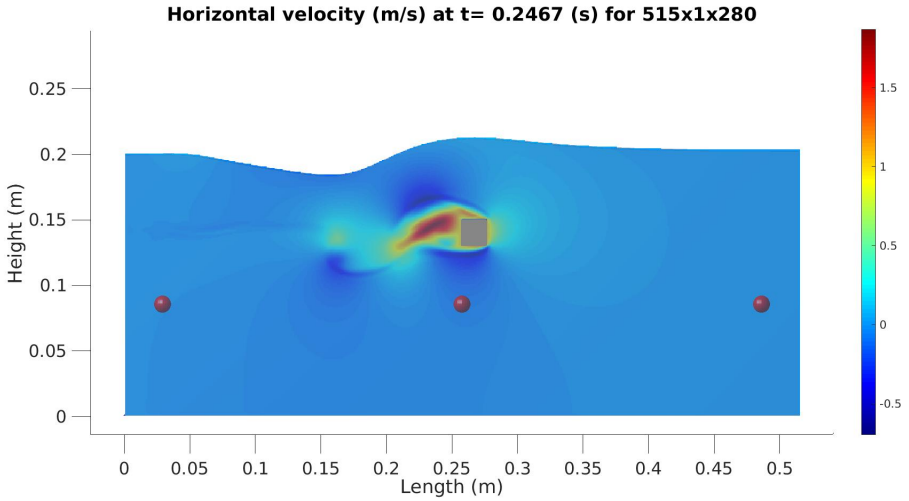

Figure 2.15: Horizontal velocity in m/s at $t = 0.2467$ s for the 515x1x280 grid.

Then, at the last extreme value the water activity has increased even more (Figure 2.16). After 0.32 seconds, the moving object has passed the second sensor and is approaching the third one. When we look at what happens behind the cube we see that there originated a pattern of swirling vortices that repeats itself. This is called a vortex street and appears at higher Reynolds numbers [5]. Water has a density (ρ) of $1.0 \cdot 10^3$ kg/m^3 and a dynamic viscosity (μ) of $1.0 \cdot 10^{-3}$ kg/ms. In the experiment the water is able to move over a distance (L) of 0.02 m, the height of the moving cube, with a velocity (U) of 1 m/s. This gives us a high Reynolds number of

$$Re = \frac{\rho U L}{\mu} = \frac{1.0 \cdot 10^3 \times 1 \times 0.02}{1.0 \cdot 10^{-3}} = 20,000$$

which confirms that during the experiment there indeed originates a vortex street.

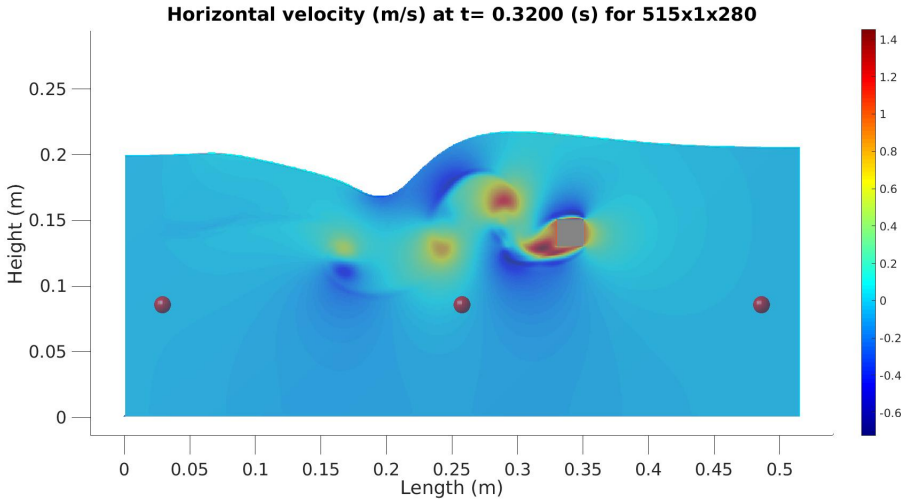

Figure 2.16: Horizontal velocity in m/s at $t = 0.3200$ s for the 515x1x280 grid.

So, for the second sensor the moment where the graphs of the different grids in Figure 2.12 start to diverge, is when the moving object has passed the second sensor and starts shedding vortices. We already mentioned that the graphs at the first and third sensor do not differ that much. We saw that at the time the cube passes the first sensor, the activity is still directly right behind the object. Therefore it is not causing much activity in the neighbourhood of the sensor, which is the reason why the graphs for the the first sensor are equal. Further, the graphs of the third sensor show only the approaching phase of the moving object. During the experiment it appears that approaching the sensors causes not as much activity as passing does. But the phase where the moving object has passed the third sensor has not been reported yet. This explains why the graphs for the third sensor are also equal to each other.

Putting everything together it looks like that the phenomenon of the vortex street at least partly explains the differing graphs for the second sensor. To check whether this is indeed the case we compare the situations of both grids at a moment in time where the difference between the graphs is almost maximal. If we look at the horizontal velocities at $t = 0.3000$ s, we see for the situation of the 515x1x280 grid in Figure 2.17 again the shedding of vortices. But for the situation of the 172x1x93 grid (Figure 2.18) there is a much less activity through the water and the activity caused by the moving object is restricted to a small area directly after the object. This is also seen in Figures 2.19 and 2.20 for the vertical velocities at $t = 0.3000$ s.

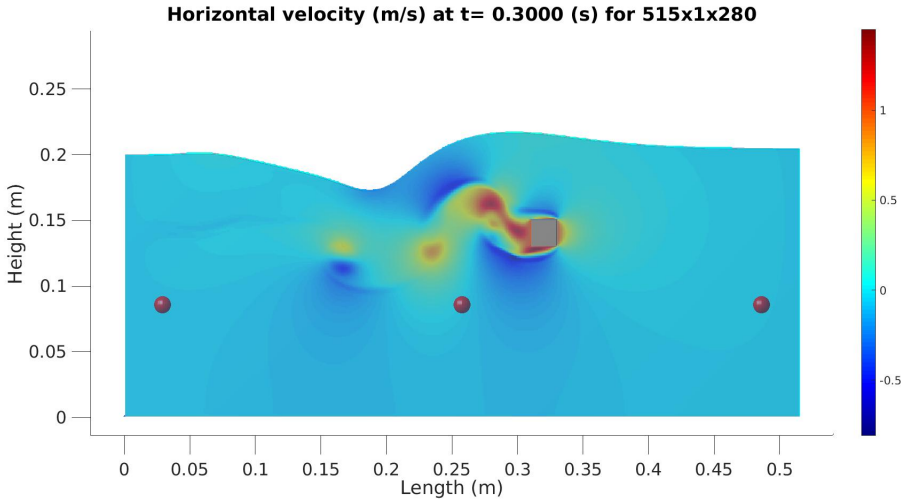

Figure 2.17: Horizontal velocity in m/s at $t = 0.3000$ s for the 515x1x280 grid.

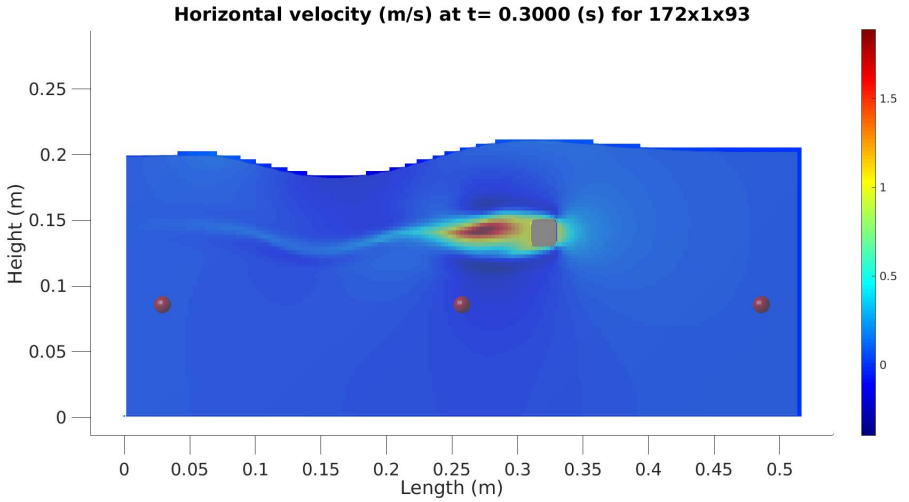

Figure 2.18: Horizontal velocity in m/s at $t = 0.3000$ s for the 172x1x93 grid.

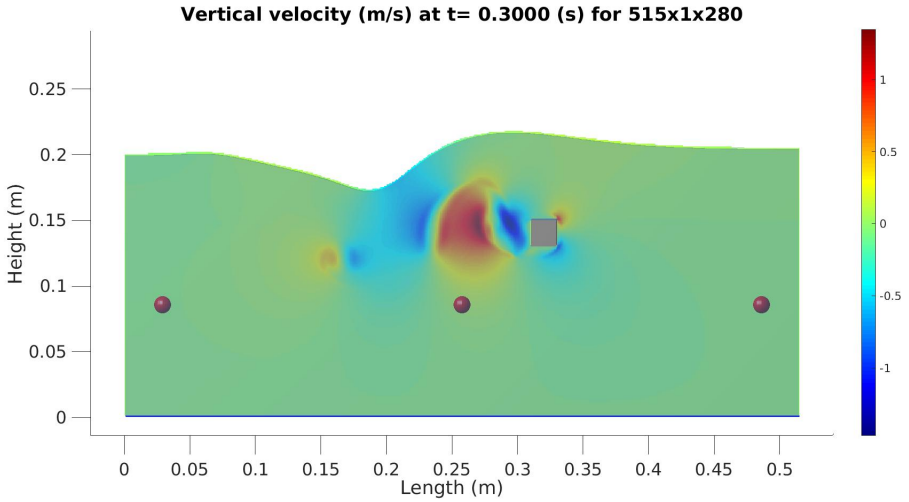

Figure 2.19: Vertical velocity in m/s at $t = 0.3000$ s for the 515x1x280 grid.

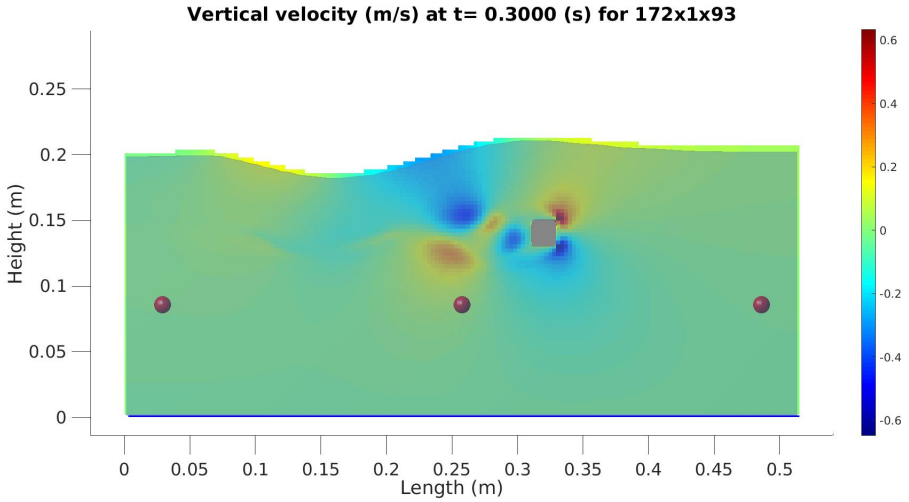

Figure 2.20: Vertical velocity in m/s at $t = 0.3000$ s for the 172x1x93 grid.

The shedding of vortices will be different in every situation, even when there is only little difference between the cases. Also in reality, every time you repeat the same experiment, you will observe a different pattern of vortices. This, together with the fact that with a coarsened grid the computation will be computed in less detail, makes that the graphs of the different grids can never be equal to each other.

Now that we know that the shedding of vortices is the reason why the graphs of the velocities differ so much, we are able to choose a grid to work with. This grid should give results that are sufficiently accurate, but it should also have an acceptable computation time. In the first try we saw

that the computation times were acceptable for all grids. However, the computation times of the same grids tested in the second try, were much larger. The 515x1x280 grid needed 2 days to complete, while in the first try it took only 7 hours. By changing the values of cflmin and cflmax to make the measurements more accurate, also the time it takes to complete a computation has changed. The small values for cflmin and cflmax led to more accurate measurements, but it also made the computation times much larger.

Therefore, cflmin and cflmax will be given larger values again: cflmin will be set to 0.25 and cflmax gets a value of 0.60. Applying these makes the 515x1x280 grid have an acceptable computation time again. Together with the fact that it also gives results with an acceptable accuracy, makes the 515x1x280 grid the most suitable grid which we will use during the rest of the research.

Chapter 3

Constant velocity versus acceleration

In the computations we have done so far, we considered the object to move with a constant velocity of 1.00 m/s at all times. In practice, however, during the first 0.05 meters the object will slowly build up to that velocity. We would like to create a situation that resembles the real experiment as much as possible. That is why we have to find out if the situation with the object having a constant velocity during the whole experiment comes close enough to the true situation in which the object starts with having zero velocity. If it appears that the case with having a constant velocity throughout the whole tank deviates too much from reality, we will use the case in which the object starts with having zero velocity. Unless this situation gives us unexpected results which can not be explained. We then will continue using the old case.

Results

Figures 3.1 and 3.2 show the horizontal velocity at $t = 0.0150$ s for respectively the case in which the moving object has a constant velocity at all times and for the case in which it starts with having an acceleration, after which it continues to go with a constant velocity as well. We see that at the same moment in time, the object with constant velocity has come a little farther than the object with acceleration. Also, in the case of the constant velocity, there is a lot more activity in the water caused by the object. Behind the cube velocities of around 1.40 m/s are reached, while the maximum in the acceleration case is around 0.15 m/s. Further, in front of the cube with constant velocity we observe that the cube has set water in motion in a lot wider range than the cube with acceleration has does.

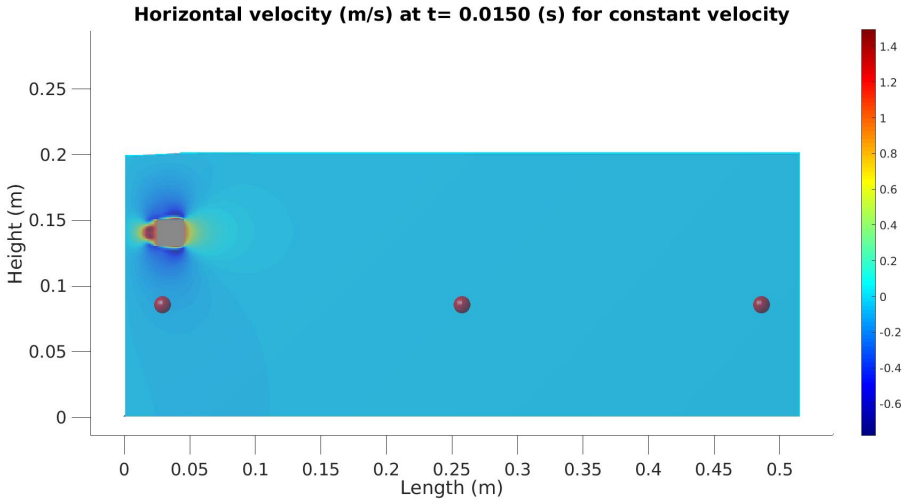

Figure 3.1: Horizontal velocity in m/s at $t = 0.0150$ s for the case in which the cube starts with having constant velocity.

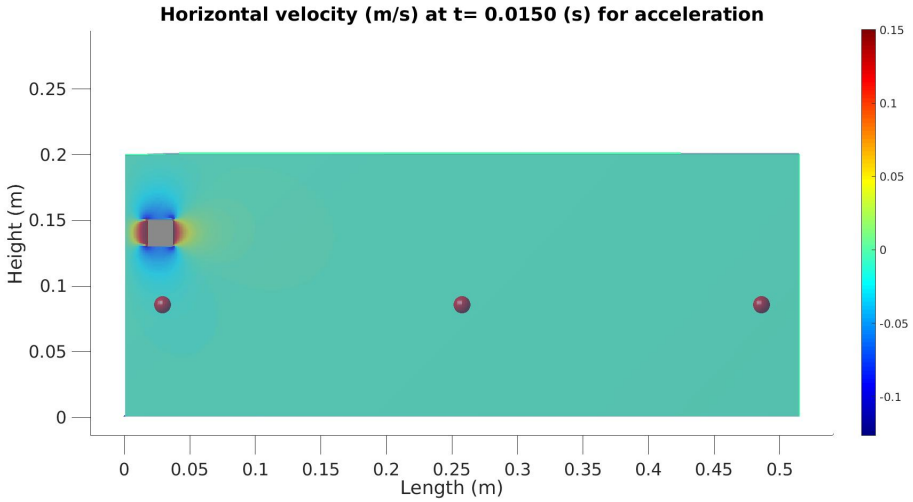

Figure 3.2: Horizontal velocity in m/s at $t = 0.0150$ s for the case in which the cube starts with having acceleration.

The difference in travelled distance between both objects and the difference of the maximum and minimum achieved values is also seen for the vertical velocity (Figures 3.3 and 3.4) and pressure (Figures 3.5 and 3.6).

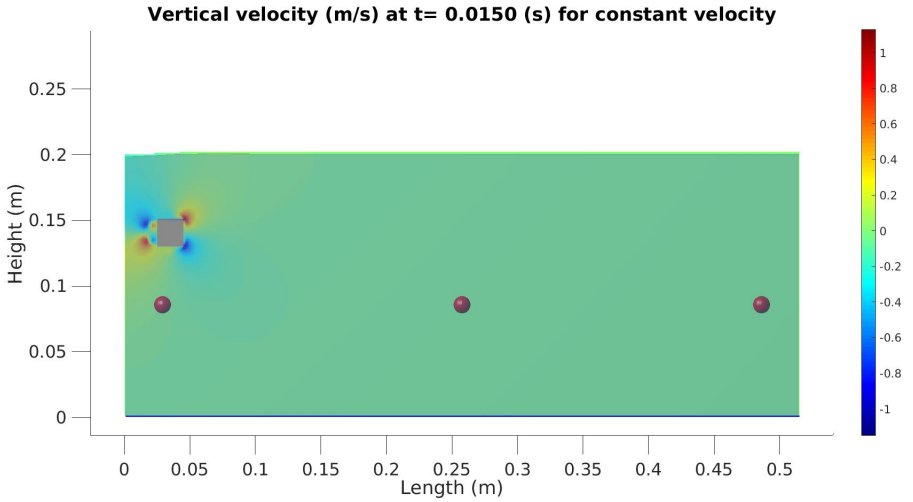

Figure 3.3: Vertical velocity in m/s at $t = 0.0150$ s for the case in which the cube starts with having constant velocity.

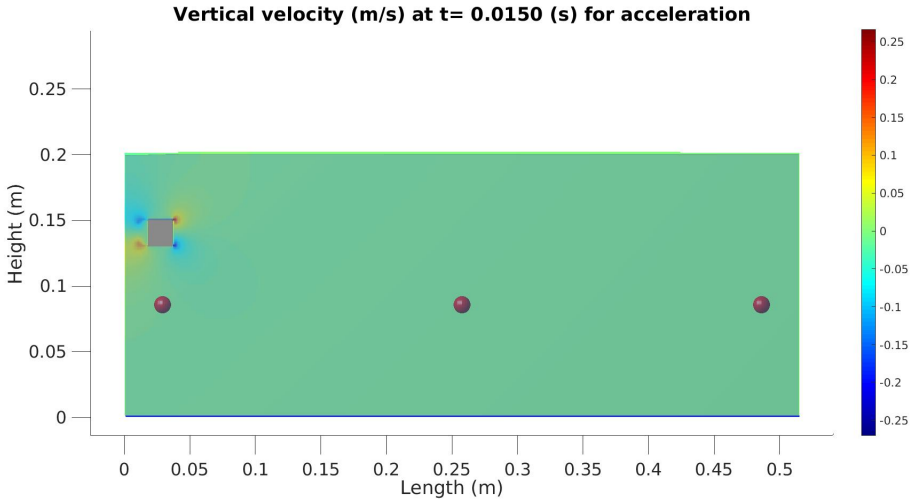

Figure 3.4: Vertical velocity in m/s at $t = 0.0150$ s for the case in which the cube starts with having acceleration.

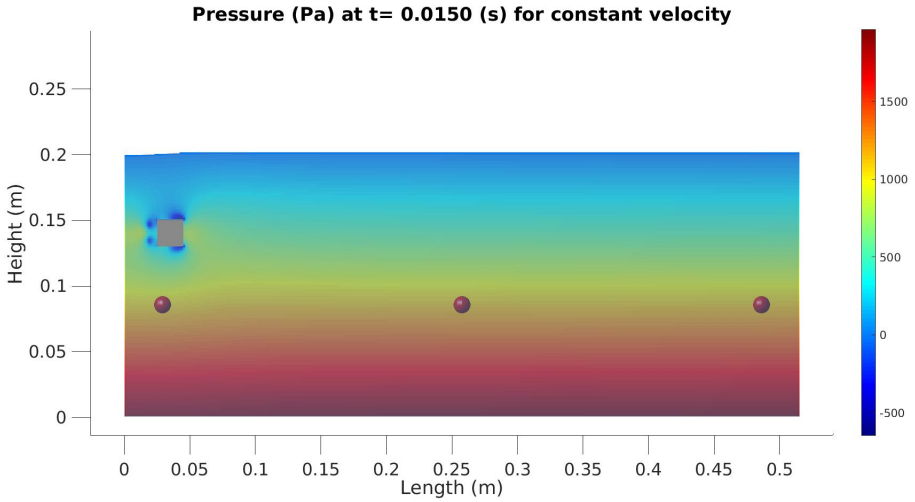

Figure 3.5: Pressure in Pa at $t = 0.0150$ s for the case in which the cube starts with having constant velocity.

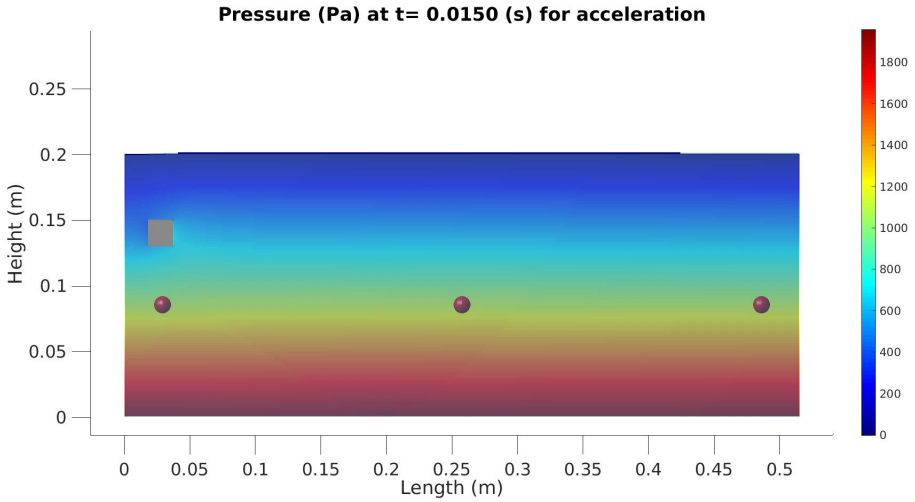

Figure 3.6: Pressure in Pa at $t = 0.0150$ s for the case in which the cube starts with having acceleration.

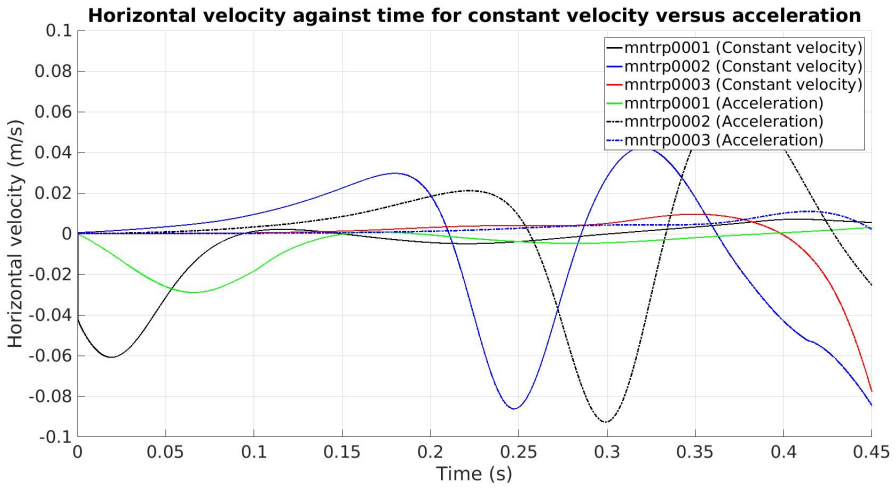

Figure 3.7: Horizontal velocity against time for the case in which the cube starts with having constant velocity versus the case in which the cube starts with having acceleration, reported by three sensors.

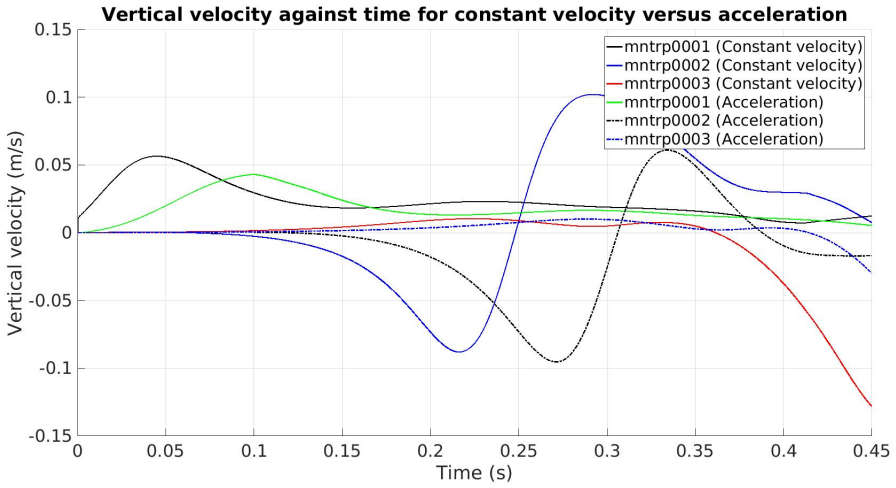

Figure 3.8: Vertical velocity against time for the case in which the cube starts with having a constant velocity versus the case in which the cube starts with having acceleration, reported by three sensors.

When we look at the graphs in Figures 3.7 and 3.8 of the horizontal and vertical velocity for both cubes, we find that the graphs for the cube with constant velocity has its maxima and minima at an earlier moment in time than the cube with having an acceleration. Also, the first maximum and minimum for the constant velocity cube have extremer values. This is because the constant velocity cube passes the sensors at an earlier moment in time and therefore sets in the beginning more water in motion around

the sensors, probably due to its higher velocity at the start. After around $t = 0.20$ s the maximum and minimum of the other case have extremer values. This is related to the onset of the vortex streets that have taken place around that same moment.

For the pressure we see the same pattern (Figure 3.9). The graphs of the constant velocity have their maxima and minima at an earlier moment in time with a more extreme value. Further, we observe that up till 0.10 seconds, the sensors of the accelerated case measure less differences in pressure. This is the time range where the cube still has an acceleration. Around $t = 0.10$ s, the accelerated cube reaches the velocity of 1.00 m/s. After this point it will continue with a constant velocity.

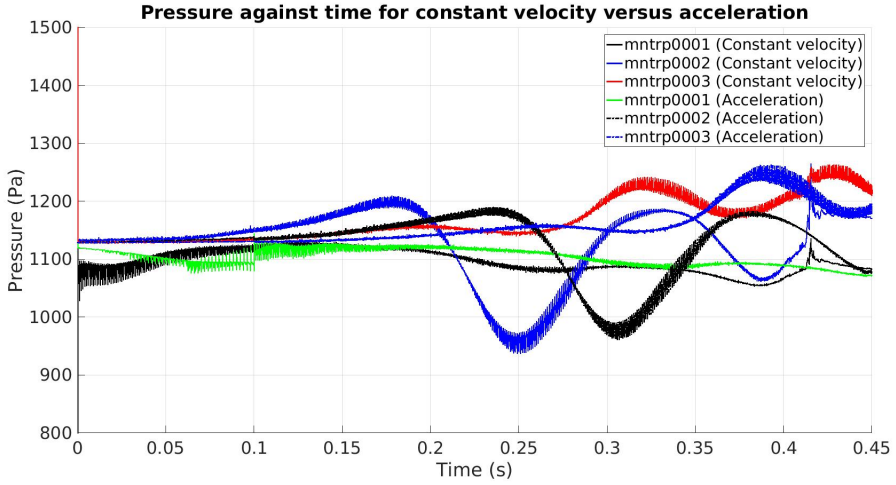

Figure 3.9: Pressure against time for the case in which the cube starts with having a constant velocity versus the case in which the cube start with having an acceleration,, reported by three sensors.

The case with the accelerated cube does not give unexpected results that can not be explained and is a better representation of the real experiment than the case in which the cube has a constant velocity at all times. So, from now on the accelerated cube will be used in the set-ups that follow.

Chapter 4

Inserting walls

The researchers of Artificial Science want to model the situation in fish. In doing so they will perform experiments letting an object move in a tank filled with water. This is what we already investigated thus far. However, fish sense flows from their surroundings via several openings in their lateral line canal. To simulate this, some horizontal walls between the moving object and the sensors are inserted. Besides this, the researchers are also interested in what happens when they would place vertical walls between the sensors. So we will also take this situation into consideration and compare the different situations to each other.

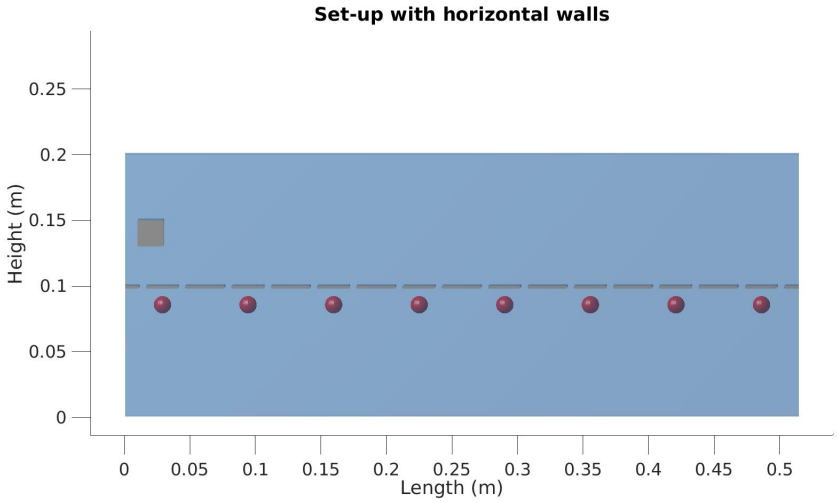

Figure 4.1: Set-up with horizontal walls that are partly separating the eight sensors from the moving object.

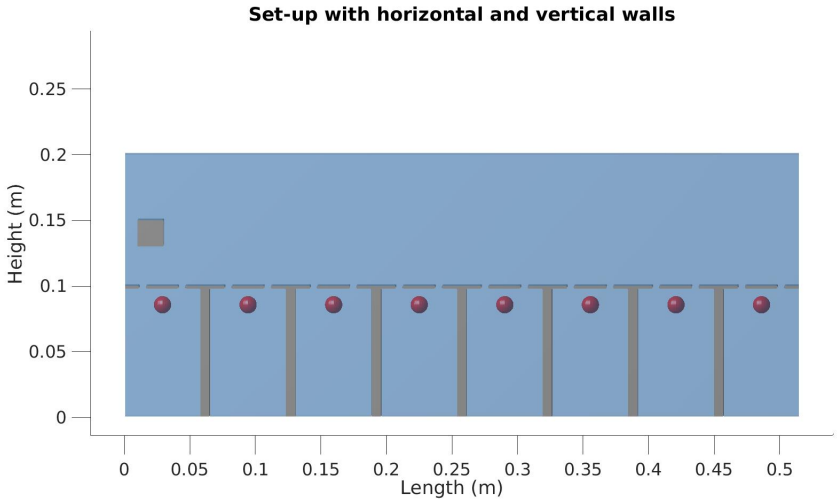

Figure 4.2: Set-up with horizontal walls that are partly separating the eight sensors from the moving object and vertical walls that are seperating the sensors from each other.

In Figures 4.1 and 4.2 we see how the set-ups look like. In order to obtain as much information as possible, in both situations eight sensors are inserted in the tank. The walls right above the sensor have a length of 0.025 m and are 0.013 m removed from the sensor. Between the horizontal walls there is a gap of 0.005 m. In the situation with both walls, the sensor is 0.029 m removed from both the left and right vertical wall.

Results

In evaluating the results of the two different situations, we again look at the horizontal velocity, vertical velocity and pressure reported by the sensors. Beginning with the horizontal velocity, Figure 4.3 shows the graphs of the horizontal velocity in m/s against time at the third and sixth sensor for the case with only horizontal walls and the case with both horizontal and vertical placed walls. We observe that up till a certain time the graphs from the same sensor follow a similar path. But after the moment where they intersect there is no longer a relation between them. Trying to understand what exactly happens during the experiment we will take a closer look at the first minimum of the graphs and the intersection for the third sensor.

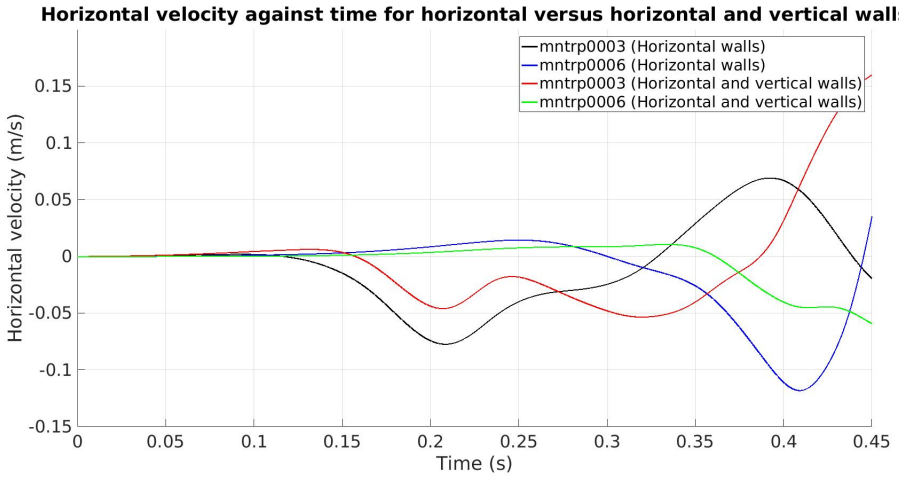

Figure 4.3: Horizontal velocity against time for the case in which horizontal walls are placed versus the case in which both horizontal and vertical walls are placed, reported by the third and sixth sensor.

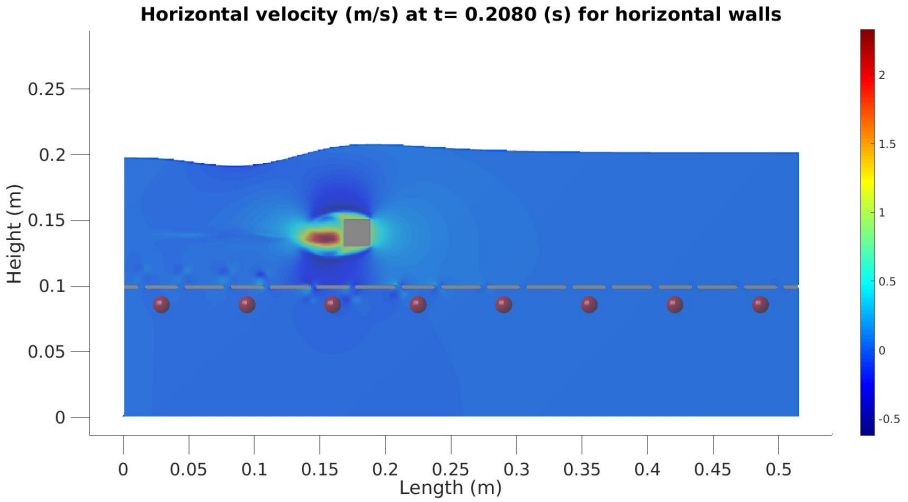

Figure 4.4: Horizontal velocity in m/s at $t = 0.2080$ s for the case in which horizontal walls are placed.

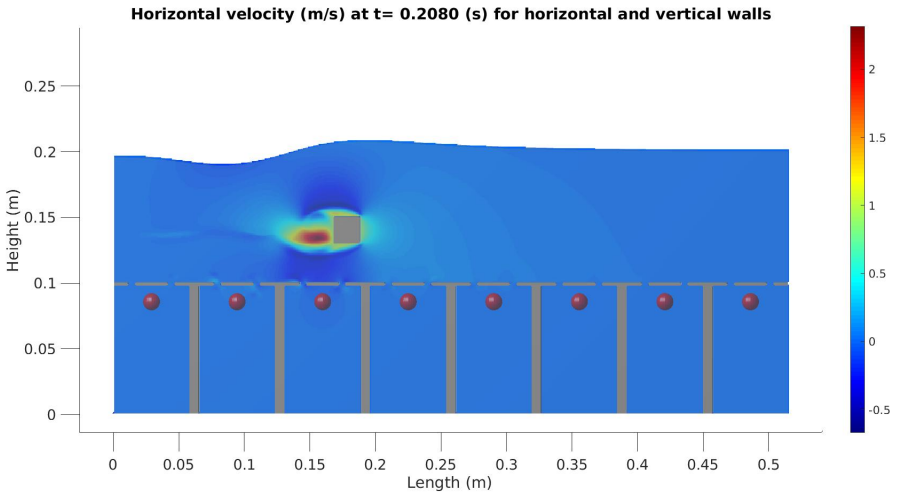

Figure 4.5: Horizontal velocity in m/s at $t = 0.2080$ s for the case in which both horizontal and vertical walls are placed.

The sensors of both cases record their first minimum around $t = 0.21$ s. In Figures 4.4 and 4.5 we see that around this moment in time the cube is passing the third sensor. In the case with only horizontal walls the cube has set the water in a higher motion than the cube in the case with both horizontal and vertical walls has done. Together with the fact that there also arose more vortices around the gaps between the horizontal walls, which can reach the sensors from the first situation, makes the sensor measure an extremer value of the minimum than the sensor does in the situation with also vertical walls. However, the activity right behind the cube is quite similar for both situations.

The point where the two graphs from the third sensor in Figure 4.3 intersect is around $t = 0.27$ s. This is the moment where the cubes are beginning to start with the shedding of vortices (Figures 4.6 and 4.7). The activity is no longer directly behind the cubes and are different in both situations. Because the vortex street appears in every situation differently, the water will be set in motion in different ways as well and therefore the sensors will also report different values. As a result, after the onset of the vortex streets there is no relation between the measurements from the case with only horizontal walls and the case with both horizontal and vertical walls anymore.

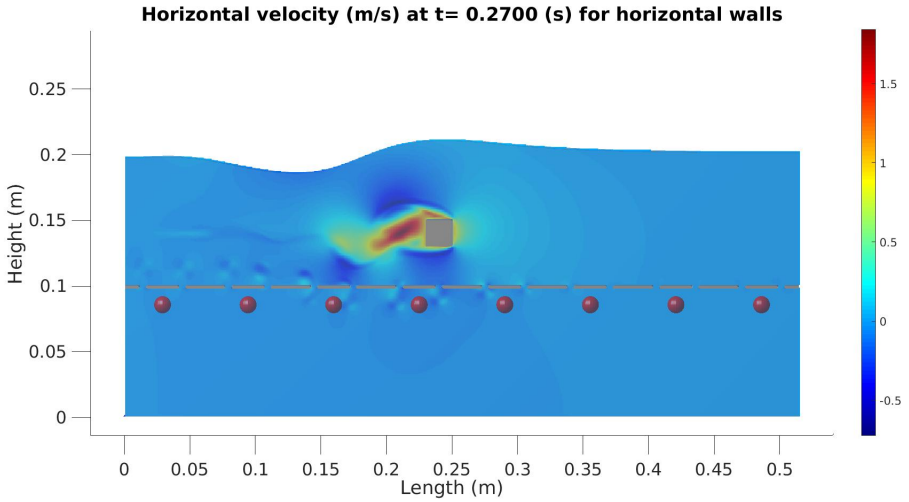

Figure 4.6: Horizontal velocity in m/s at $t = 0.2700$ s for the case in which both horizontal and vertical walls are placed.

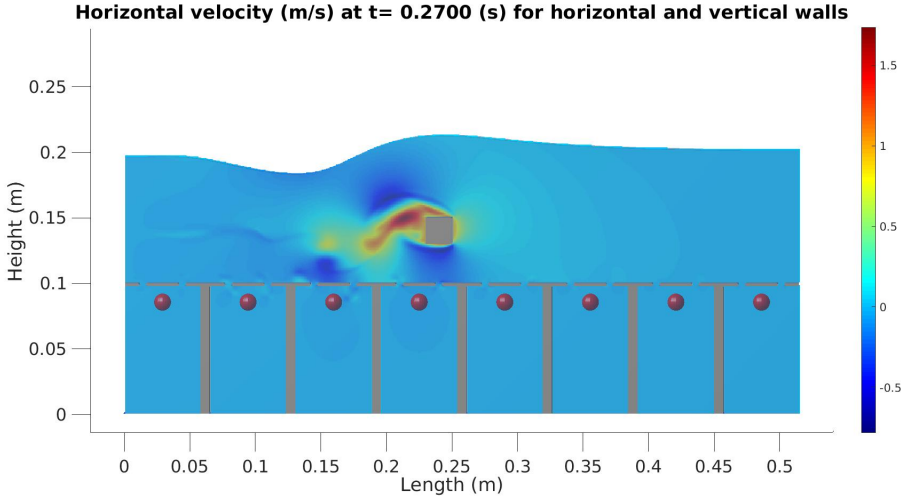

Figure 4.7: Horizontal velocity in m/s at $t = 0.2700$ s for both horizontal and vertical walls.

Looking at the graphs at the third and sixth sensor of the vertical velocity for the case with only horizontal walls and the case with both horizontal and vertical walls, we find that the sensors for the case with only horizontal walls report a change in vertical velocity at an earlier moment in time than the sensors of the case with both horizontal and vertical walls do. But where the sensors of the first case start with registering a negative value, the sensors of the second case both start with registering a positive value. To find out what happens during the experiment, we will investigate what happens at several moments in time. Beginning with the first minimum of the graph at the third sensor from the horizontal walls case.

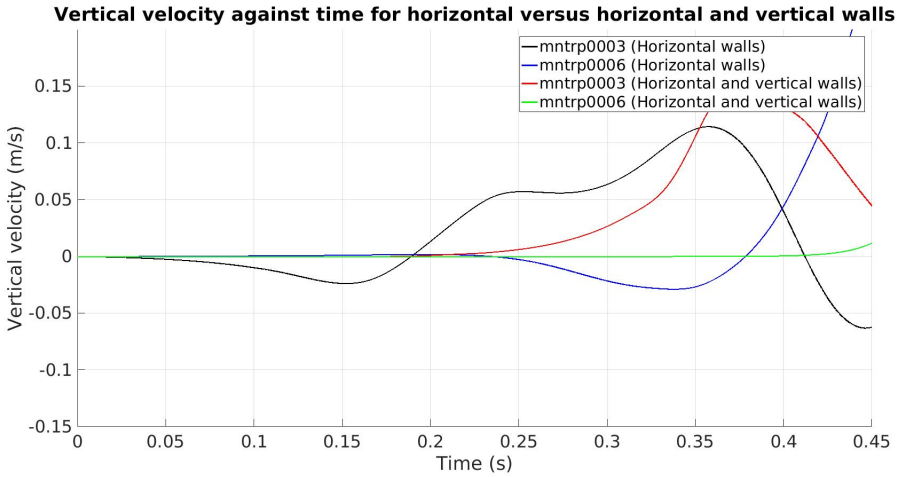

Figure 4.8: Vertical velocity against time for the case in which horizontal walls are placed versus the case in which both horizontal and vertical walls are placed, reported by the third and sixth sensor.

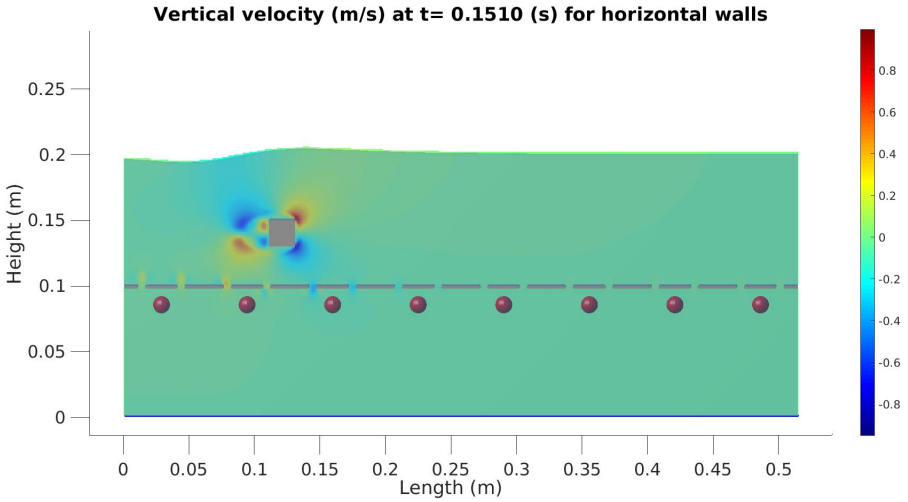

Figure 4.9: Vertical velocity in m/s at $t = 0.1510$ s for the case in which horizontal walls are placed.

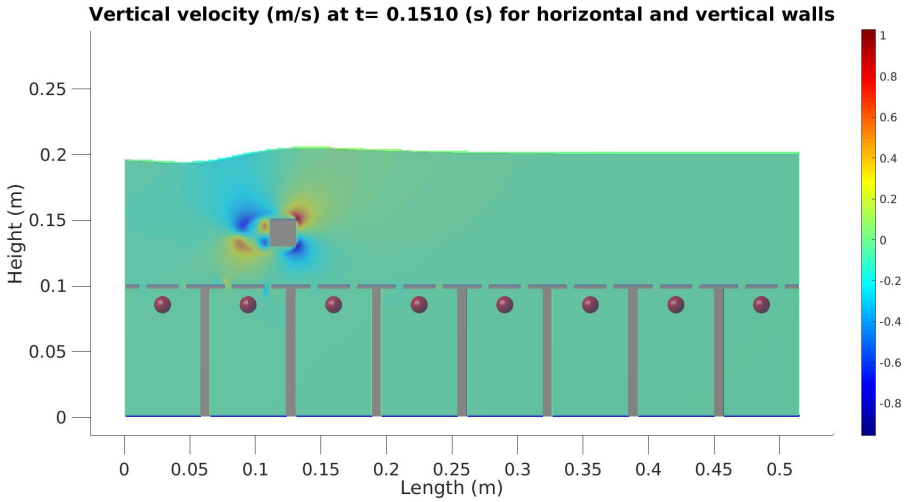

Figure 4.10: Vertical velocity in m/s at $t = 0.1510$ s the case in which both horizontal and vertical walls are placed.

This minimum is attained around $t = 0.15$ s. Figures 4.9 and 4.10 tell us that at this moment both cubes are approaching the third sensor. In doing so, the cube in the case with only horizontal walls causes a change in vertical velocity in the gaps above the first three sensors. While in the case with both horizontal and vertical walls a change in vertical velocity is seen in only the gaps above the second sensor. This is also the reason why the graph at the third sensor for the first case shows a minimum, while the graph for the second case does not show any difference. Further, we see that the activity directly around the cube is the same for both situations.

According to Figure 4.8, around $t = 0.35$ s the third sensor of both cases record a positive value of the vertical velocity. In Figures 4.11 and 4.12 we see that this is caused by a vortex that is in the neighbourhood of the sensor. The vortex is a result of the shedding of vortices by the moving cube. The pattern of this phenomenon in the two cases look like each other, but they are not totally the same. This is because the shedding of vortices will be different in every situation. As we already concluded for the horizontal velocity, also for the vertical velocity it applies that when there is a vortex street present, no relation could be found between the results reported by the same sensor of the two different cases. Which makes that the graphs of the two situations are not related either.

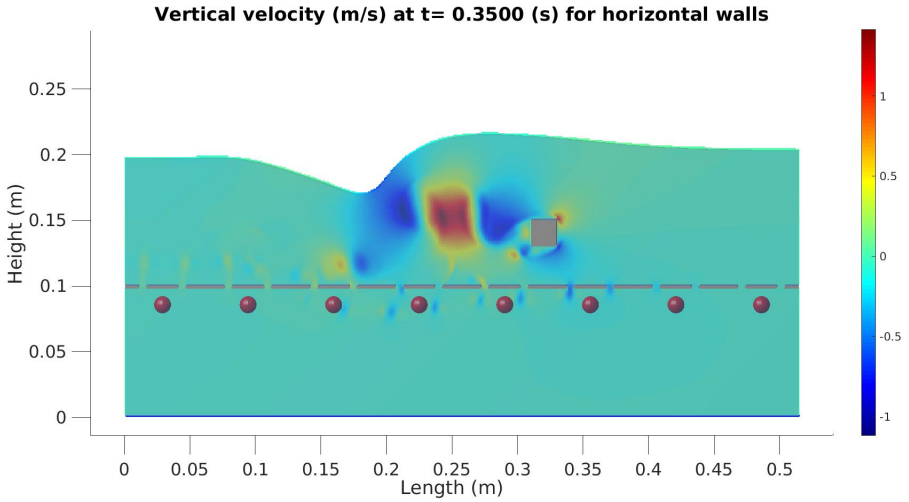

Figure 4.11: Vertical velocity in m/s at $t = 0.3500$ s the case in which horizontal walls are placed.

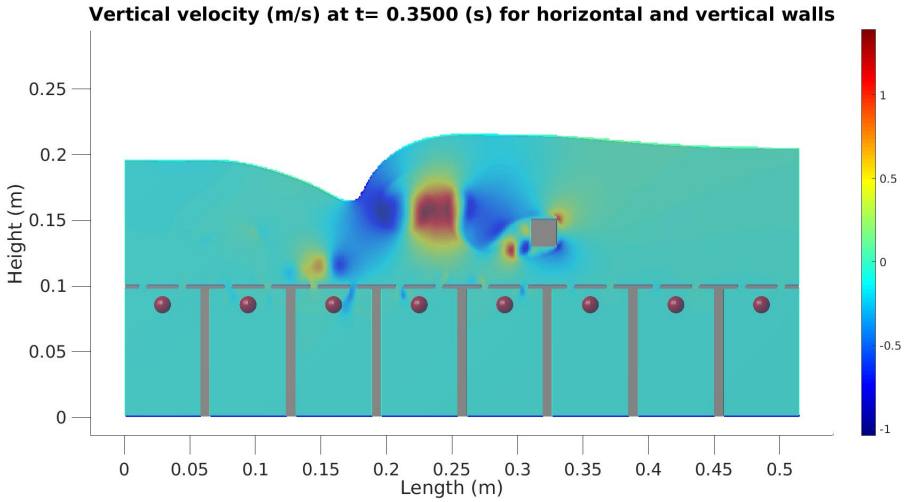

Figure 4.12: Vertical velocity in m/s at $t = 0.3500$ s the case in which both horizontal and vertical walls are placed.

The graphs for the velocities show more and extremer maxima and minima for the case with only horizontal walls than for the case with both horizontal and vertical walls. However, in Figure 4.13 we see that regarding the pressure, this is the other way around. The graphs for the case with both horizontal and vertical walls show clear extreme values, while the other graphs stay more constant. Further, although the graph of the sixth sensor for the both horizontal and vertical walls case show a clear maximum and minimum, it has a much extremer maximum value and a less extremer minimum value of the pressure, compared to the graph of the third sensor from the same case. To investigate why this is, we will take a closer look at what happens at these extreme values measured by the third and sixth sensor.

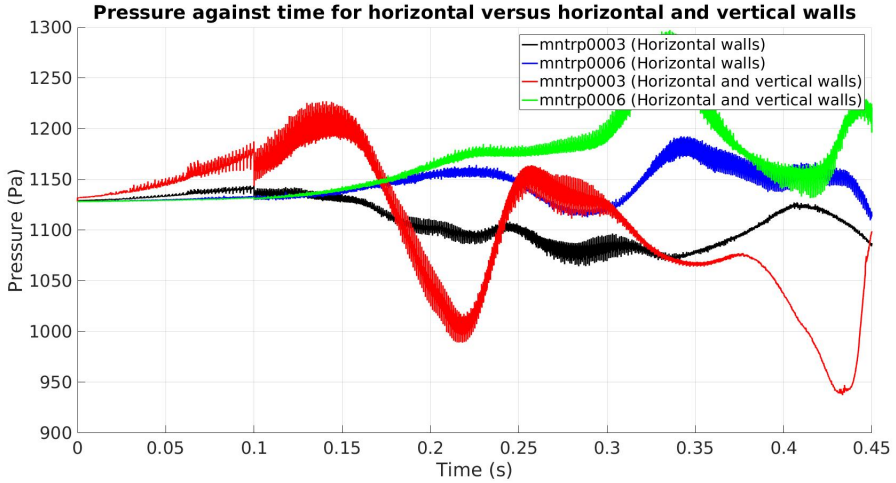

Figure 4.13: Pressure against time for the case in which horizontal walls are placed versus the case in which both horizontal and vertical walls are placed, reported by the third and sixth sensor.

The first maximum that is reported by the third sensor of the case with both horizontal and vertical walls is around $t = 0.13$ s, when the cube is approaching this sensor (Figure 4.15). For the case with only horizontal walls (Figure 4.14), we observe that at this moment in time, around every sensor the same values of the pressure are seen. Only directly around the cube, there are some changes in pressure. Similar changes in pressure around the cube are also present in the case with both horizontal and vertical walls. However, the pressure values around the sensors do not correspond to the situation in the other case. In approaching the third sensor of the case with both horizontal and vertical walls, the movement of the cube causes a rise in pressure in the third compartment and a drop in pressure in the second compartment. This explains the maximum of the graph in Figure 4.13.

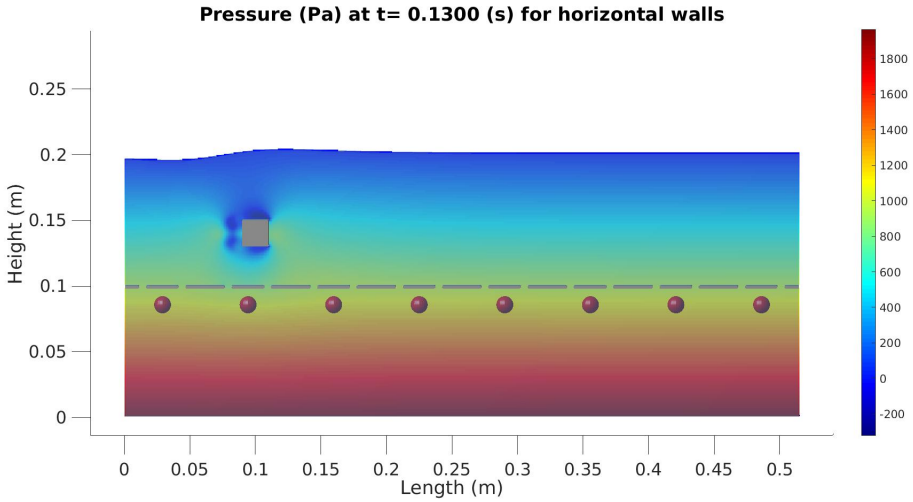

Figure 4.14: Pressure in Pa at $t = 0.1300$ s for the case in which horizontal walls are placed.

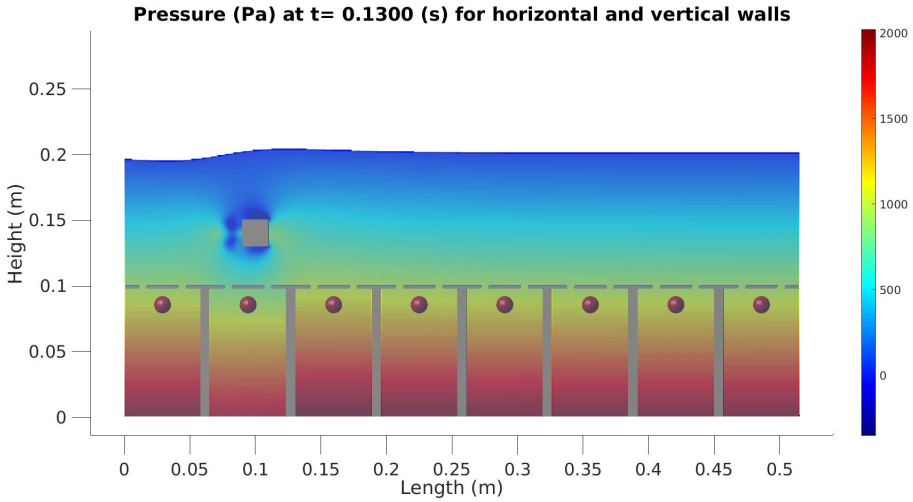

Figure 4.15: Pressure in Pa at $t = 0.1300$ s for the case in which both horizontal and vertical walls are placed.

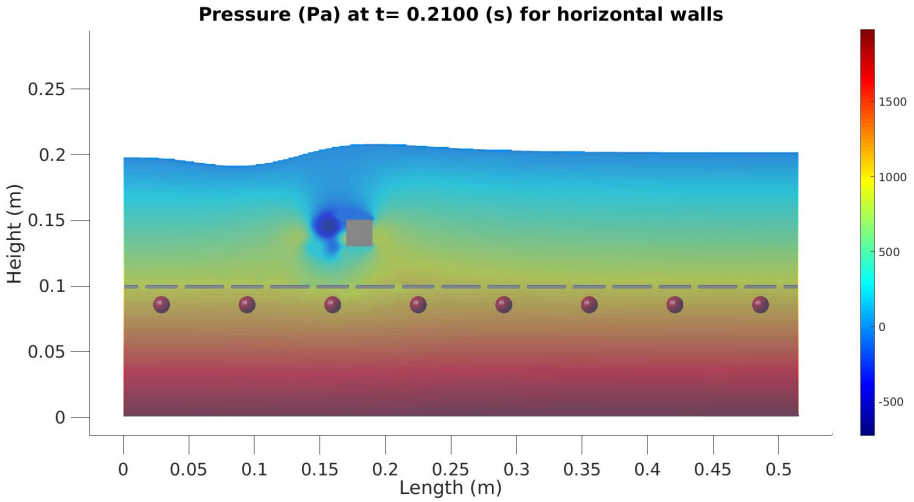

Figure 4.16: Pressure in Pa at $t = 0.2100$ s for the case in which both horizontal and vertical walls are placed.

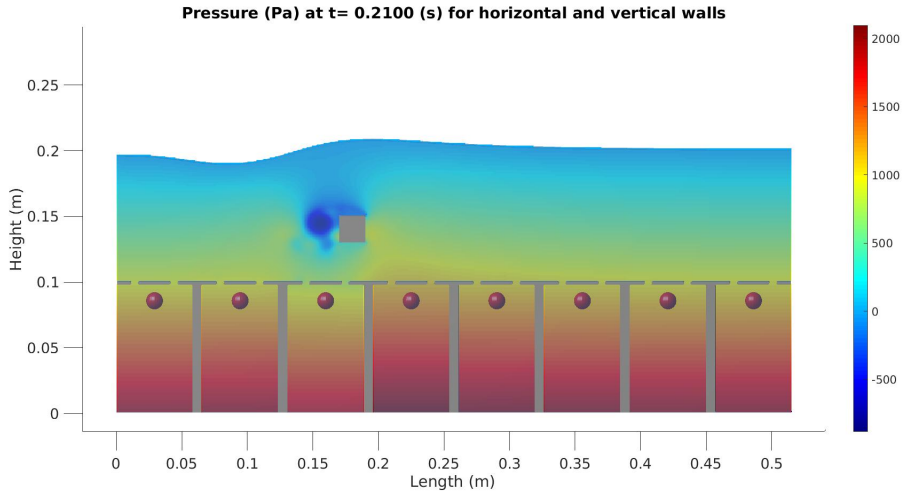

Figure 4.17: Pressure in Pa at $t = 0.2100$ s for the case in which both horizontal and vertical walls are placed.

Figures 4.16 and 4.17 tell us that at $t = 0.2100$ s the cube is passing the third sensor. We observe that the pressure directly around the cube is for both cases the same. Looking at the case for only horizontal walls, we see that through the whole tank the pressure has lowered a bit. But the pressure around the sensors has stayed relatively the same. There still are no enormous differences at one specific sensor. In the case for both horizontal and vertical walls, however, we see in Figure 4.15 that, by passing the third compartment, the cube causes a rise in pressure in at least the two compartments in front of it and evokes a drop in pressure in the third

compartment. This is the reason why the graph of the third sensor for this case in Figure 4.13 shows us a minimum around $t = 0.21$ s.

In Figure 4.13, it is observed that the graph of the sixth sensor for the case with both horizontal and vertical walls has a much extremer maximum value and a less extremer minimum value of the pressure compared to the graph of the third sensor from the same case. To find out why this is, we will take a look at what happens around $t = 0.42$ s where the minimum is attained. Again the phenomenon of vortex shedding of is visible (Figures 4.18 and 4.19). Because of the presence of the vortex street, the water around the cube is set in a different motion than when the cube was passing the third sensor. This also causes different values of the maxima and minima registered by the sensors.

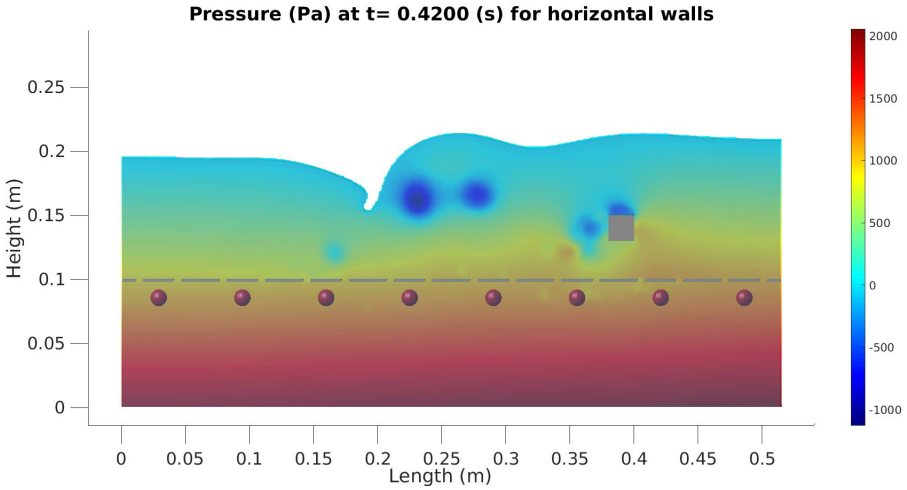

Figure 4.18: Pressure in Pa at $t = 0.4200$ s for the case in which horizontal walls are placed.

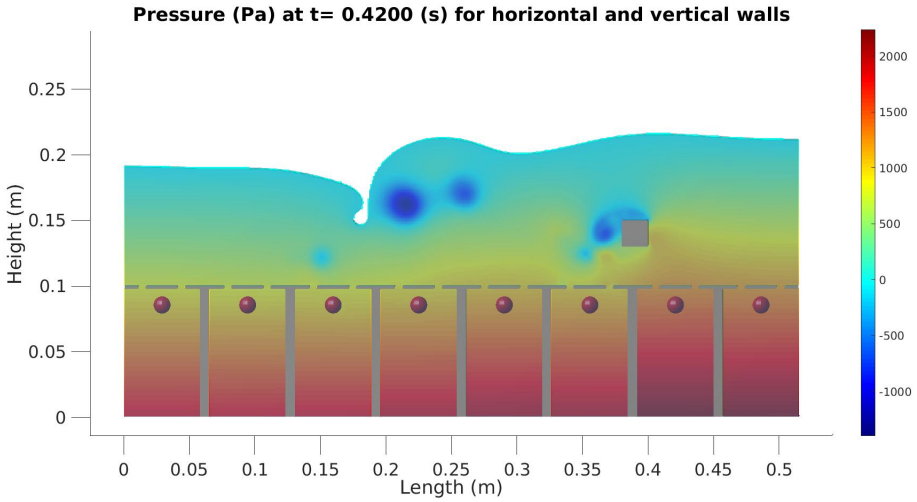

Figure 4.19: Pressure in Pa at $t = 0.4200$ for the case in which both horizontal and vertical walls are placed.

In conclusion, comparing the case with only horizontal walls to the case with both horizontal and vertical walls gives us that for both velocities, the sensors report a more extreme value at the same moment in time for the case with only horizontal walls. For the pressure, it is the other way around. In this case the maxima and minima of the both horizontal and vertical walls case have more extreme values. But after the onset of the vortex street, we see that no relation can be found between the graphs of the different cases anymore.

Chapter 5

Cube versus ball

Up to now we considered the moving object to be a cube. However, in the real experiment the moving object that will be used is a ball. We would like to apply this to our research as well. We expect that the change of shape will result in different measurements. To investigate what kind of effect this exactly has on the measurements, in this section the two situations will be compared to each other. This will be done using the same set-up as in the case with both horizontal and vertical walls from the previous chapter. With the only difference that in one case the cube will be replaced by a ball.

Results

Firstly, considering the horizontal velocity again, we see that the graphs for the third sensor are the same up till around $t = 0.15$ s (Figure 5.1). After this moment the graph of the cube shows for the same moments in time a lower value than the graph of the ball, also staying parallel for around 0.15 seconds. At a certain time we observe that there is no relation between the graphs of the cube and the ball anymore.

The graphs of the sixth sensor are quite similar up till around $t = 0.35$ s. After that moment we see the graphs diverge from each other. To discover what happens during the experiment, we will highlight some important moments in time.

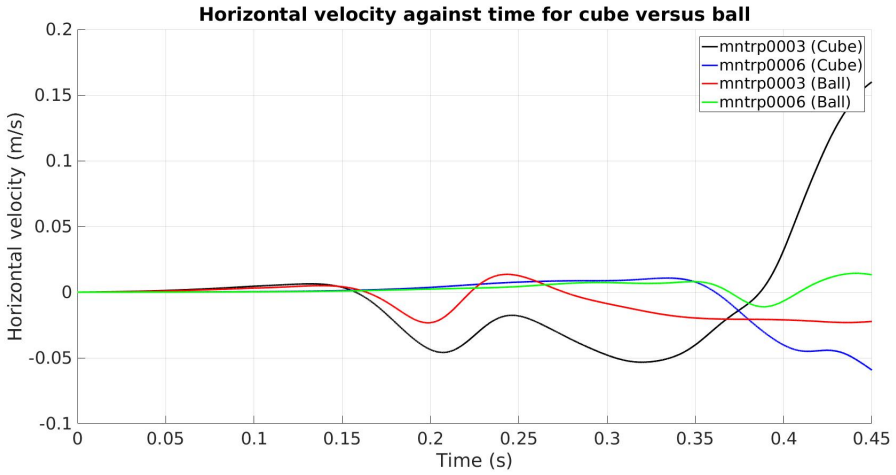

Figure 5.1: Horizontal velocity against time for the case with a cube versus the case with a ball, reported by the third and sixth sensor.

From Figure 5.1 we know that around $t = 0.20$ s both graphs of the third sensor have their first minimum. However, these minima do not have the same value. The graph of the cube has an extremer value than the graph of the ball. In Figures 5.2 and 5.3 it is shown that in approaching the third sensor, the activity in the case of the cube is right behind the object, while the activity in the case of the ball goes more downwards. This indicates that the start of the shedding of vortices happens at an earlier moment in time for the ball than for the cube. The difference in activity behind the objects is also the explanation for the difference in minima of the two graphs.

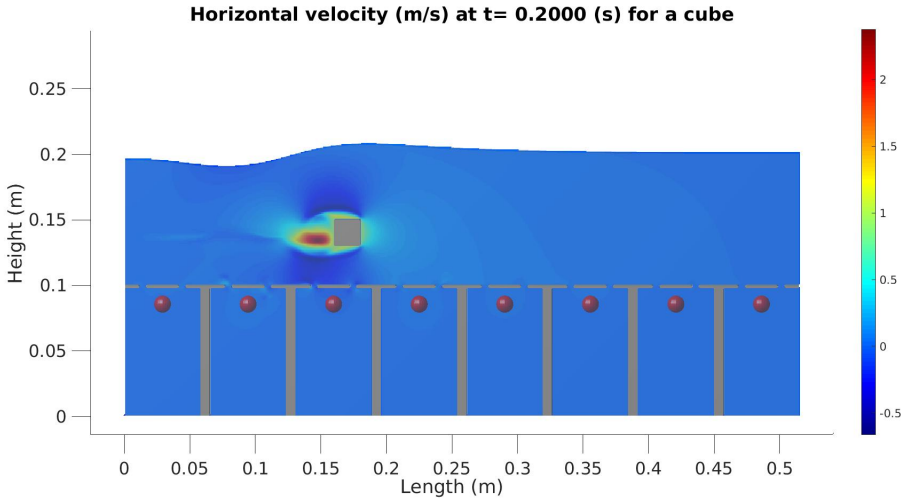

Figure 5.2: Horizontal velocity in m/s at $t = 0.2000$ s for the case with a cube.

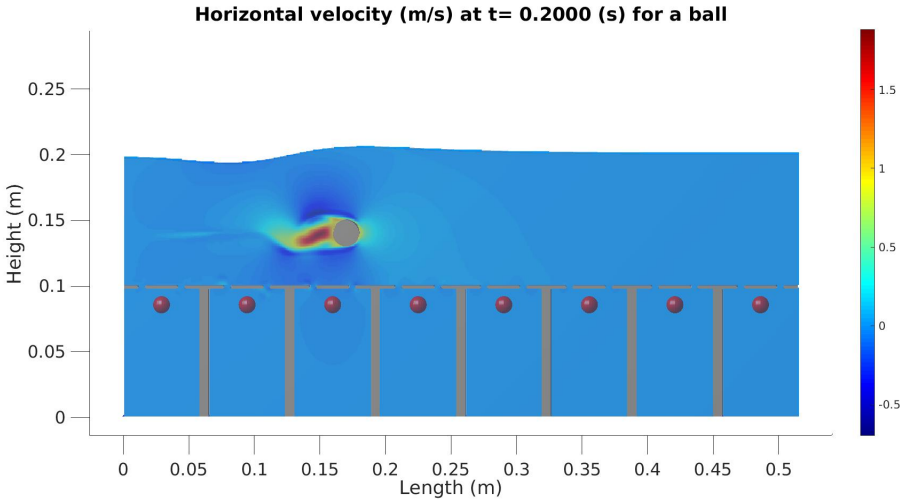

Figure 5.3: Horizontal velocity in m/s at $t = 0.2000$ s for the case with a ball.

The point where the graphs for the third sensor in Figure 5.1 stop being parallel is around $t = 0.33$ s. At this moment in both cases a vortex street is present as shown in Figures 5.4 and 5.5. A vortex is shedded in the neighbourhood of the third sensor in both situations. However, because the shedding of vortices never happens in the same way, the vortex in the case of the cube is located at a different place and has a different velocity than the vortex in the case of the ball. This is why, from this moment onwards, different values of the horizontal velocity are reported by the same sensor.

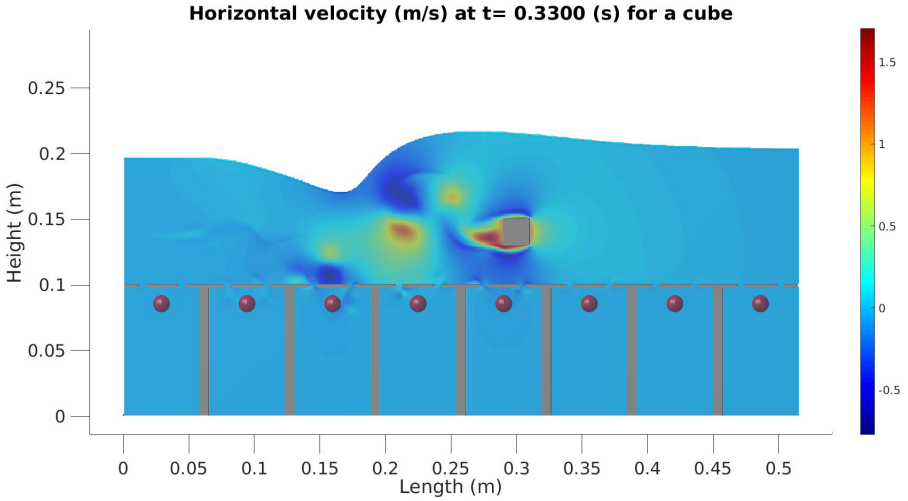

Figure 5.4: Horizontal velocity in m/s at $t = 0.3300$ s for the case with a cube.

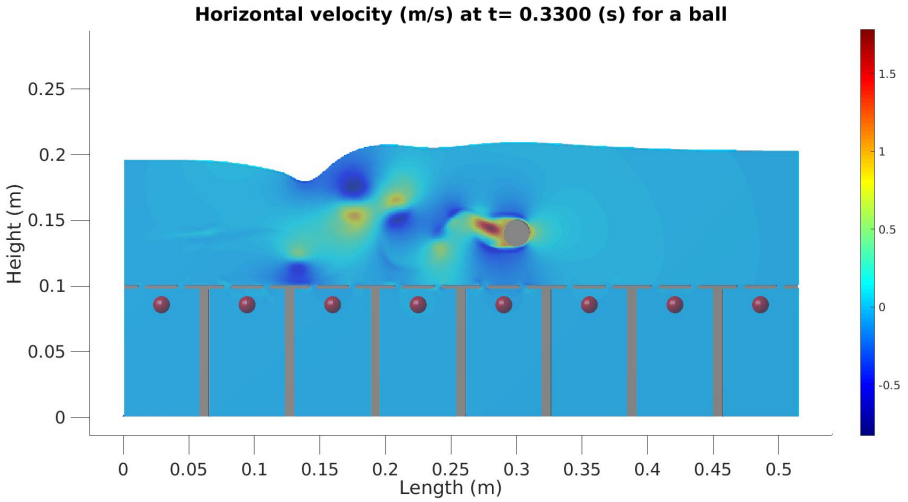

Figure 5.5: Horizontal velocity in m/s at $t = 0.3300$ s for the case with a ball.

Looking at the graphs for the vertical velocity in Figure 5.6, we observe that the third sensor from the case of the ball and the sixth sensor from both cases barely register a difference in vertical velocity. Up till around $t = 0.20$ s this is also true for the third sensor from the case of the cube. But after 0.20 seconds the graph for this case starts to grow with having its maximum around $t = 0.375$ s.

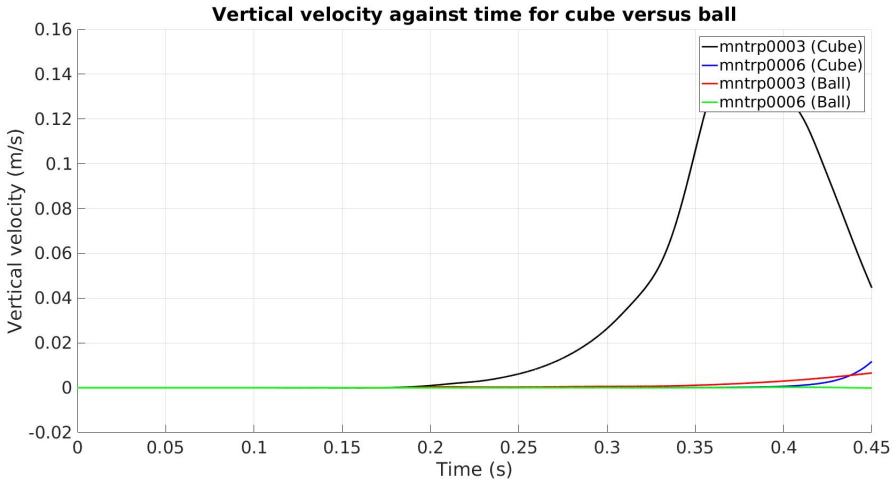

Figure 5.6: Vertical velocity against time for the case with a cube versus the case with a ball, reported by the third and sixth sensor.

Figures 5.7 and 5.8 tell us that at this moment in time, by both moving objects a vortex is shedded near the third sensor. But the vortex in the case of the cube is of a different size and magnitude and is therefore able to reach the third sensor, while the vortex in the case of the ball does not set the water below the horizontal walls in motion. Moreover, according to the graph of this case, during the experiment no other vortex was able to do that either.

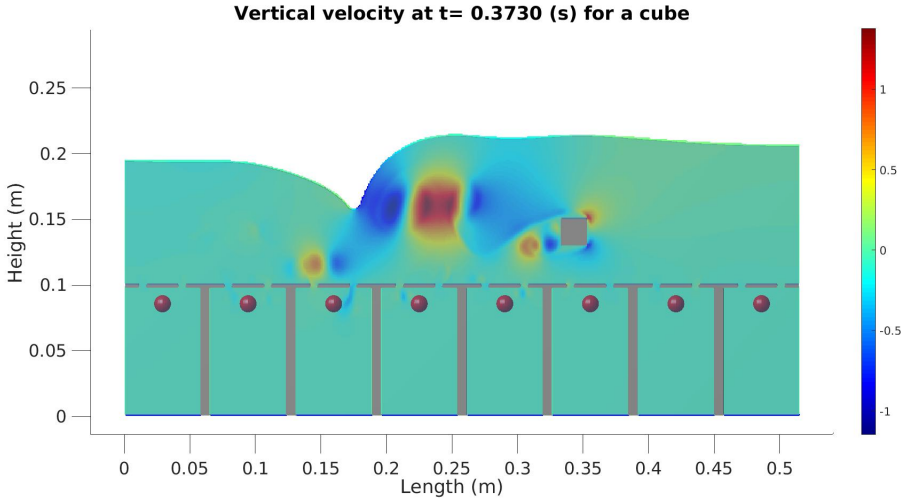

Figure 5.7: Vertical velocity in m/s at $t = 0.3730$ s for the case with a cube.

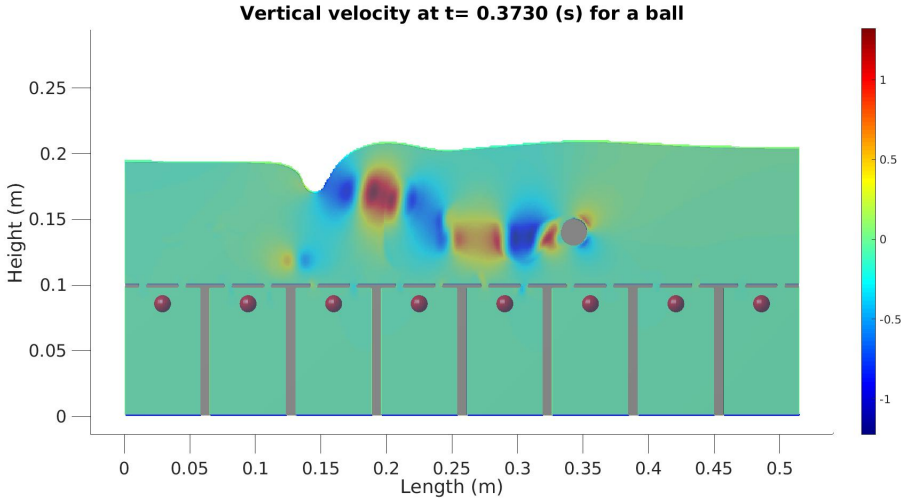

Figure 5.8: Vertical velocity in m/s at $t = 0.3730$ s for the case with a ball.

In Figure 5.9 we see that the graphs of the pressure at the third sensor for the cases with the cube and the ball are parallel from the start until around $t = 0.19$ s. At this moment, the graph belonging to the case with the ball decreases to a lower minimum value around $t = 0.21$ s than for the case with the cube around $t = 0.22$ s. In the remainder of the diagram, the two graphs appear to have quite similar slopes, with small deviations relative to each other.

Looking at the graphs of the pressure at the sixth sensor, we also only see small deviations between the cases for the cube and the ball up till around $t = 0.36$ s. However, around $t = 0.39$ s a large difference in pressure between the cases for the cube and the ball is measured. After this moment, the two graphs partly converge again.

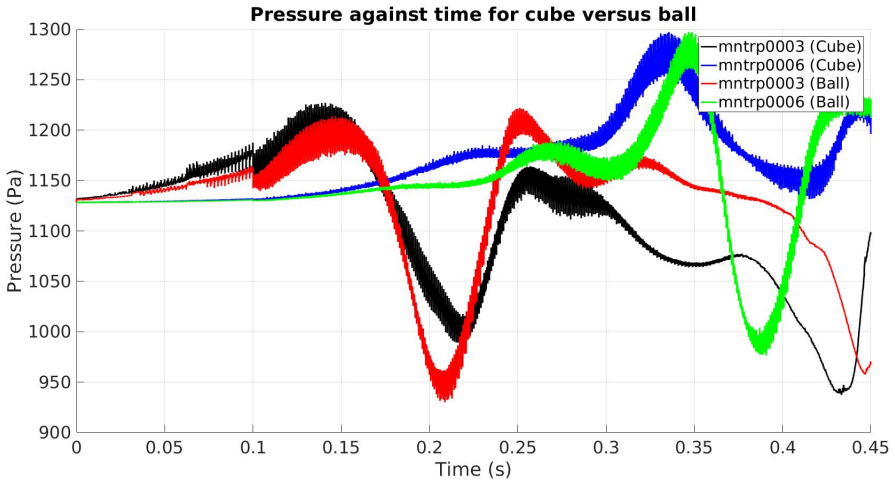

Figure 5.9: Pressure against time for the case with a cube versus the case with a ball, reported by the third and sixth sensor.

In Figures 5.10 and 5.11 it is shown what happens at the point where the graphs of the third sensor stop following a parallel path. At $t = 0.1900$ s the object is passing the third sensor. While doing this, in the case of the cube the most activity is seen directly behind it, while for the case with the ball we observe that the activity behind the ball curves upwards. This indicates that the onset of the vortex street in the case of the ball takes place at an earlier moment in time than the onset of the vortex street in the case of the cube. So, because after approximately $t = 0.19$, seconds the activity behind both objects is starting to differ in direction, which has also an effect on the direction of the water around it, from this moment on the two sensors start measuring different values of the pressure.

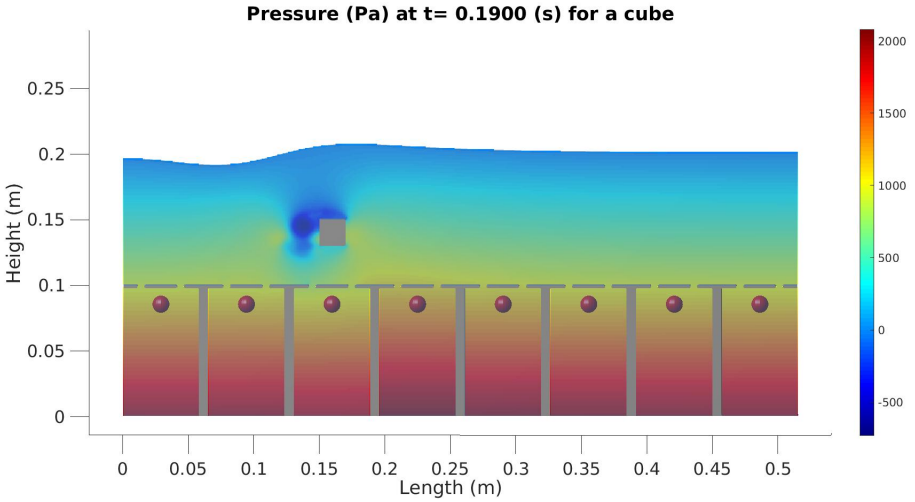

Figure 5.10: Pressure in Pa at $t = 0.1900$ s for the case with a cube.

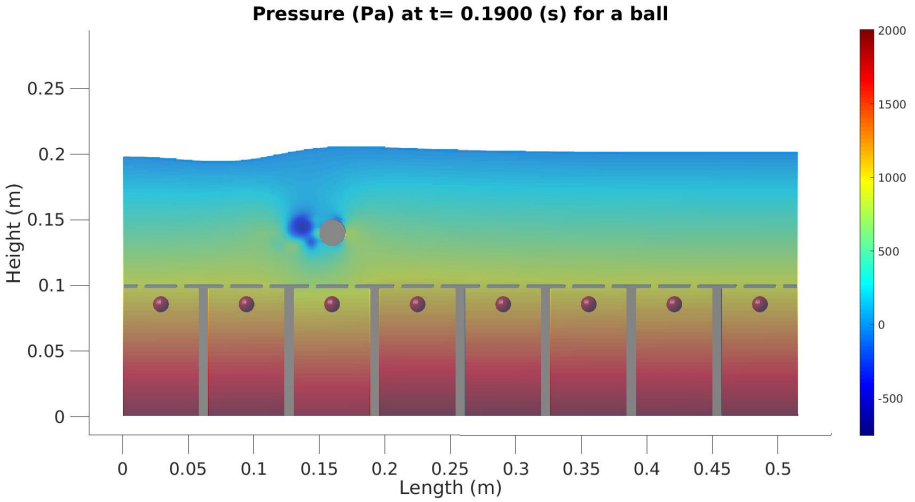

Figure 5.11: Pressure in Pa at $t = 0.1900$ s for the case with a ball.

At $t = 0.3900$ s both objects are located right above the sixth sensor (Figures 5.12 and 5.13). We see that the activity around the cube starts at the top of the object, making a curve downwards. While the activity of the ball begins from below making a curve upwards. This causes a big difference in pressure reported by both sixth sensors. Further, we observe that at this time, in both situations the vortex street is present. However, the pattern of the shedded vortices are not similar, which makes the graphs differ as well.

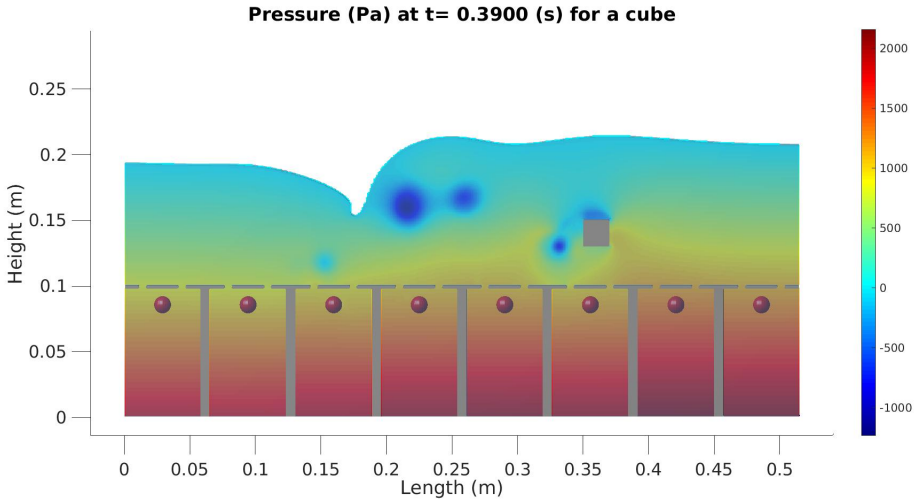

Figure 5.12: Pressure in Pa at $t = 0.3900$ s for the case with a cube.

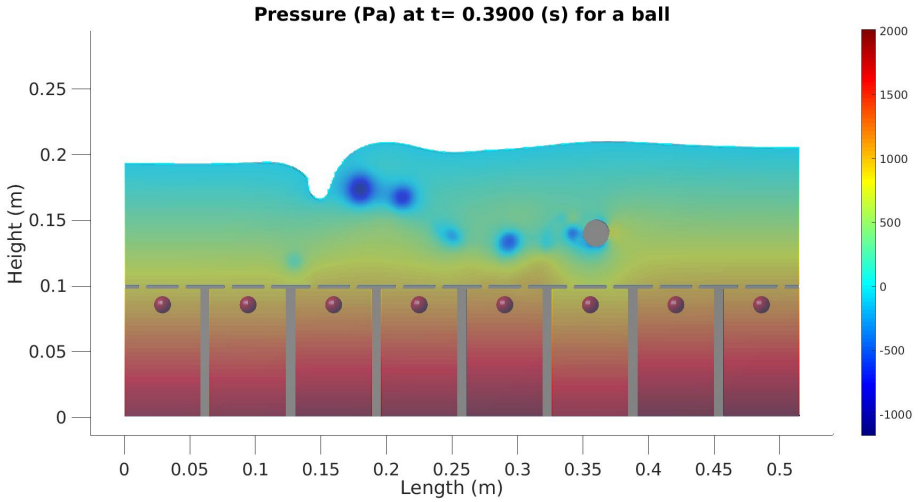

Figure 5.13: Pressure in Pa at $t = 0.3900$ s for the case with a ball.

Thus, comparing the case with the cube to the case with the ball, we find that the ball begins at an earlier moment in time with the shedding of vortices. Also, the pattern of the vortices of the different cases differ. Therefore different values of the velocities and pressure are reported at the same sensors.

Chapter 6

The experiment considered in the three-dimensional space

In the previous sections, the cases were all considered in two dimensions. However, when performing the experiment in real-life a third dimension will be present. So, in order to resemble the true experiment as much as possible, adding a third dimensions will be the next step. In doing this, two different situations will be considered. In the first situation the horizontal (and vertical) walls and sensors are centered in the middle of the tank. For the second situation the walls and sensors are placed at the right side of the tank. In each situation, the case with only horizontal walls will be compared to the case with both horizontal and vertical walls.

It is expected that with adding an extra dimension, the calculations will be more expensive and will take more time to complete. Therefore, the first computations will be done using a coarser grid, with the following dimensions: 172x50x94. Also, local grid coarsening will be applied to some parts of the tank that are less interesting. Such that, these will be considered with a grid that is a factor two bigger than the original grid, which should make the computations go a little faster.

6.1 The walls and sensors placed in the center of the tank

Beginning with the situation in which the walls and sensors are located in the center of the tank, we will use the set-up of Figure 6.1 for the case with only horizontal walls and the set-up of Figure 6.2 for the case with both horizontal and vertical walls. The local grid coarsening will be applied to the right and left side of the walls, as shown in Figure 6.3.

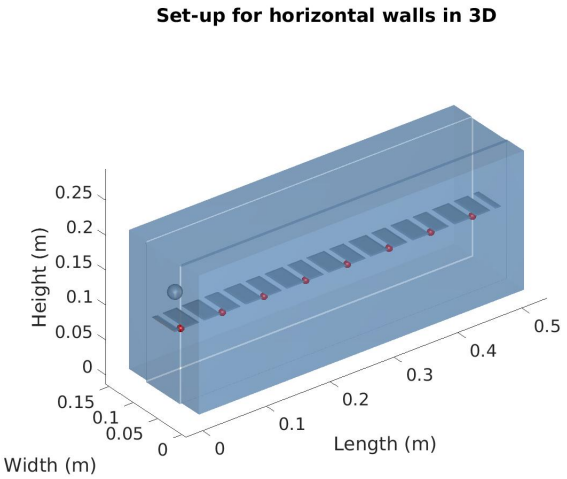

Figure 6.1: Three-dimensional set-up for the case in which both horizontal and vertical walls are placed in the center of the tank.

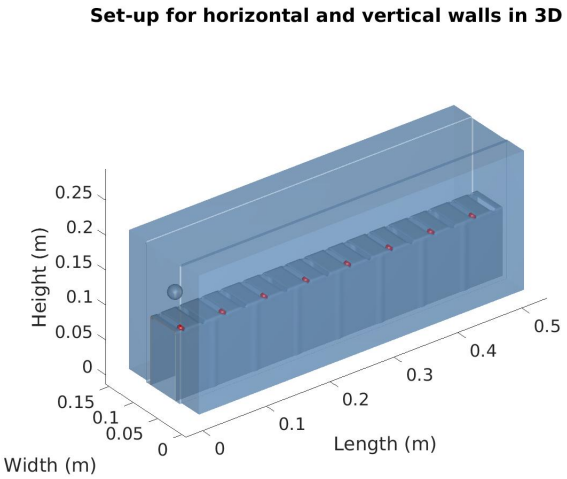

Figure 6.2: Three-dimensional set-up for the case in which both horizontal and vertical walls are placed in the center of the tank.

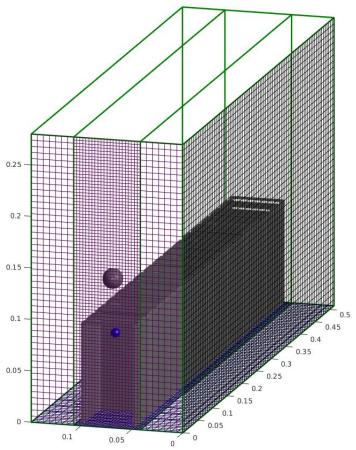

Figure 6.3: By means of local grid coarsening, less computational cells are placed near the sides of the tank.

Results

Figure 6.4 shows us the graphs for the U velocity against time, for both the case with only horizontal walls and the case with both horizontal and vertical walls, at the third and sixth sensor. The curves for the both horizontal and vertical walls case obtain higher values than those for the horizontal walls case. Remarkable is that these graphs follow an almost entire parallel path. This is in contrast to what we have seen in the two-dimensional simulations, where we saw that, because of the onset of a vortex street at a certain point, no relation could be found between two relevant graphs. Further, the values of the U velocity that are reported by the sensors are much smaller than in the two-dimensional cases. To find out what happens, we take a closer look at the maxima and minima registered by the third sensors.

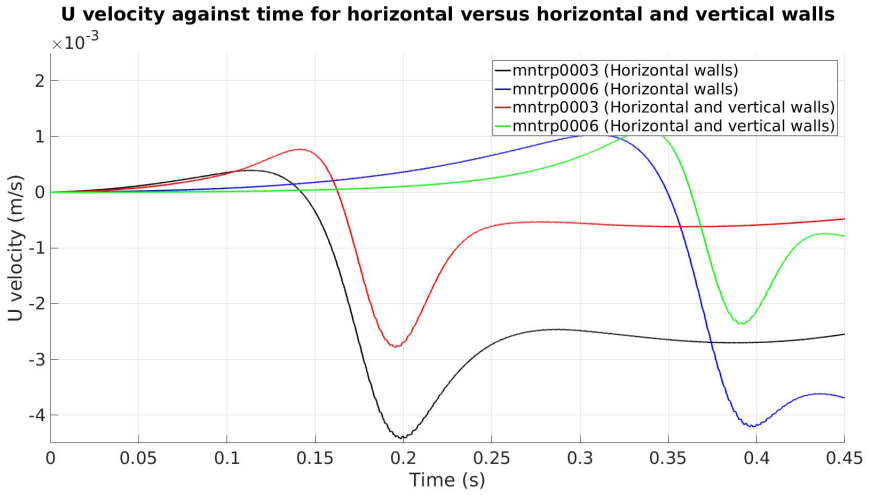

Figure 6.4: U velocity against time for the case with horizontal walls versus the case with both horizontal and vertical walls, reported by the third and sixth sensor.

The maximum value of the U velocity of both cases reported by the third sensor is obtained around $t = 0.14$ s. Figures 6.5 and 6.6 show that at this moment, the ball is approaching the third sensor. While doing this, the activity is right behind the ball and relatively little water in the tank has been set in motion. In front of the ball of the case with both horizontal and vertical walls, some lighter parts are seen. Indicating higher velocities in that region. This is also seen in front of the ball of the other case, but the parts in that case are less lighter. This is in accordance with the graph in Figure 6.4.

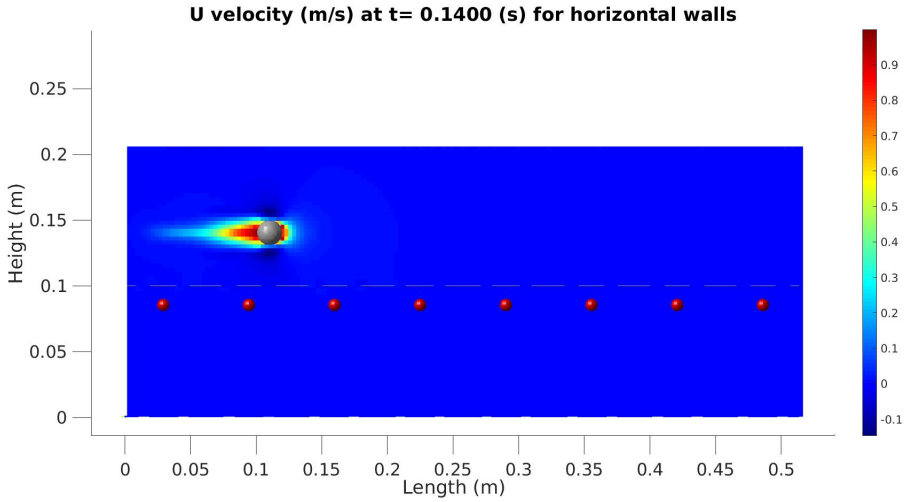

Figure 6.5: Front view. U velocity in m/s at $t = 0.1400$ s for the case with horizontal walls.

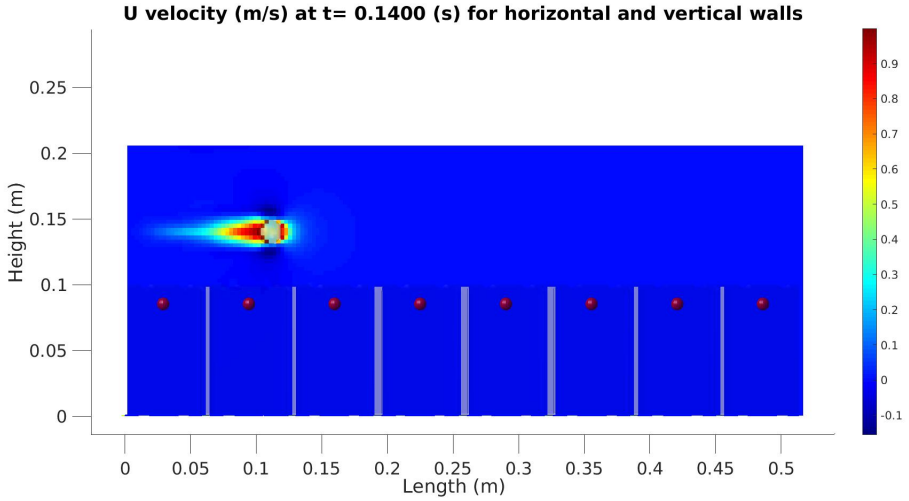

Figure 6.6: Front view. U velocity in m/s at $t = 0.1400$ s for the case with both horizontal and vertical walls.

Figures 6.7 and 6.8 tell us what happens at the minimum in Figure 6.4 of both graphs for the third sensor. We see that both balls are passing the third sensor, with having the highest activity, although in a larger area, still right behind it. Again there is not much water set in motion in the rest of the tank. According to the graphs, a difference in minimum value of the U velocity around $t = 0.20$ s between the two cases should be visible, but there is hardly any difference in color and thus velocity. This is probably because the difference in velocity is too small compared to the velocities that are being obtained right behind the object.

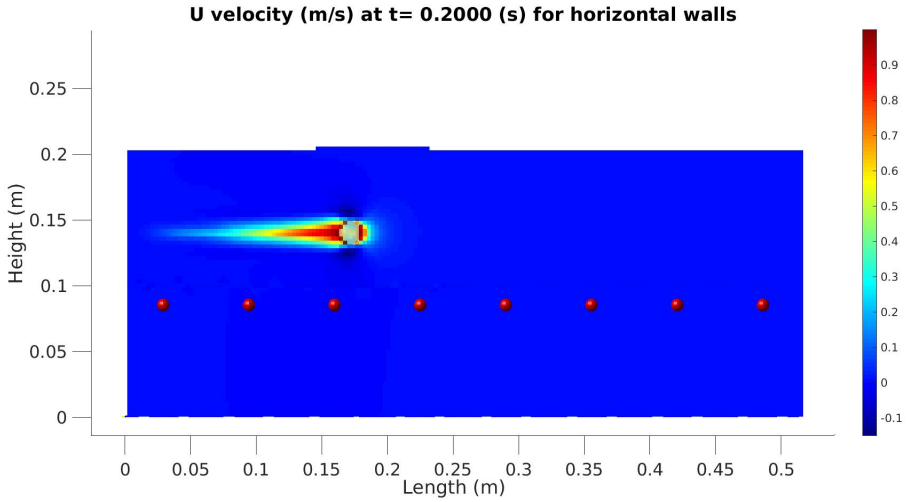

Figure 6.7: Front view. U velocity in m/s at $t = 0.2000$ s for the case with horizontal walls.

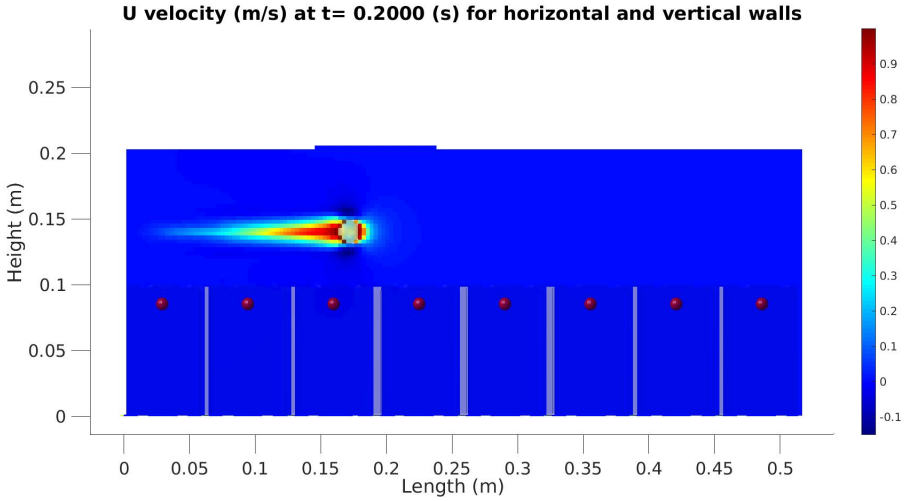

Figure 6.8: Front view. U velocity in m/s at $t = 0.2000$ s for the case with both horizontal and vertical walls.

When we look at the graphs of the V velocity in Figure 6.9, we see that the values of the V velocity are even smaller than the values of the U velocity. So, the maxima of the graphs from the case with only horizontal walls that are seen are actually small differences. The graph registered by the third sensor has its maximum around $t = 0.20$ s, which is, as we already saw when evaluating the U velocity, the moment where the object is passing the third sensor.

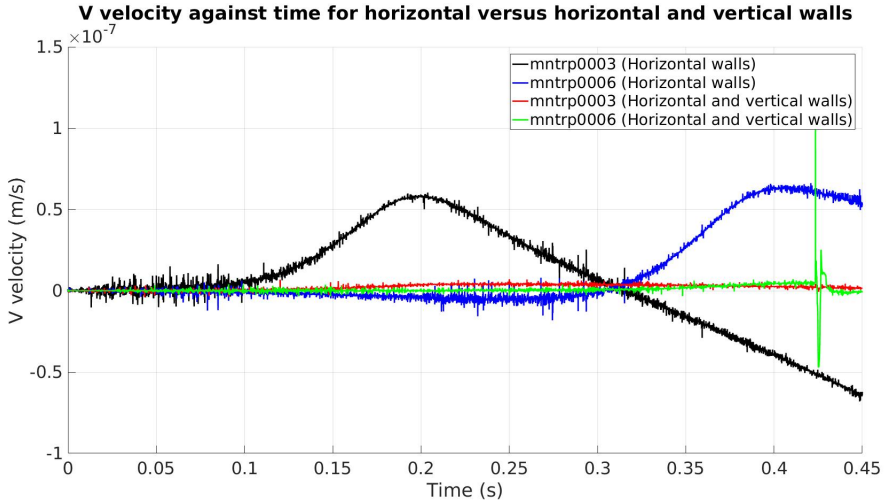

Figure 6.9: V velocity against time for the case with horizontal walls versus the case with both horizontal and vertical walls, reported by the third and sixth sensor.

Figures 6.10 and 6.11 show the side view of the tank at again $t = 0.2000$ s. The figures are quite similar. Both show a slight decrease in V velocity at theright side of the ball and a slight increase in V velocity at the left side of the ball. But again there is hardly any difference in velocity seen in the neighbourhood of the sensors nor in the water of the rest of the tank.

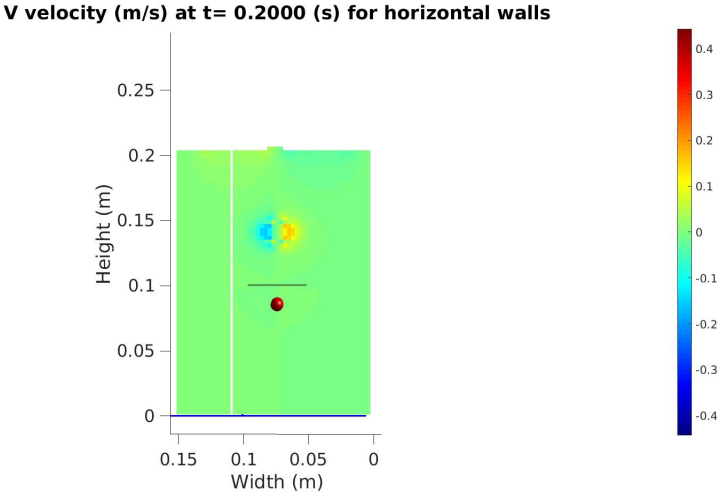

Figure 6.10: Side view. V velocity in m/s at $t = 0.2000$ s for the case with horizontal walls.

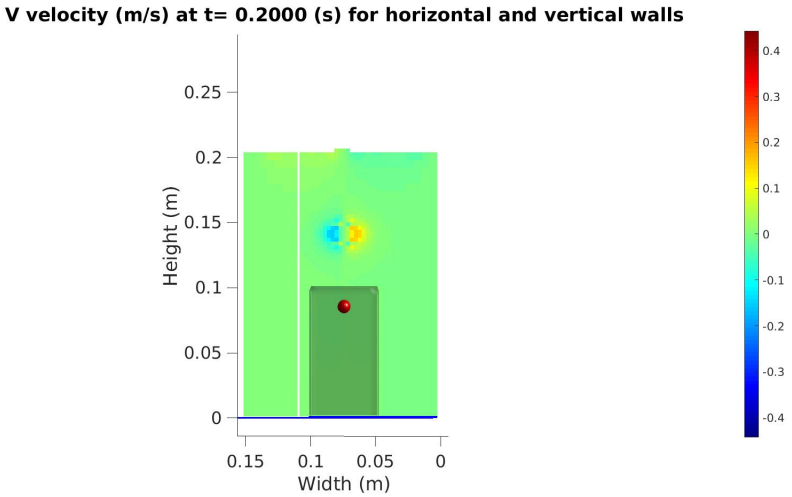

Figure 6.11: Side view. V velocity in m/s at $t = 0.2000$ s for the case with both horizontal and vertical walls.

Considering the last velocity, W, we observe that the graphs of this velocity for the case with only horizontal walls again, show bigger differences than the graphs for the case with both horizontal and vertical walls. The reported values are again smaller than those obtained in the two-dimensional simulations. Both graphs for the third sensor have their minimum around $t = 0.16$ s, while around $t = 0.25$ s only the horizontal walls case has its maximum. We will take a look at what happens at these moments in time.

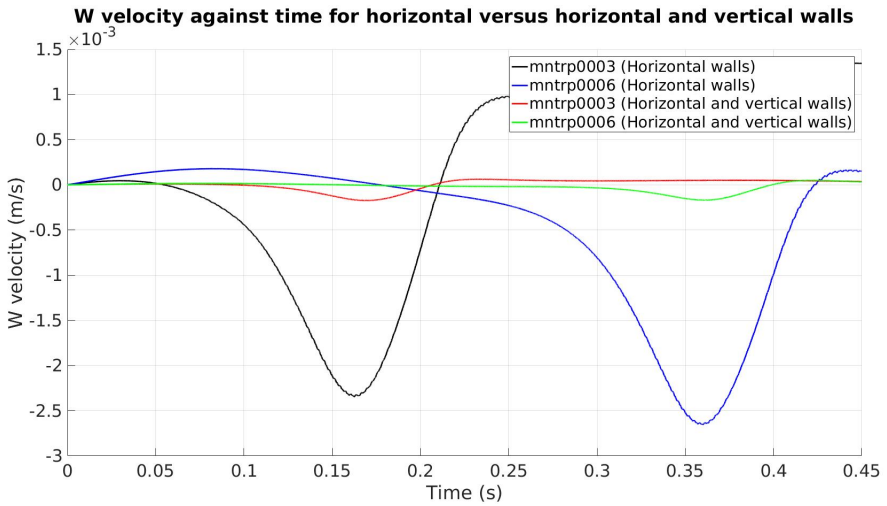

Figure 6.12: W velocity against time for the case with horizontal walls versus the case with both horizontal and vertical walls, reported by the third and sixth sensor.

At $t = 0.1600$ s both balls are approaching the third sensor. This causes a change in W velocity, with an increase in W velocity in the upper right part and lower left part and a decrease in W velocity in the lower right part and the upper left part (Figures 6.13 and 6.14). We can see in Figure 6.13, for the case with only horizontal walls, that the water between the gaps above the third sensor is also set in motion, while this does not happen in the case for both horizontal and vertical walls. This is the reason why the third sensor of the horizontal walls case reports an extremer value of the minimum than the third sensor in the other case.

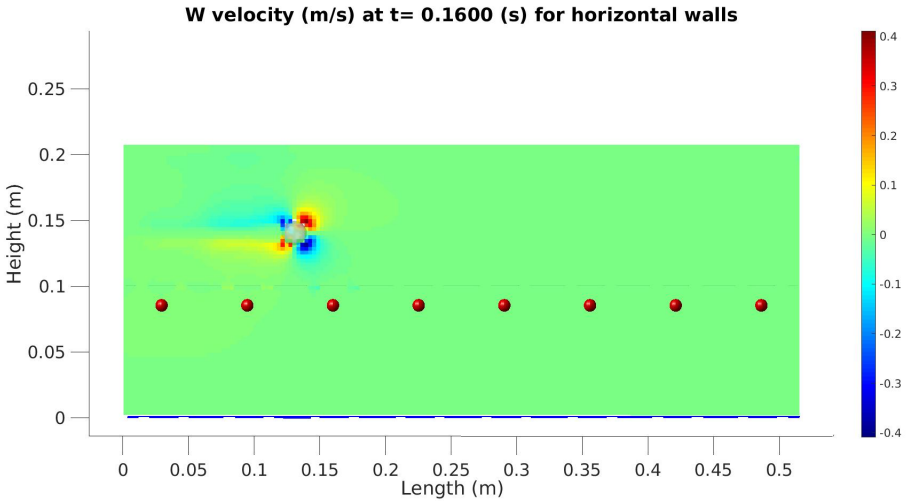

Figure 6.13: Front view. W velocity in m/s at $t = 0.1600$ s for the case with horizontal walls.

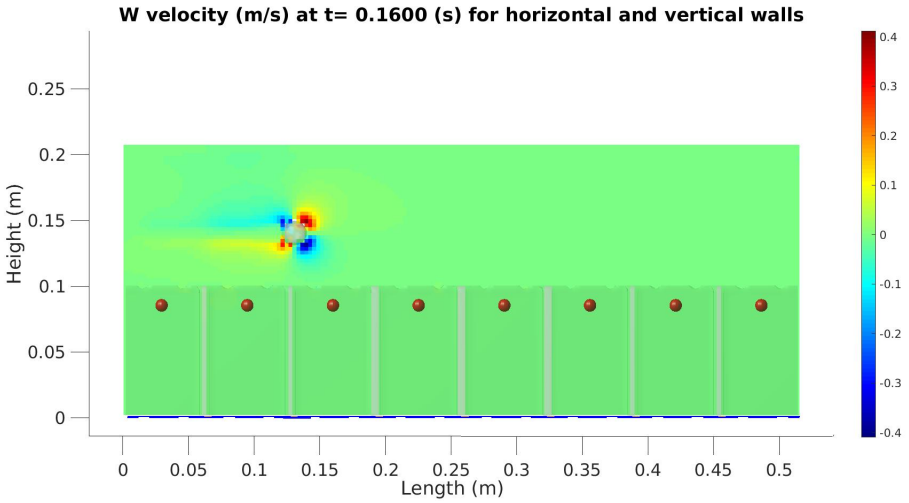

Figure 6.14: Front view. W velocity in m/s at $t = 0.1600$ s for the case with both horizontal and vertical walls.

The maximum of the graph of the horizontal walls case is obtained around $t = 0.25$ s. At this moment the ball has already passed the third sensor and is right above the fourth sensor, as is shown in Figures 6.15 and 6.16. For the case with only horizontal walls, we observe that in the gaps located above the third sensor a positive value of the W velocity has arisen, while for the other case there is no difference in velocity visible. This is the reason why the graph for the case with horizontal walls shows a maximum and the graph for the case with both horizontal and vertical walls does barely change.

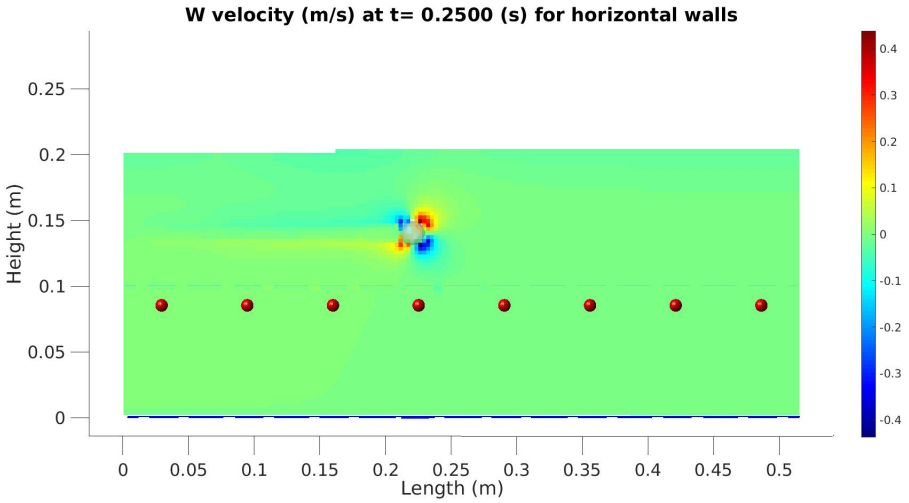

Figure 6.15: Front view. W velocity in m/s at $t = 0.2500$ s for the case with horizontal walls.

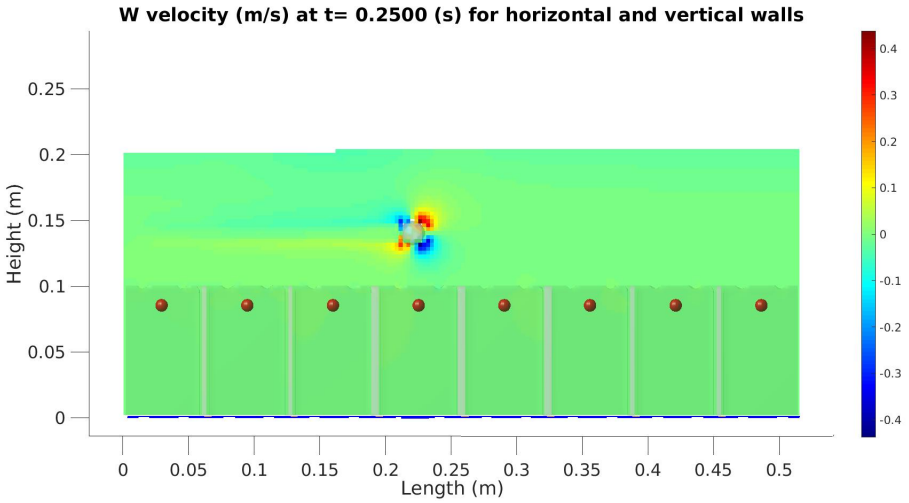

Figure 6.16: Front view. W velocity in m/s at $t = 0.2500$ s for the case with both horizontal and vertical walls.

While we saw for the velocities that the graphs of the case with both horizontal and vertical walls had smaller differences than the graphs of the case with only horizontal walls, for the pressure this is the other way around. This has also been observed the two-dimensional simulations Chapter 4. The sensors of the both horizontal and vertical walls case report more extreme values of the pressure than the sensors of the horizontal walls. However, the change in pressure is again smaller than in the two-dimensional space. Further, we see that the maxima and minima that in both cases, are obtained around the same time.

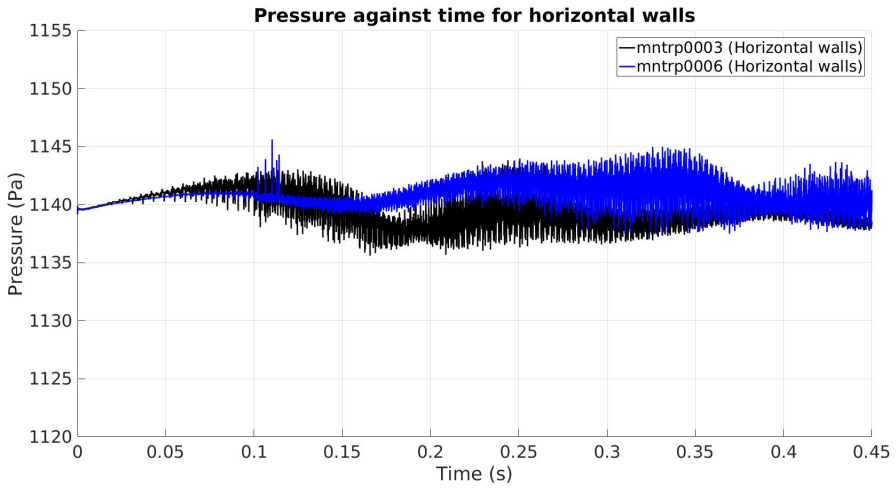

Figure 6.17: Pressure against time for the case with horizontal walls, reported by the third and sixth sensor.

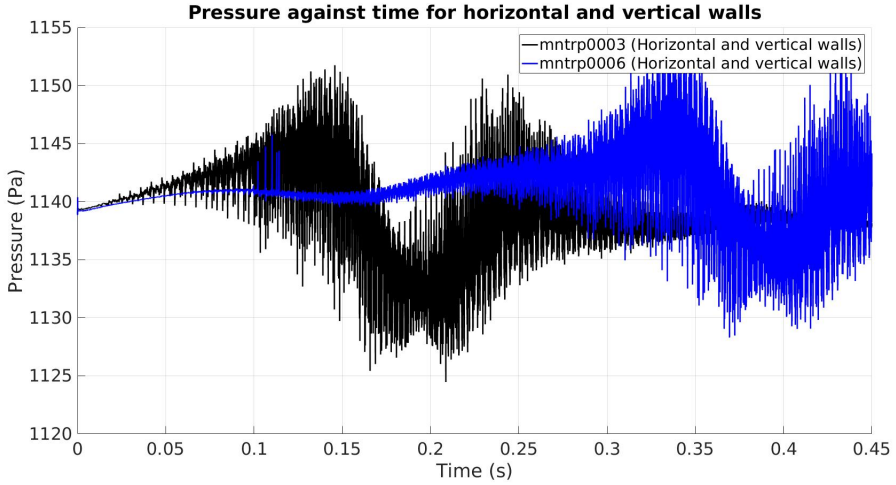

Figure 6.18: Pressure against time for the case with both horizontal and vertical walls, reported by the third and sixth sensor.

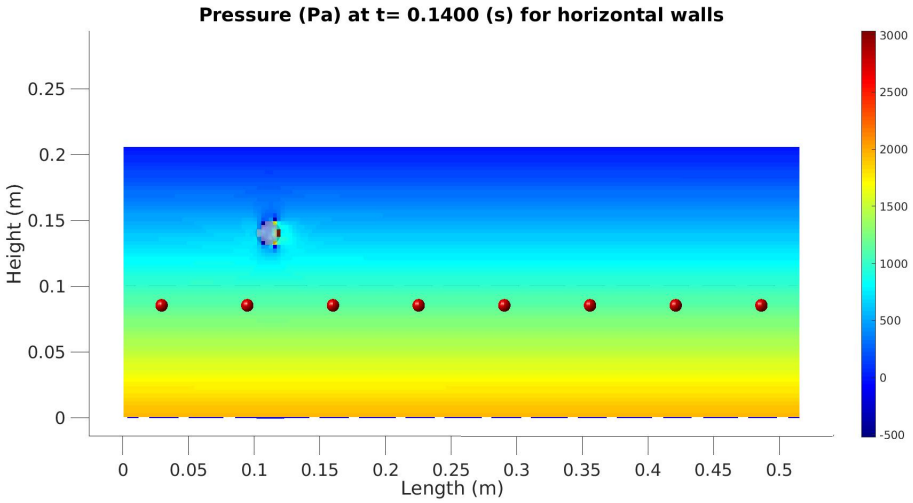

Figure 6.19: Front view. Pressure in Pa at $t = 0.1400$ s for the case with horizontal walls.

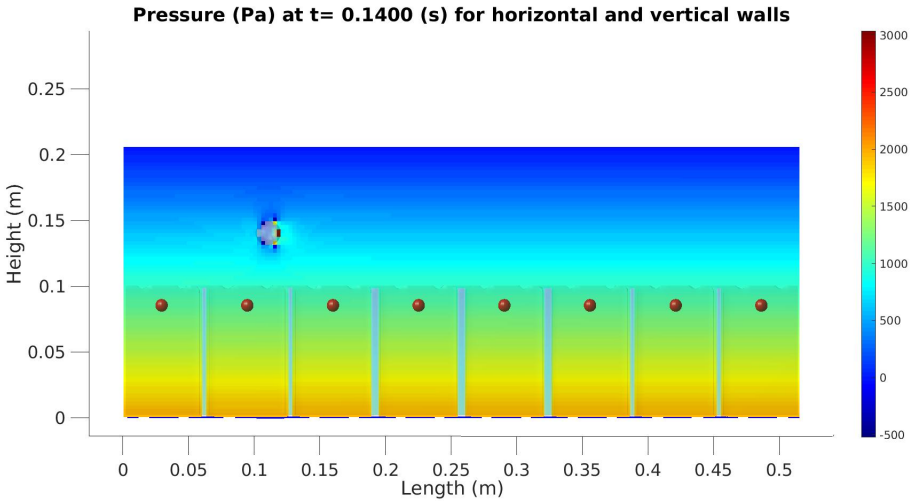

Figure 6.20: Front view. Pressure in Pa at $t = 0.1400$ s for the case with both horizontal and vertical walls.

In Figures 6.19 and 6.20, we see that, at the moment of the first maximum, the objects are approaching the third sensor. The minima of the two cases have place around $t = 0.20$ s, when both balls are passing the third sensor (Figures 6.21 and 6.24).

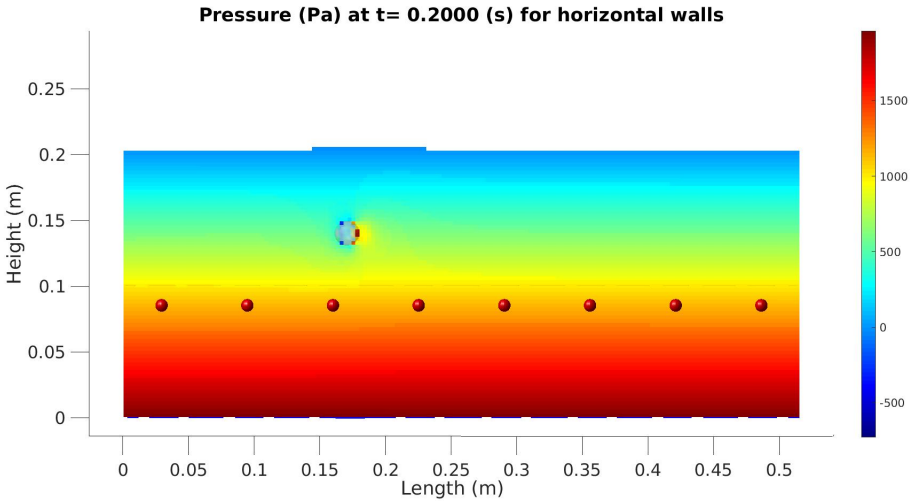

Figure 6.21: Front view. Pressure in Pa at 0.2000 s for the case with horizontal walls.

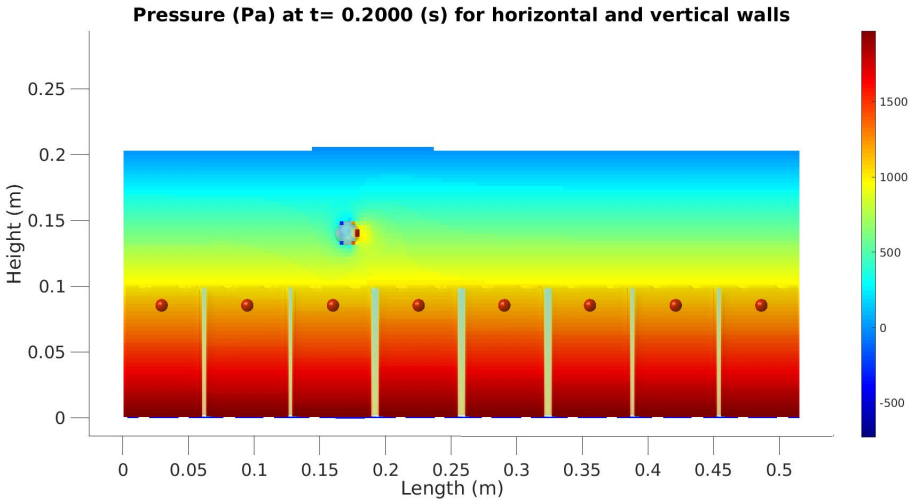

Figure 6.22: Front view. Pressure in Pa at 0.2000 s for the case with both horizontal and vertical walls.

At the moment the last extreme value is measured by the third sensor, the objects have passed the third sensor and are right above the fourth sensor, as shown in Figures 6.23 and 6.24. However, the differences in pressure are again not clearly visible in the Figures. This is because the differences are much smaller compared to the values in pressure obtained elsewhere in the tank.

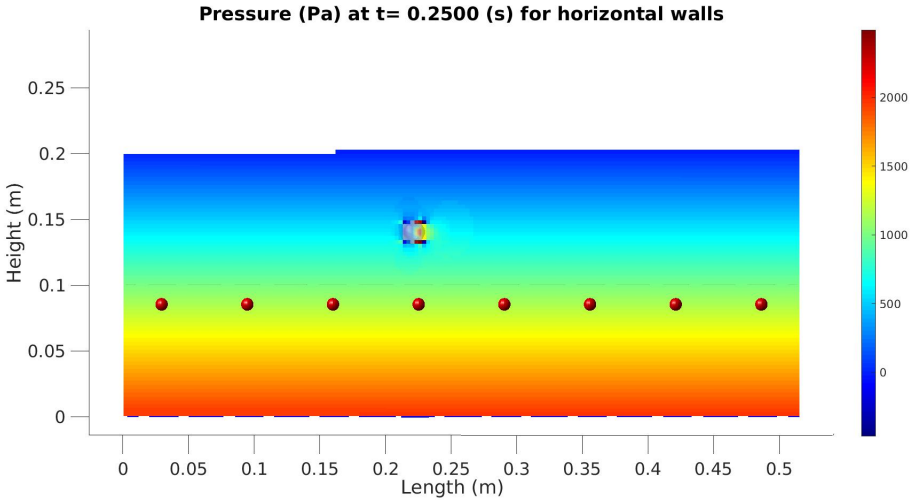

Figure 6.23: Front view. Pressure in Pa at $t = 0.2500$ s for the case with horizontal walls.

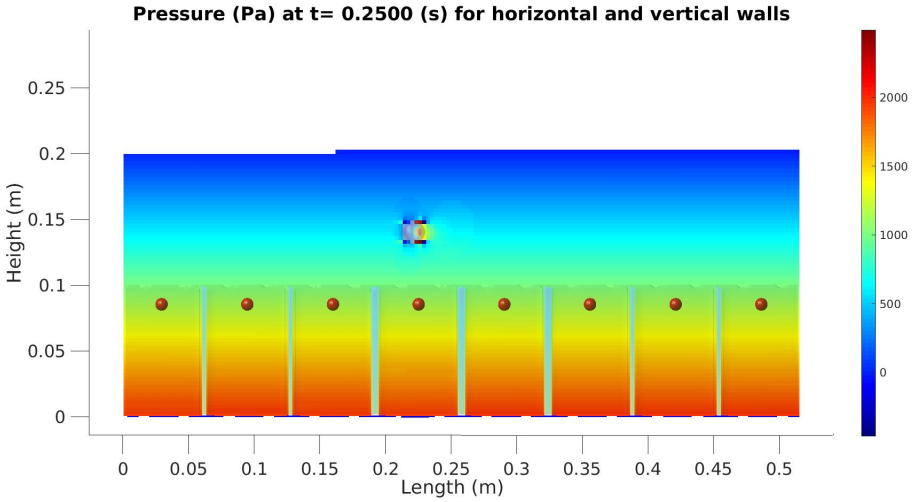

Figure 6.24: Front view. Pressure in Pa at $t = 0.2500$ s for the case with both horizontal and vertical walls.

Remarkable is that, in all Figures for the three-dimensional simulations thus far, barely any activity in the rest of water is seen, let alone a vortex street. From Chapter 2.2 we know that, when working with the coarser grid, 172x1x93, compared to the 515x1x280 grid, no vortex street can be obtained, because of the low accuracy of this grid. However, we see in the Figure of the 172x1x93 grid (Figure 2.18) of that section that some waves have originated at the water surface and that the tail of the activity behind the object shows a curve, while this is not present in the three-dimensional simulations. The fact that we barely see any changes in values throughout the tank, can partly be explained by the adding of the third dimension. Adding an extra dimension leads to more numerical diffusion of the water, which means that the water will be set in a lower motion. Hence, this added third dimension and the coarsened grid are probably the cause of the smaller differences in velocities and pressure compared to the two-dimensional cases.

6.2 The walls and sensors placed at the right side of the tank

Now that the centered case has been evaluated, we are going to take a look at the other case in which the walls and sensors are located at the right side of the tank. While doing this, we will also compare this situation to the centered situation. This will be done by using the set-ups of the previous section for the centered case and by using the set-ups depicted Figures 6.25 and 6.26 for the case with walls and sensors at the right side. Although almost everything has moved to the right, as can be seen in these figures, the ball does stay in the center. Further, in this case the local grid coarsening will be applied to only the left side of the walls, which is shown in Figure 6.27.

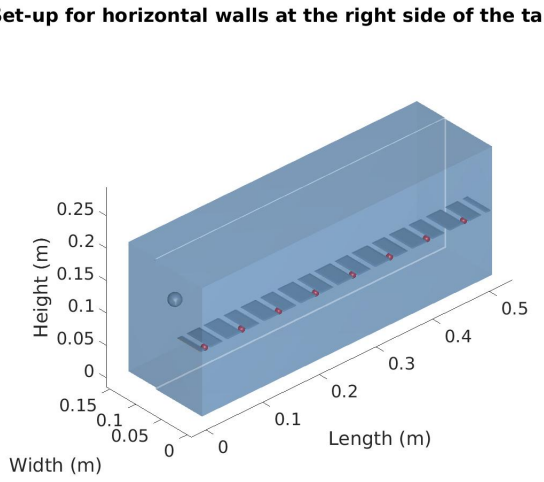

Figure 6.25: Set-up for the case in which the horizontal walls are placed at the right side of the tank in 3D.

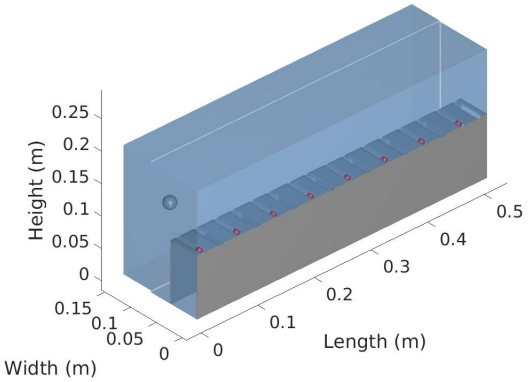

Figure 6.26: Set-up for the case in which both horizontal and vertical walls are placed at the right side of the tank in 3D.

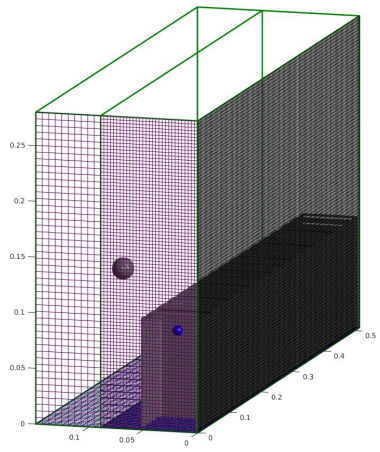

Figure 6.27: By means of local grid coarsening, less computational cells are placed at theleft side of the tank.

Results

Starting with evaluating the U velocity, we observe in Figure 6.28, that the pattern of the graphs of the case with walls and sensors placed at the right side, are quite similar to the graphs of the case in which they are centered. However, they do differ a bit in maximum and minimum values. To find out what exactly causes these differences, we will take a closer look at these extreme values at the third sensor, for the situation with only horizontal walls in both cases of wall positioning.

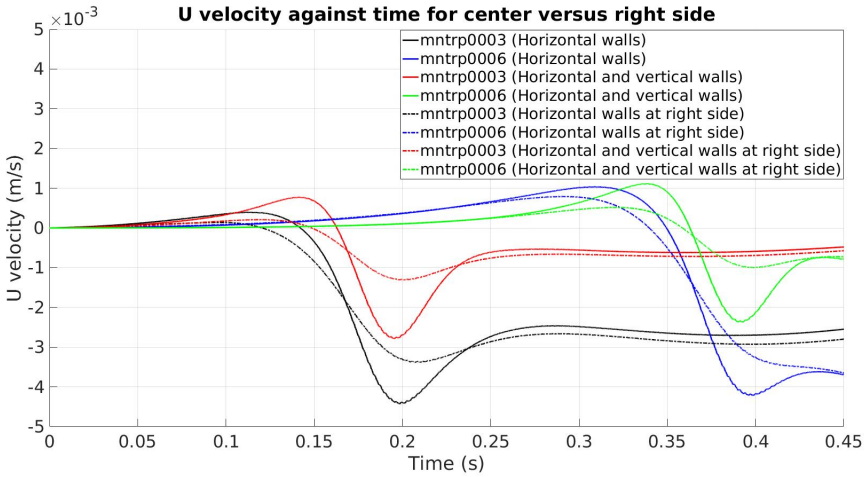

Figure 6.28: U velocity against time for the case with the horizontal walls in the center versus the case with both horizontal and vertical walls in the center versus the case with the horizontal walls at the right side versus the case with both the horizontal and vertical walls at the right side, reported by the third and sixth sensor.

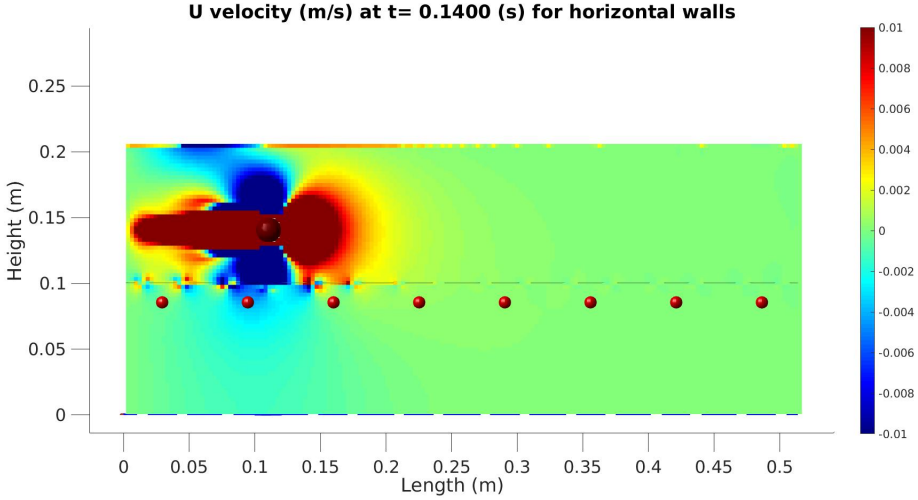

Figure 6.29: Front view. U velocity in m/s at $t = 0.1400$ s for the case with the horizontal walls in the center.

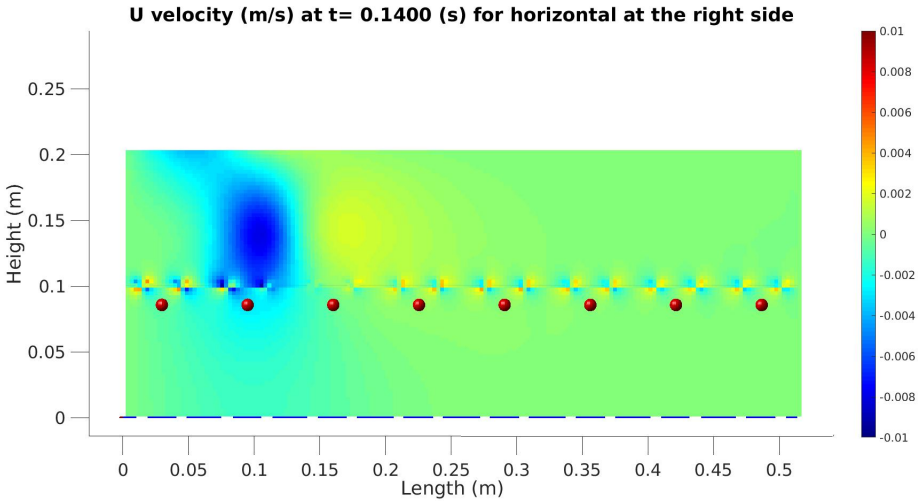

Figure 6.30: Front view. U velocity in m/s at $t = 0.1400$ s for the case with the horizontal walls at the right side.

The first extreme value is obtained around $t = 0.14$ s, the moment when the ball is approaching the third sensor. In Figure 6.29 we can see that a lot of activity is present around the ball. Figure 6.30 shows that the intensity of this activity is much less when the sensors are placed at the right side of the tank. Much less extreme values of the U velocity are registered at that side of the tank. Moreover, we observe that the area around the third sensor, in the case in which the walls and sensors are located at the right side, is a little bit bluer coloured than the area around the third sensor of the other case. This means that a lower value of the U velocity is reached, which is also displayed by the graphs in Figure 6.28.

Around $t = 0.20$ s the minimum values of the graphs of both cases are obtained. In Figure 6.31 we see that at this moment in time the object is passing the third sensor and by doing this, it causes a high negative U velocity of the water right beneath it. That is why the area directly around the third sensor is also set in a higher motion. Again, this effect is smaller in the case in which the water has to travel a little further to reach the walls and sensor. Less extreme values are obtained in the area around the sensor of this case, as shown in Figure 6.32. Too much numerical diffusion may enhance this effect in the simulations. Grid refinement studies may confirm this, but would take much too long computing time.

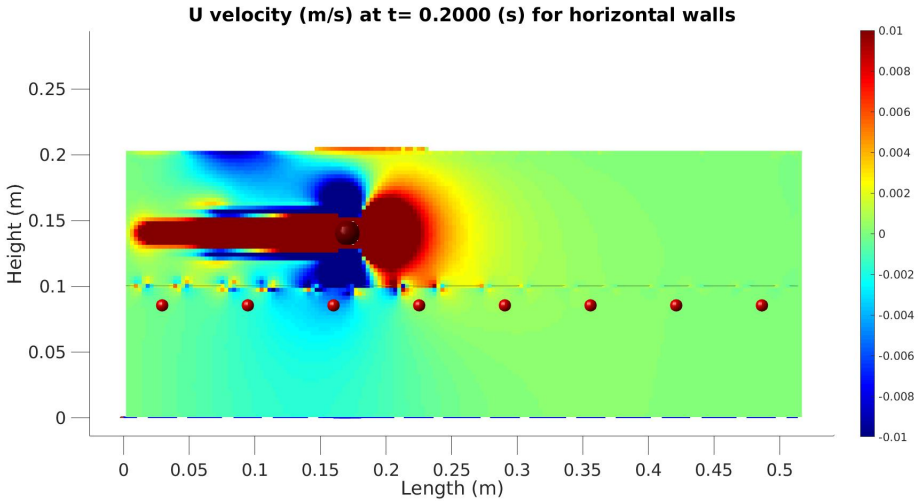

Figure 6.31: Front view. U velocity in m/s at $t = 0.2000$ s for the case with the horizontal walls in the center.

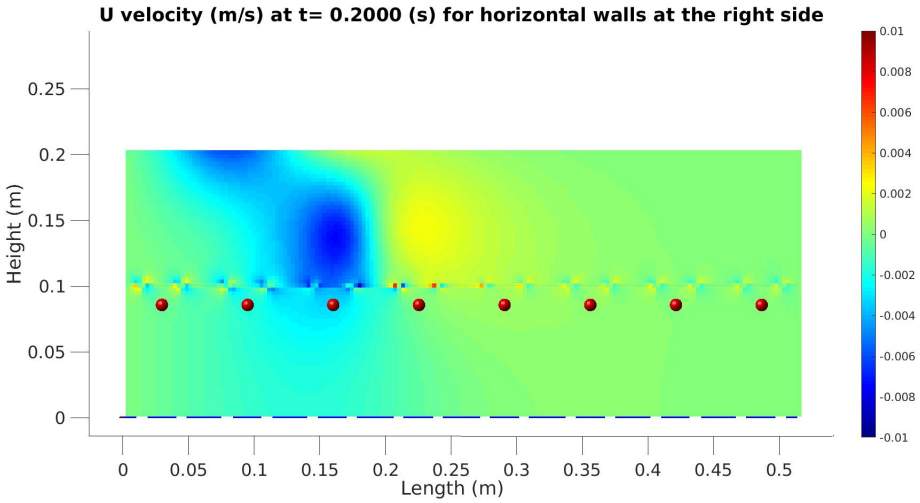

Figure 6.32: Front view. U velocity in m/s at $t = 0.2000$ s for the case with the horizontal walls at the right side.

Figure 6.33 shows the graphs of the V velocity at the third and sixth sensor for both cases, with walls and sensors placed in the center of the tank and the walls and sensors placed at the right side of the tank. We observe that, compared to the other case, the graphs for the case with everything centered show no changes in V velocity. From section 6.1, we know that for this case there actually are changes measured, but these changes are just too small for being noticed in this figure.

Further, we observe that, looking at the graphs for the cases with the walls and sensors located at the right, the graph for the case with horizontal walls and the graph for the case with both horizontal and vertical walls follow an almost similar path. The only difference is that the ones for the horizontal walls reach more extreme values.

When comparing the graphs of the third sensor to the graphs of the sixth sensor for both cases, we see that they follow a different path. Therefore, while evaluating in more detail what happens at the extreme values, this time we will also consider the situation at the sixth sensor.

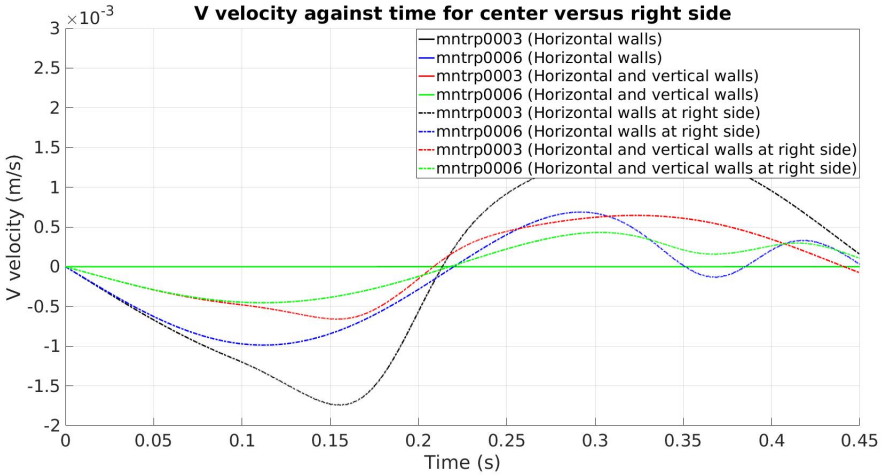

Figure 6.33: Front view. V velocity against time for the case with the horizontal walls in the center versus the case with both horizontal and vertical walls in the center versus the case with the horizontal walls at the right side versus the case with both the horizontal and vertical walls at the right side, reported by the third and sixth sensor.

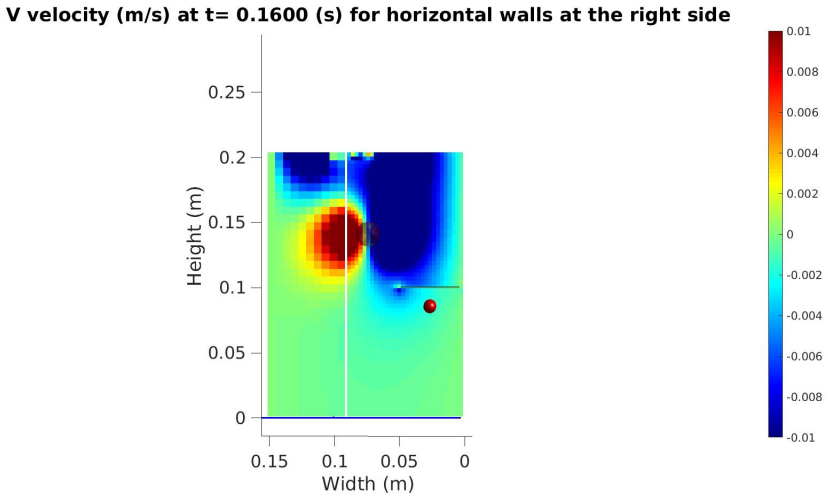

Figure 6.34: Side view. V velocity in m/s at $t = 0.1600$ s for the case with the horizontal walls at the right side.

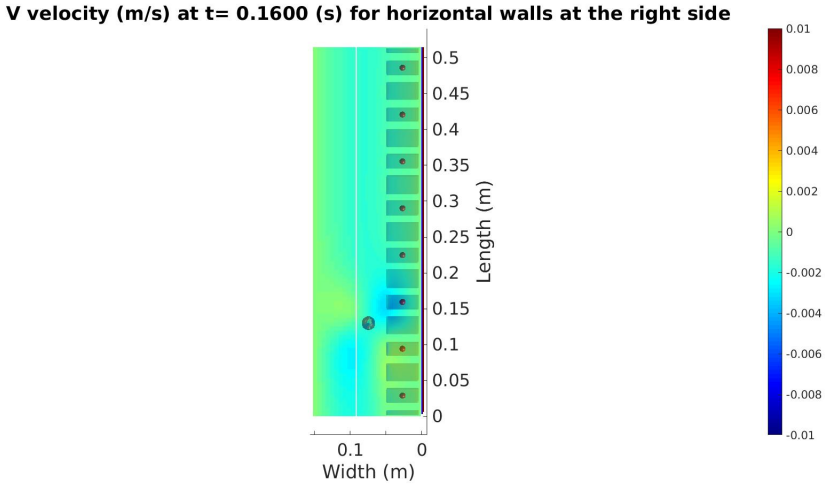

Figure 6.35: Top view. V velocity in m/s at $t = 0.1600$ s for the case with the horizontal walls at the right side.

Starting with the situation at the third sensor, Figure 6.33 tells us that the minimum, in the case with the walls and sensors placed at the right side of the tank, is reached around $t = 0.16$ s, when the ball is approaching the third sensor. We can see in Figure 6.34, that at that moment, at the left side of the ball positive values of the V velocity are obtained, while at the right side negative values are given, but in a much bigger range. Further, the water in the area around the sensor is also set in motion, causing this sensor to report negative values of the V velocity as well. Figure 6.35 shows that the water in the rest of the tank is also already set in motion, with a

small velocity going from the left to the right side of the tank.

In the centered case, the water that is set in motion is restricted to only the area directly around the moving object, as shown in Figure 6.37. The moving of the object does not have an effect at the water that is under the horizontal walls (Figure 6.36), hence the sensor does not report a change in V velocity. This is because the ball moves exactly over the center of the sensor, pushing the water from the middle to both sides with equal magnitude. Therefore, together with the presence of the horizontal wall, it is not possible to set the water around the sensor in motion. This is also true for the other sensors in the centered case. The ball moves in the same manner over all sensors, causing the same situation such that no change in V velocity can be reported by the sensors, which confirms what was seen in the graphs of Figure 6.33.

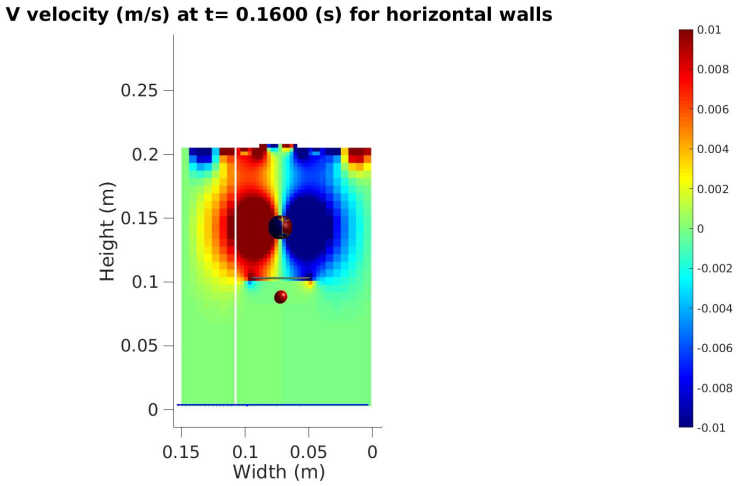

Figure 6.36: Side view. V velocity in m/s at $t = 0.1600$ s for the case with the horizontal walls in the center.

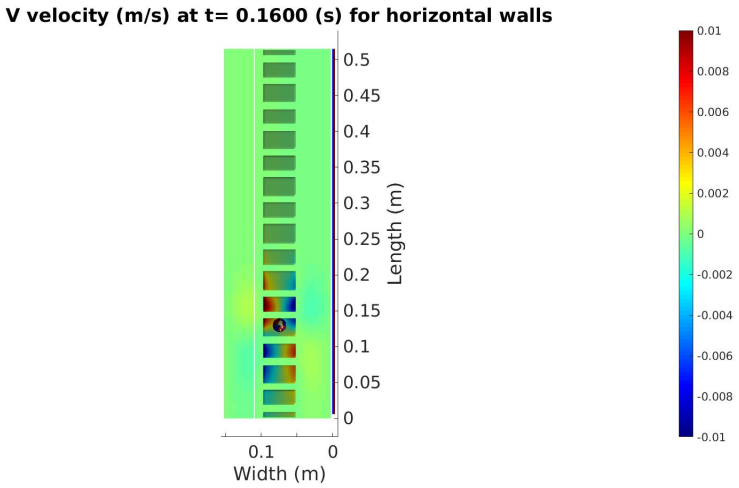

Figure 6.37: Top view. V velocity in m/s at $t = 0.1600$ s for the case with the horizontal walls in the center.

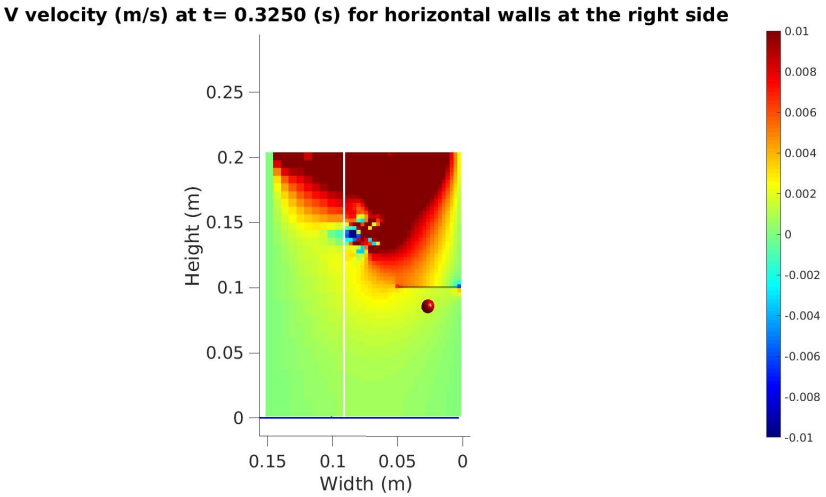

Figure 6.38: Side view. V velocity in m/s at $t = 0.3250$ s for the case with the horizontal walls at the right side.

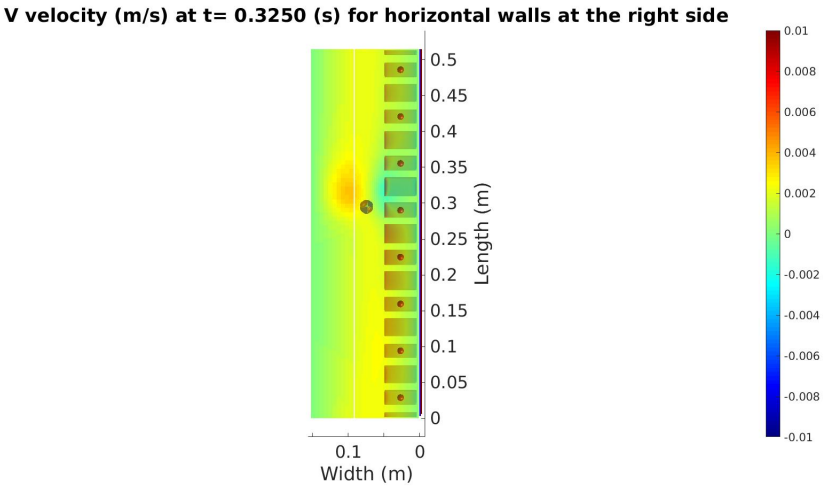

Figure 6.39: Top view. V velocity in m/s at $t = 0.3250$ s for the case with the horizontal walls at the right side.

Around $t = 0.325$ s a maximum is obtained for the case with horizontal walls placed at the right side. In Figure 6.38, we see that at this moment in time, the water has only a positive value of the V velocity, meaning that the water is going from the right to the left side of the tank. This is not only the case for the area in which the third sensor is located, but for the whole tank, as shown in Figure 6.39. It is remarkable that the water throughout the tank is now moving from the right to the left side, while in the previous case considered it went in the opposite direction. The water has probably clashed to the right walls of the tank, and after that it has returned causing a movement from the right to the left side.

Then, considering the graph for the horizontal walls case at the sixth sensor, in Figure 6.33 we observe that it reaches a minimum around $t = 0.11$ s. At this moment a great part of the water is moving from the left to the right (Figure 6.40). Therefore, a negative value of the V velocity is reported by the sixth sensor. This is, however, also true for more areas in the tank as shown in Figure 6.41. Positive values are only seen closely around the moving object that pushes the water to both sides.

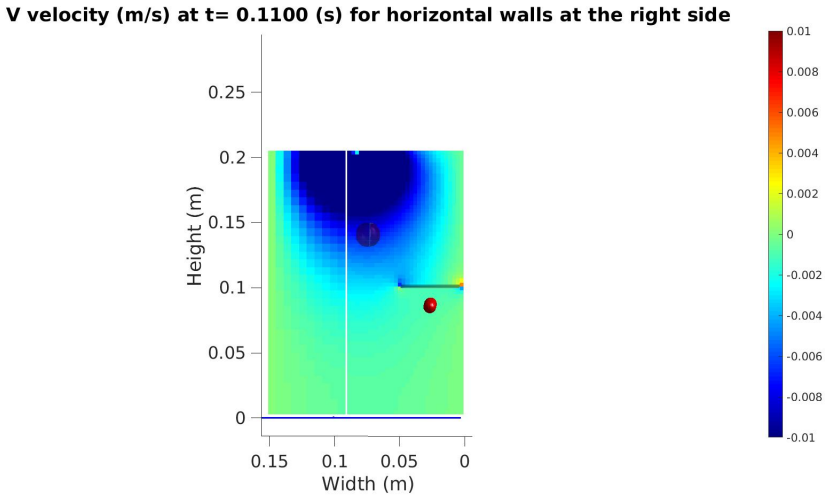

Figure 6.40: Side view. V velocity in m/s at $t = 0.1100$ s for the case with the horizontal walls at the right side.

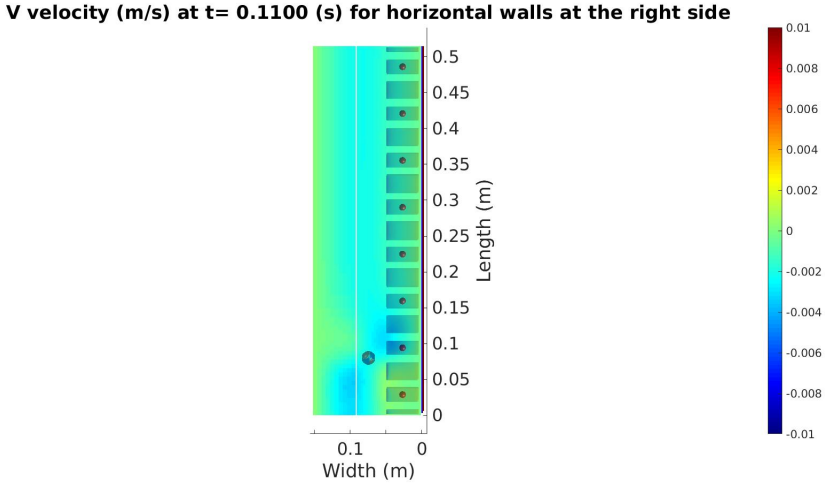

Figure 6.41: Top view. V velocity in m/s at $t = 0.1100$ s for the case with the horizontal walls at the right side.

After 0.29 seconds, the situation has changed. Figure 6.42 shows that the water is now moving from the right to the left. Again, this is not only for the area around the sixth sensor, but is seen in the rest of the tank as well (Figure 6.43). This is what we also observed when we evaluated the events at the third sensor. At a certain moment the direction of the water has switched, probably because the water has clashed against the wall of the tank and then returned.

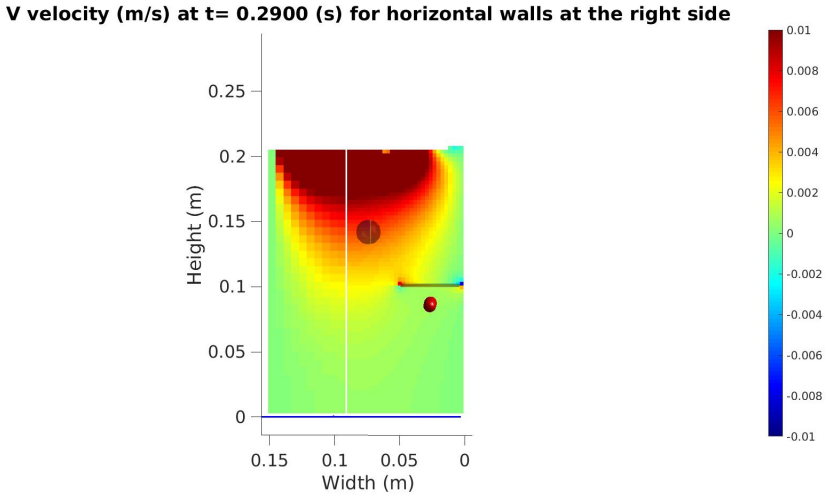

Figure 6.42: Side view. V velocity in m/s at $t = 0.2900$ s for the case with the horizontal walls at the right side.

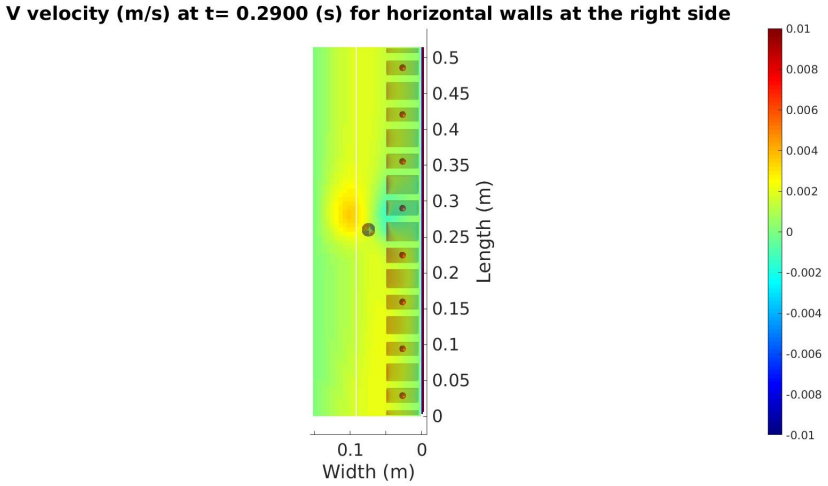

Figure 6.43: Top view. V velocity in m/s at $t = 0.2900$ s for the case with the horizontal walls at the right side.

The last extreme value that is reported by the sixth sensor takes place around $t = 0.37$ s. Figure 6.45 tells us that at this moment the water is mostly still moving from the right to the left side of the tank. However, this is not true for the area around the sixth sensor. This sixth sensor is being approached by the moving object, which pushes water to the left and right side (Figure 6.44). The pushing of the water to the right side causes a decrease in V velocity near the sixth sensor.

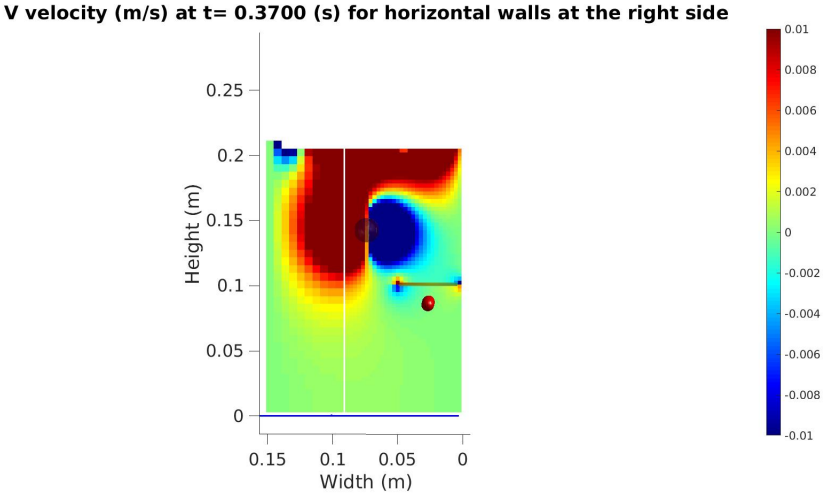

Figure 6.44: Side view. V velocity in m/s at $t = 0.3700$ s for the case with the horizontal walls at the right side.

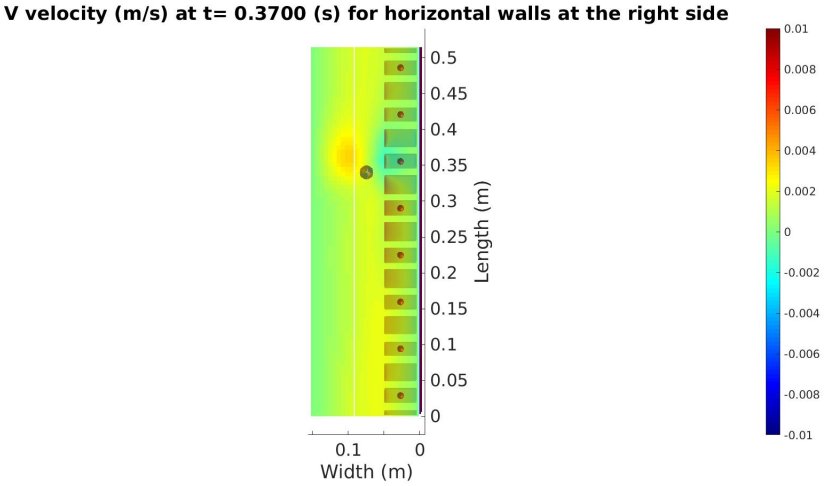

Figure 6.45: Top view. V velocity in m/s at $t = 0.3700$ s for the case with the horizontal walls at the right side.

Considering the W velocity in Figure 6.46, we find that the sensors in the cases in which also vertical walls are present barely reported any difference in W velocity. In section 6.1 we already that, for the centered case, the small change in W velocity was related to the approaching of a sensor by the ball. Although this also happens in the present case in which the walls and sensors are placed at the right side, the water first has to travel a while before it reaches the sensor. And along the way numerical diffusion may take place, which is the reason why there are no changes in W velocity measured by the sensor in this case.

For the cases with only horizontal walls, we observe that the graphs of the centered sensors follow a similar path, but at a different moment in time. The graphs for the right placed sensors, however, do not follow a similar path. Both graphs for the right side case do start in a same manner, but soon after the first hundreds of seconds they already start to differ in pattern. With the graph of the third sensor having four extreme values and the graph of the sixth sensor having only two extreme values. Also, these graphs can not be related to the graphs of the centered case. To find out what happens in the case in which the horizontal walls and sensors are placed at the right side, we are going to take a closer look at the extreme values measured by the third sensor.

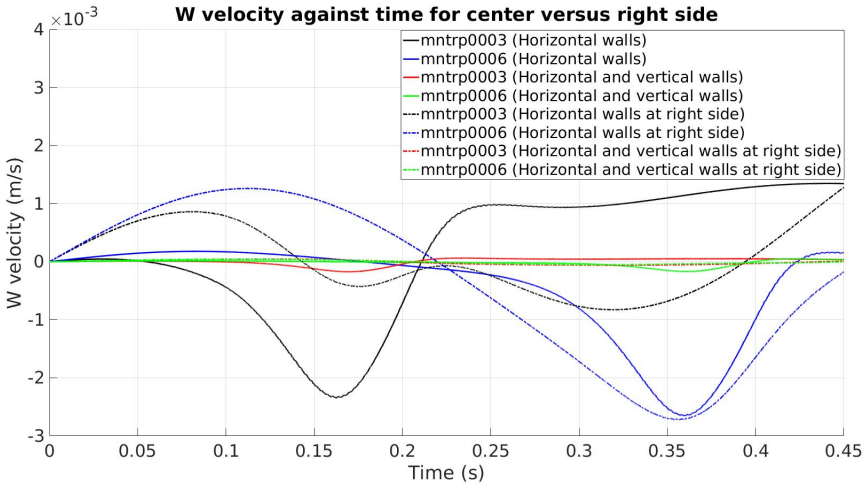

Figure 6.46: W velocity against time for the case with the horizontal walls in the center versus the case with both horizontal and vertical walls in the center versus the case with the horizontal walls at the right side versus the case with both the horizontal and vertical walls at the right side, reported by the third and sixth sensor.

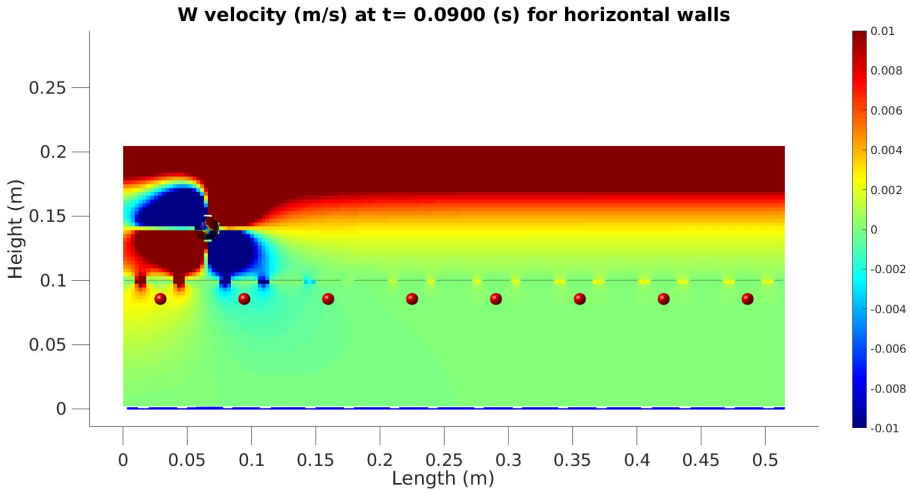

Figure 6.47: Front view. W velocity in m/s at $t = 0.0900$ s for the case with the horizontal walls in the center.

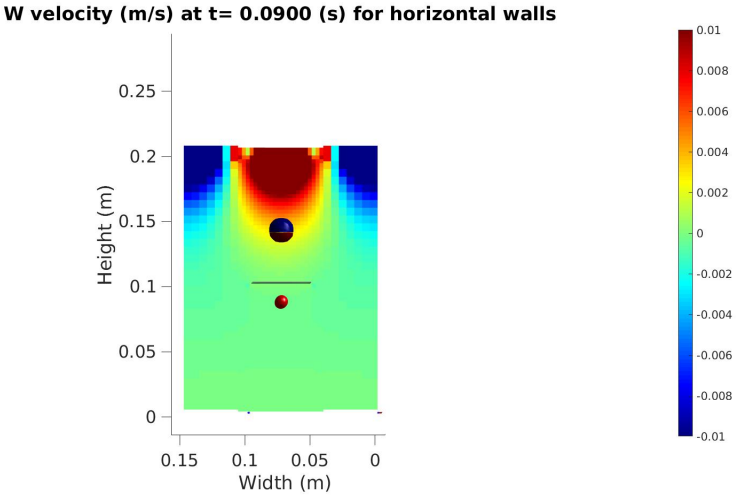

Figure 6.48: Side view. W velocity in m/s at $t = 0.0900$ s for the case with the horizontal walls in the center.

The first extreme value is a maximum obtained around $t = 0.09$ s. In Figure 6.47, we see that at that moment the ball is approaching the second sensor, mainly causing a positive value of the W velocity in the area around the first sensor and a negative value of the W velocity near the second sensor in the centered case. However, in one of the gaps above the third sensor there is also some change in W velocity visible. This probably has an effect at the area beneath and is the reason why the graph of the third sensor shows an increase around $t = 0.09$ s. In the side view of the centered situation, shown in Figure 6.48, we observe that positive values of the W velocity are obtained

right above the object, and in the upper left and upper right corner negative values are seen.

This is different in the sight view of the right side case, as shown in Figure 6.49. When the ball is moving through the water, it pushes the water to all sides, but while pushing it to the bottom right side the water clashes via the horizontal walls against the wall at the right side, such that it is being pushed upwards causing for a positive value at the right side of the tank. Then at the left side of the tank the water is moved downwards. Figure 6.50 shows that positive values of the W velocity are obtained for the entire right side of the tank, but these values are more extreme for the sensors already passed and less extreme for the sensor to be approached.

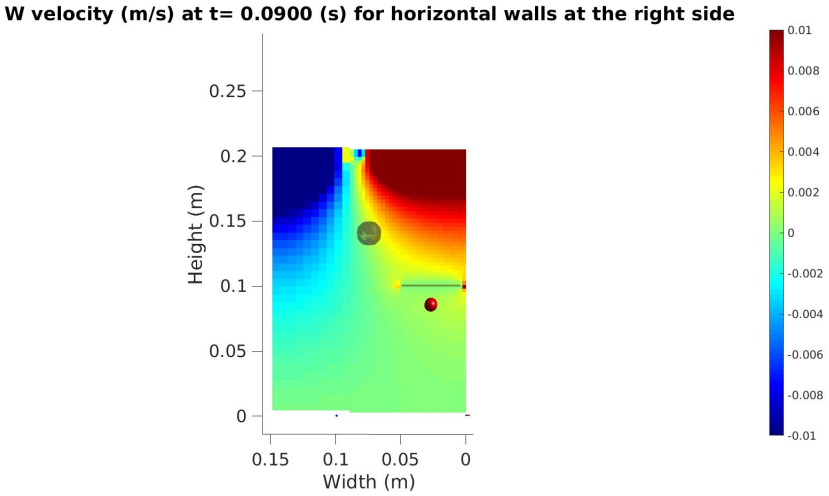

Figure 6.49: Side view. W velocity in m/s at $t = 0.0900$ s for the case with the horizontal walls at the right side.

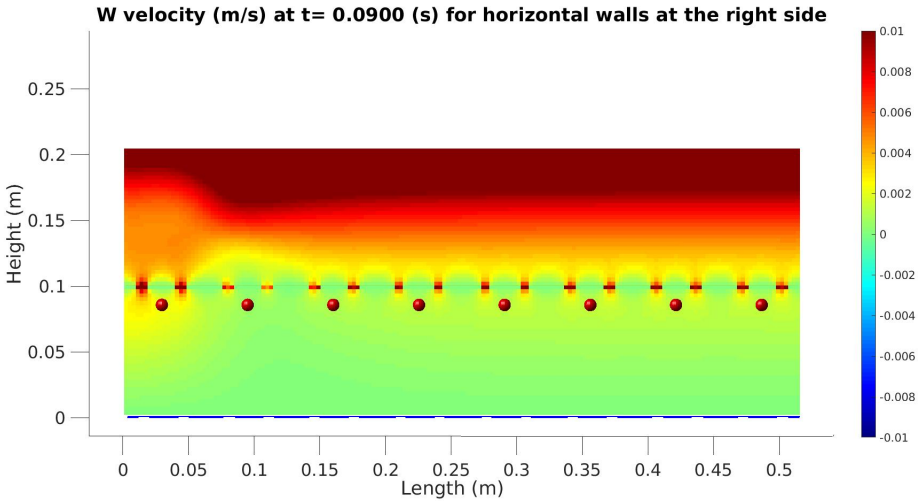

Figure 6.50: Front view. W velocity in m/s at $t = 0.0900$ s for the case with the horizontal walls at the right side.

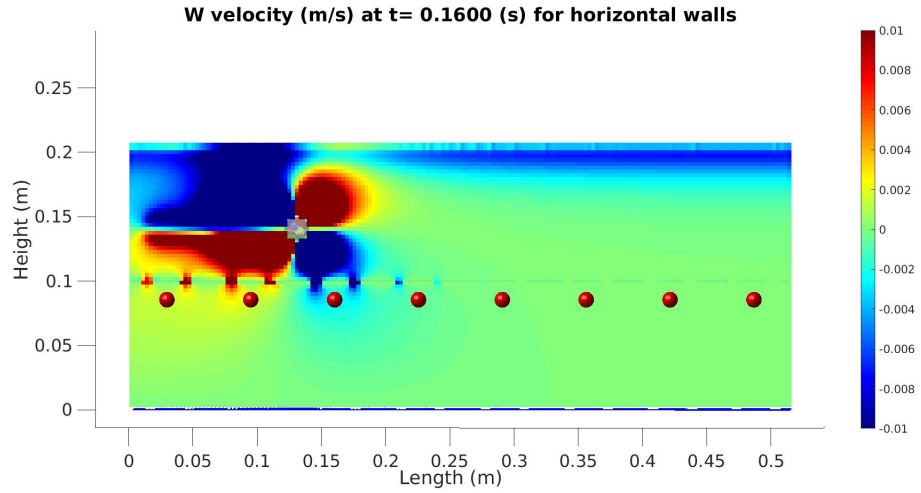

Figure 6.51: W velocity in m/s at 0.1600 s for the case with the horizontal walls in the center.

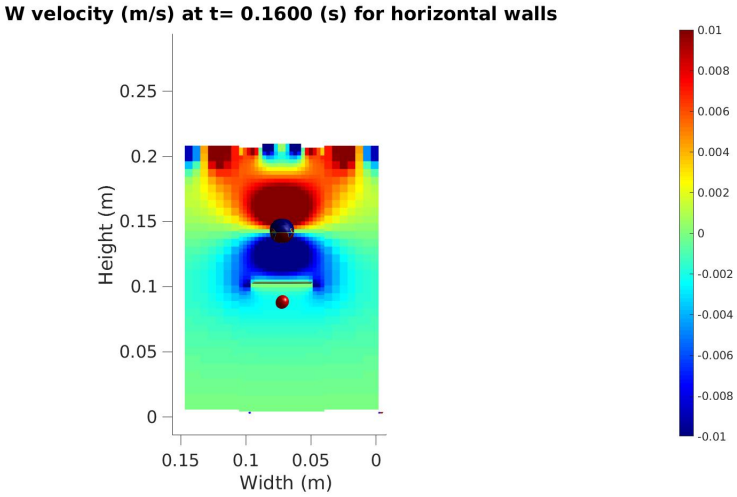

Figure 6.52: W velocity in m/s at 0.1600 s for the case with the horizontal walls in the center.

The maximum around $t = 0.16$ s is the second extreme value reported by the third sensors. In Figure 6.51 of the centered case, we can see that the object is approaching the third sensor and has already passed the first and second sensor. The water in the area of the first two sensors is being pulled upwards by the flow of the water that is caused by the movement of the ball. In front of the ball it is pushed downwards, causing negative values of the W velocity in the neighbourhood of the third sensor. This can also be seen in Figure 6.52, the side view of the tank at the third sensor. Above the ball the water is pushed upwards while beneath the ball the water is pushed downwards, also causing for movement of the water under the horizontal wall.

This is also seen in the side view of the case in which the walls and sensors are placed at the right side of the tank (Figure 6.53). In this case, however, the water flow that is pushed downwards is bended to the left by the presence of the horizontal wall. The water above the horizontal wall, is then pulled upwards by the flow. Hence, the area under the horizontal wall is barely set in motion, which can also be seen in Figure 6.54. While in the areas of all other sensors still a slight positive W value is seen, the water around the third sensor seems not to be put in motion.

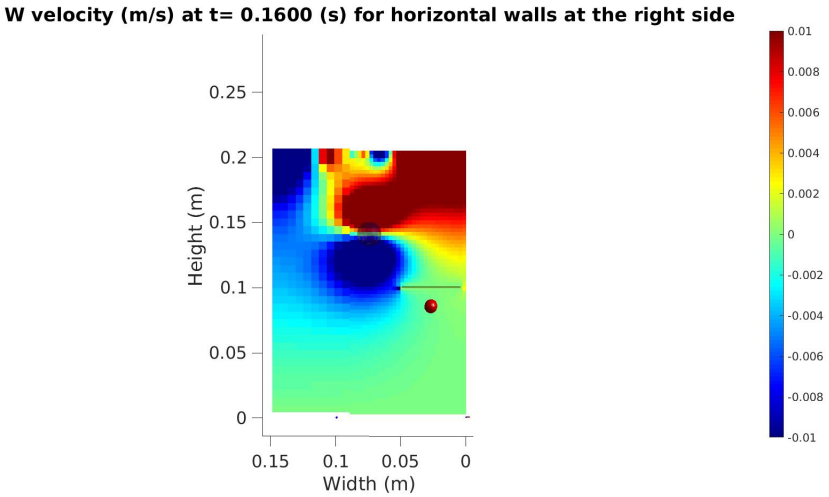

Figure 6.53: Side view. W velocity in m/s at $t = 0.1600$ s for the case with the horizontal walls at the right side.

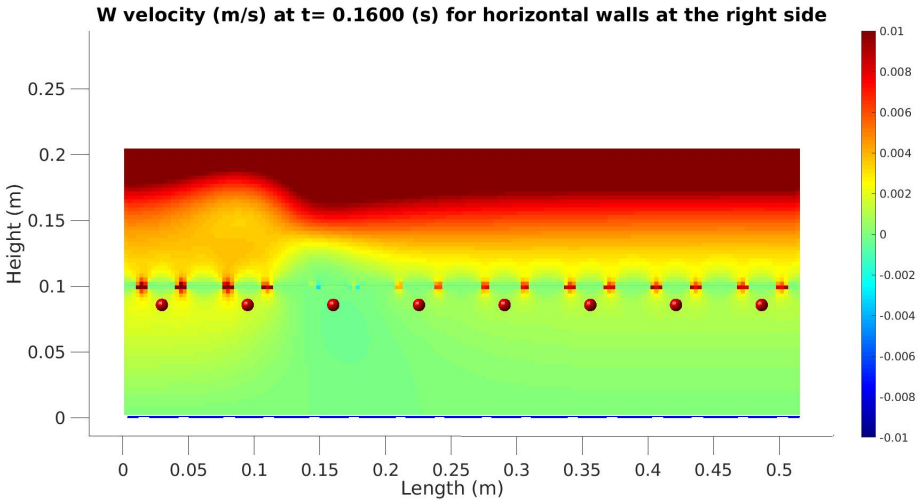

Figure 6.54: Front view. W velocity in m/s at $t = 0.1600$ s for the case with the horizontal walls at the right side.

Figure 6.55 shows what happens at $t = 0.2250$ s in the case in which the walls and sensors are centered. At this moment, the ball has also passed the third sensor. By moving the object through the water, in the upper half part of the area behind the object the water is pulled downwards, while in the lower half part of the area behind the object the water is pulled upwards. This causes a positive value of the W velocity in the area around the third sensor as well, as can also be seen in Figure 6.56.

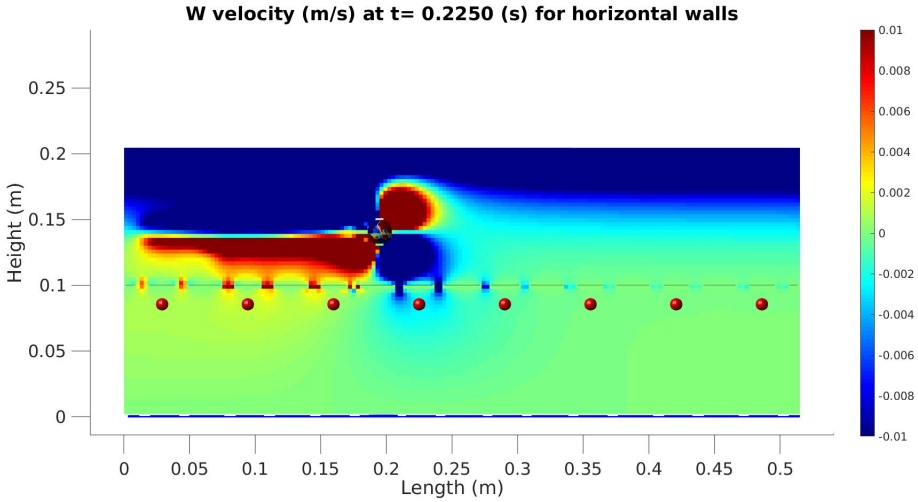

Figure 6.55: Front view. W velocity in m/s at $t = 0.2250$ s for the case with the horizontal walls in the center.

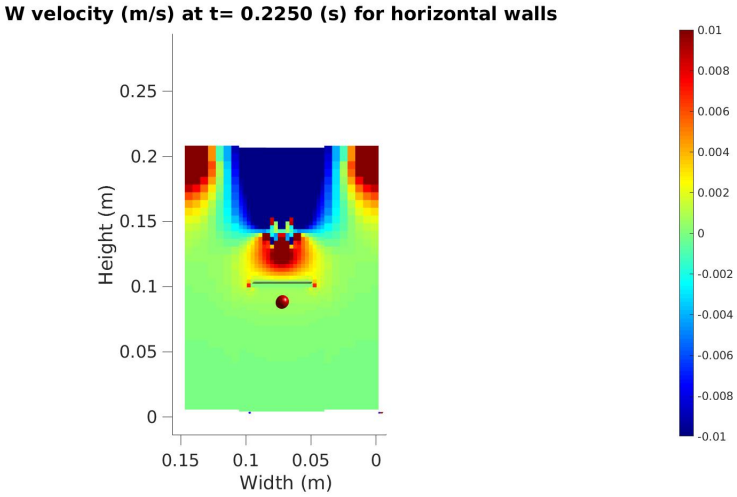

Figure 6.56: Side view. W velocity in m/s at $t = 0.2250$ s for the case with the horizontal walls in the center.

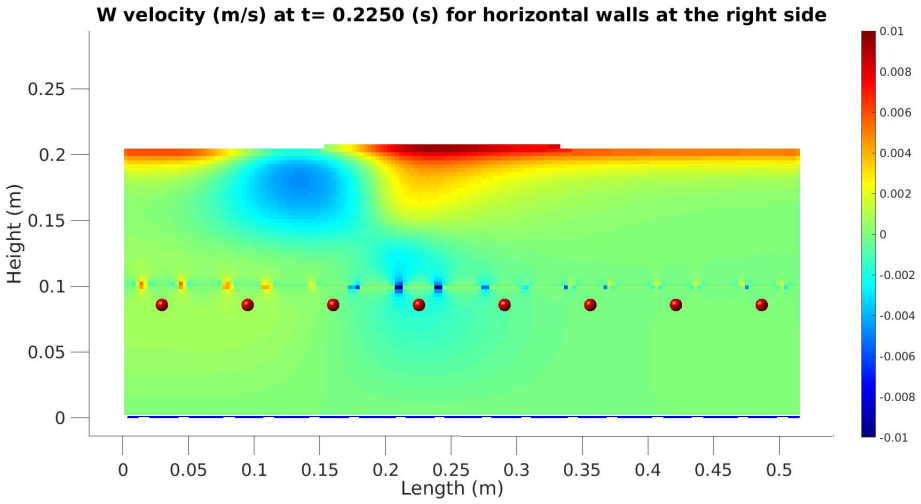

Figure 6.57: Front view. W velocity in m/s at $t = 0.2250$ s for the case with the horizontal walls at the right side.

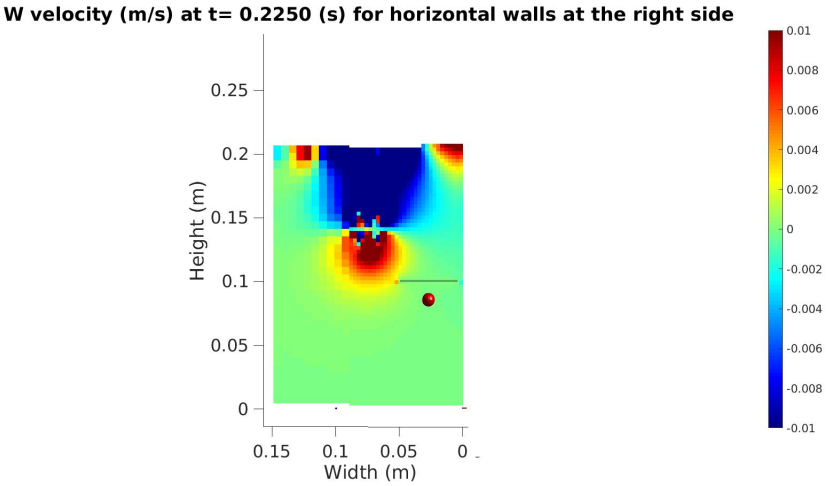

Figure 6.58: Side view. W velocity in m/s at $t = 0.2250$ s for the case with the horizontal walls at the right side.

The side view of the right side case at $t = 0.2250$ (Figure 6.58) is almost similar to the other side view. Only the values of the water velocities in both upper corners seem to differ a bit. This similarity is unexpected when looking at the previous evaluated side views of the right side case. In Figures 6.49 and 6.53, we saw that in the right corner a positive W value was obtained and in the left corner a negative W value was obtained. Apparently we have reached a moment in time where the water flow, possibly caused by the horizontal walls and the position of them, is making the W values switch. This can also be seen in Figure 6.57, where the areas around the sensors

have a smaller W value than before.

Evaluating the last extreme value of the graph of the right side case in Figure 6.46 around $t = 0.325$ s, we find in Figure 6.59 that at this moment the ball is passing the fifth sensor. The third sensor has been passed for a while now, but the water in the area around it is still being pulled upwards by the flow of the water caused by the movement of the ball. However, in Figure 6.60 we can see that compared to the situation at $t = 0.2250$ s, the effect has decreased. Lower values of the W velocity are obtained in both the area above the ball and below the ball.

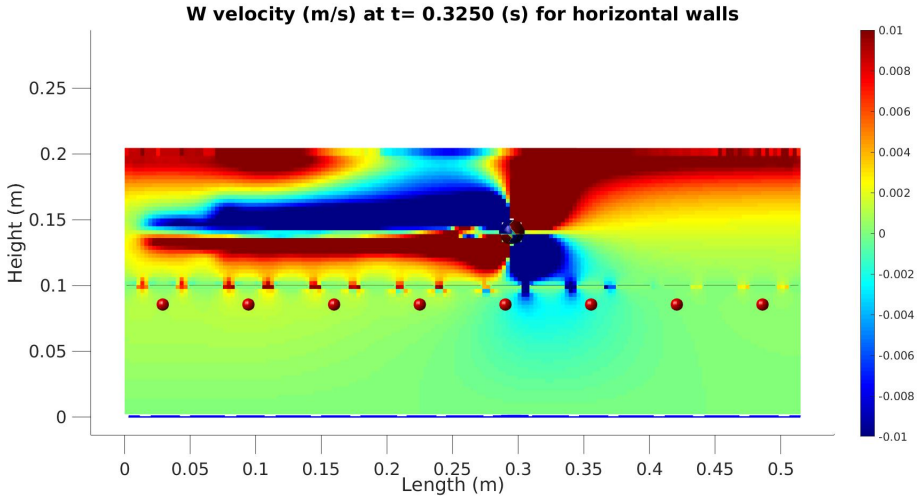

Figure 6.59: Front view. W velocity in m/s at $t = 0.3250$ s for the case with the horizontal walls in the center.

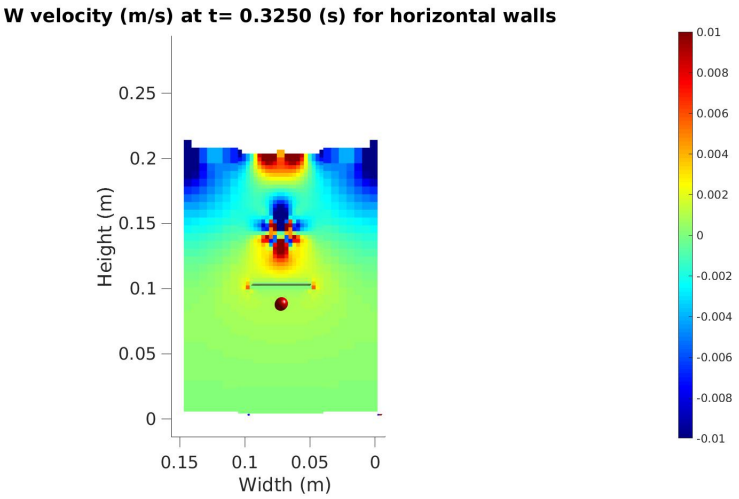

Figure 6.60: Side View. W velocity in m/s at $t = 0.3250$ s for the case with the horizontal walls in the center.

When looking at the side view of the case in which the walls and sensors are located at the right side of the tank, we observe that, compared to the situations of the first moments in time, the W values have switched (Figure 6.61). While in the first two situations positive values of the W velocities were obtained at the right side of the tank, due to the changed flow of the water, now negative values are obtained at the right side of the tank. This is also seen in Figure 6.62, where in the areas around all sensors negative values of the W velocity are observed.

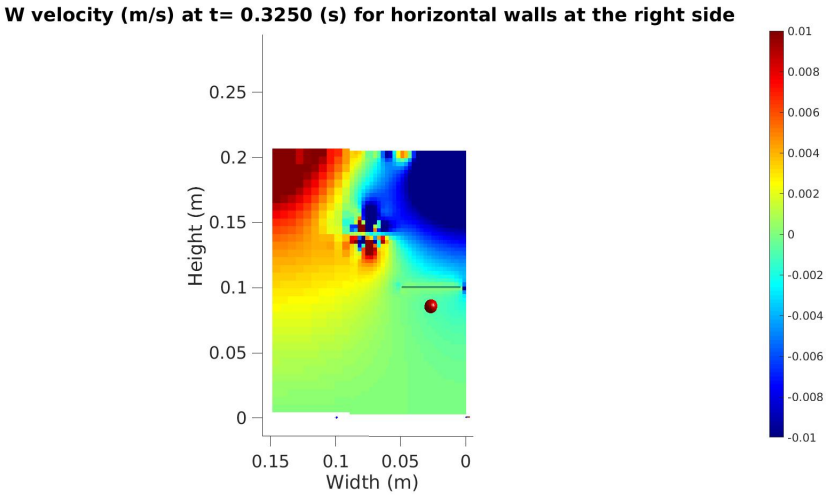

Figure 6.61: Front view. W velocity m/s at $t = 0.3250$ s for the case with the horizontal walls at the right side.

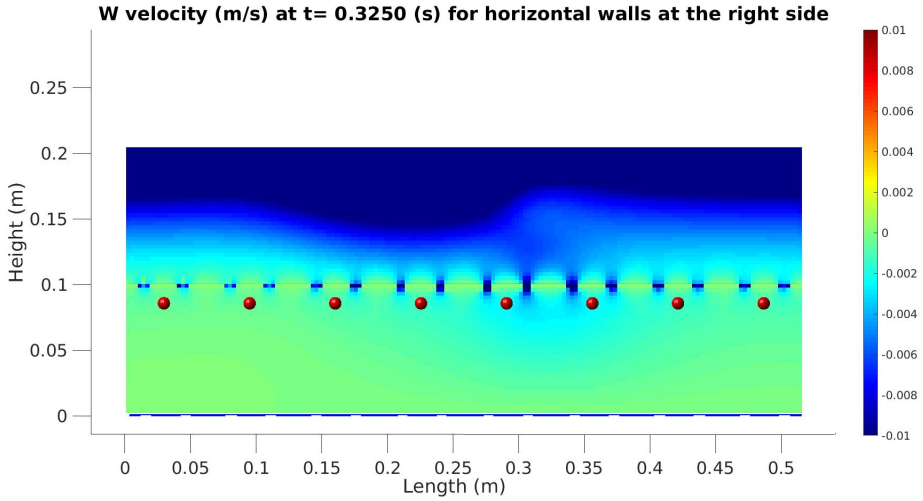

Figure 6.62: Side view. W velocity in m/s at $t = 0.3250$ s for the case with the horizontal walls at the right side.

In Figures 6.63 and 6.64, we find the graphs for the pressure in different cases. All graphs at a same sensor seem to follow a similar path, wit their extreme values around the same moment in time. However, the graphs for the case with the walls and sensors placed at the right side of the tank lie under the graphs of the centered case, indicating that there are lower values of the pressure at the right side of the tank. Further, we again observe that the graphs for the case with both horizontal and vertical walls show extremer values of the pressure than the graphs of the only horizontal walls case. There is also a difference in obtained values, when comparing the graphs of the right side case to the centered case. The sensors of the first mentioned case report smaller differences in pressure than the sensors in the other case.

As also done for the velocities, we will evaluate the pressure in more detail by looking at what happens at the maxima and minima of the graphs for both the centered and the right side case, but only considering the situation with horizontal walls.

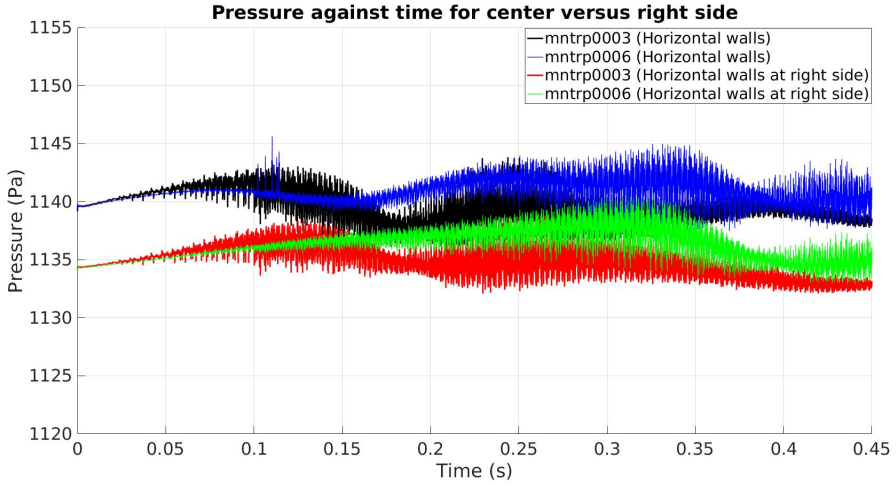

Figure 6.63: Pressure against time for the case with the horizontal walls in the center versus the case with the horizontal walls at the right side, reported by the third and sixth sensor.

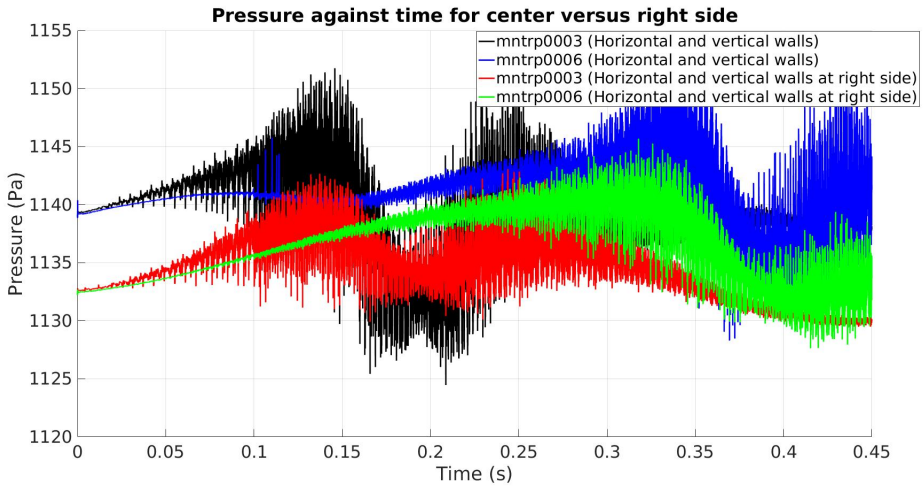

Figure 6.64: Pressure against time for the case with both horizontal and vertical walls in the center versus the case with both the horizontal and vertical walls at the right side, reported by the third and sixth sensor.

The first maximum that is reported by the third sensors of the cases with only horizontal walls takes place around $t = 0.13$ s, the moment when the ball is approaching the third sensor. Figure 6.65 shows that in the centered case the pressure in the area of the sensor that is being passed decreases, while the pressure in the area of the third sensor that is being approached increases. This is also true for the case in which the walls and sensors are at the right side of the tank. However, the values of the pressure in this situation are lower and the differences are smaller. Possibly caused by diffusion that occurred along the way and the different value of pressure that is obtained at the right side of the tank.

Further, we observe that the values between 1130 and 1145 Pa are only obtained in a small strip that contains all sensors. Everything above this strip has a value below 1130 Pa and everything below this strip has a value above 1145 Pa. This is probably because of the hydrostatic pressure, which means that in the layers above and below the sensor array respectively lower and higher values of the pressure are obtained.

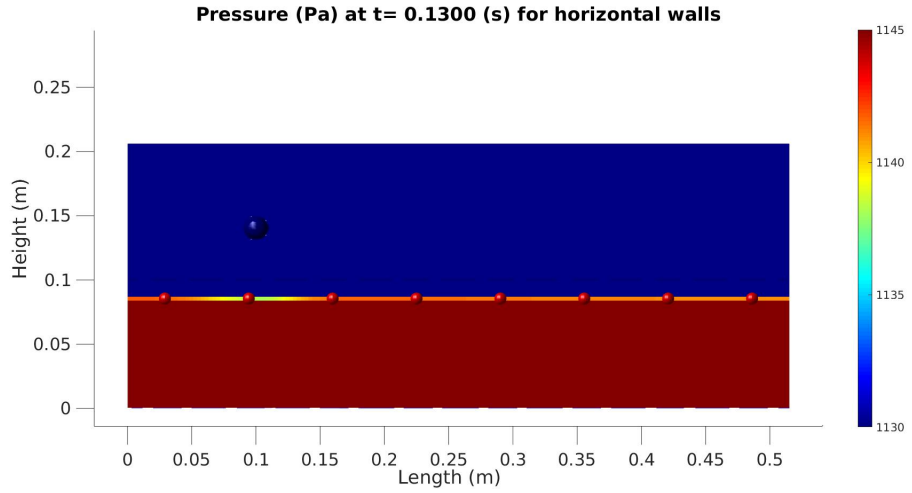

Figure 6.65: Front view. Pressure in Pa at $t = 0.1300$ s for the case with the horizontal walls in the center.

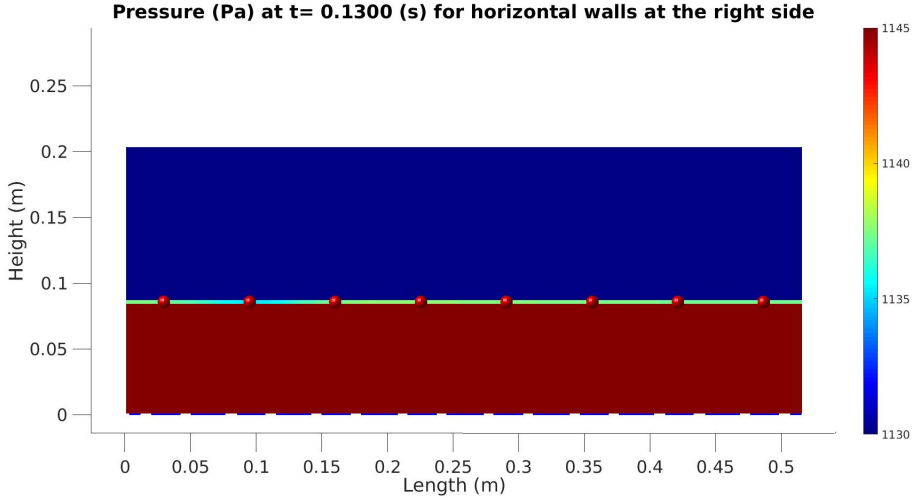

Figure 6.66: Front view. Pressure in Pa at $t = 0.1300$ s for the case with the horizontal walls at the right side.

At $t = 0.1900$ s in both cases the ball is passing the third sensor, which means that the pressure in the area around this sensor decreases and the pressure around the fourth sensor is increasing, as is also seen in Figures 6.67 and 6.68. Again, the values of the pressure measured by the sensor at the right side are lower and the differences are smaller than the ones in the centered case.

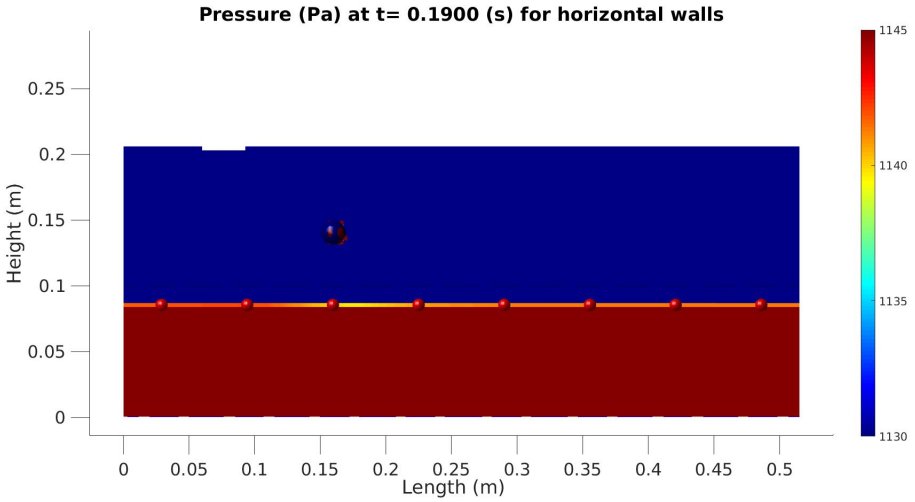

Figure 6.67: Front view. Pressure in Pa at 0.1900 s for the case with the horizontal walls in the center.

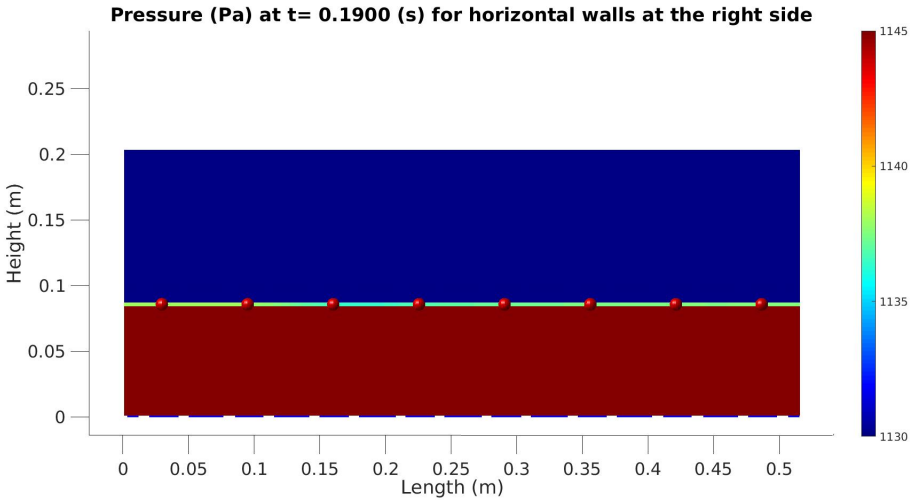

Figure 6.68: Front view. Pressure in Pa at 0.1900 s for the case with the horizontal walls at the right side.

To Summarise, comparing the centered case to the case in which the walls and sensors are placed at the right side of the tank, tells us that for the U velocity the cases are quite similar. With the only difference that the maximum and minimum of the right side case are less extreme than the ones in the centered case.

Evaluating the V velocity tells us that for the centered case the V velocity can hardly be measured, because of the direction in which the water is pushed and the presence of the horizontal walls. In the case in which the walls and sensors are placed at the right side, however, both negative and positive values of the V velocity are measured. In the first part of the experiment the water has a negative V value, while in the last part the water has a positive value. This is probably because at a certain moment the water hits the wall of the tank and returns. When the ball approaches a sensor, this sensor will report a decrease in V velocity. When it passes a sensor an increase in V velocity is seen.

For the W velocity, we see in the centered case a clear pattern. When a sensor is approached, the W velocity in the area around this sensor is decreasing. When a sensor has been passed, the water around this sensor is pulled upwards by the flow that is caused by the movement of the ball. For the case in which the walls and sensors are located at the right side of the tank, it is more complicated. During the first hundreds of seconds positive values of the W velocity are obtained at the right side of the tank, caused by the water that is pushed upwards via the horizontal walls and the wall of the tank. The horizontal wall at the right side is probably also the cause of the change in the flow direction of the water, which causes negative W values halfway the experiment.

Then lastly, for the pressure we observed, that if the ball approaches a sensor this sensor will measure an increase in pressure. If the ball is passing a sensor this sensor will report a decrease in pressure. This effect is smaller and the obtained values of the pressure are lower at the right side of the tank possibly due to the diffusion that occurs along the way.

Chapter 7

Conclusions

In this study, the model of the lateral line canal in fish has been simulated with the program ComFLOW, to find out what the most suitable settings for a modelled canal should be. This is done by first finding the most suitable grid, which is a grid that has a reasonable computing time, but yet obtains sufficiently accurate measurements of the velocities and pressure as well. Several grids sizes have been considered, simulating a two-dimensional simplified set-up in which a cube is moving above a sensor in a tank partially filled with water. Unfortunately, the grids with the dimensions of 773x1x420, 1030x1x560 and 1030x1x560 appeared too complex. The computations of the first two grids needed several days to complete, while the most fine grid did not even started. From the other grids that did have a reasonable computing time, the 515x1x280 grid gave the most accurate measurements and thus appeared to be the most suitable grid for this study.

During the search for the most suitable grid, we found that the graphs of the velocities, computed with different grid sizes, can never converge. Each time another grid is used, we see a different graph. This appeared to be caused by the onset of the vortex street caused by the moving object at a certain moment in time. The shedding of vortices will be different in every situation, even when there is only little difference between the cases. Also in reality, every time you repeat the same experiment, you will observe a different pattern of vortices causing different measurements as well.

The extension of the simplified case, by giving the moving object an acceleration from the start, reveals that, at the beginning of the numerical experiment, lower values of the velocities and pressure are obtained than for the case in which the moving cube still has a constant velocity. Also, we found that the signals reach the sensors at a later moment in time, due to the lower velocity of the moving object at the start. These are physically reasonable results and thus the moving object got an acceleration at the start in the simulations that followed as well.

In Chapter 4 walls have been inserted and two different cases have been

considered and compared to each other: the case in which only horizontal walls are placed and the case in which both horizontal and vertical walls are inserted. Until the onset of the vortex street, the sensors in the case with only horizontal walls report extremer values of the velocities than the sensors of the other case. While the sensors in the case with both horizontal and vertical walls register a bigger difference in the extreme values of the pressure. After the onset of the vortex street, vortices are shedded in different manners and no relation can be found between the measurements of the sensors in both cases anymore.

When replacing the cube by a ball, we saw that for the first part of the numerical experiment, the signals received by the sensor in the case with the cube are quite similar to the signals received by the sensor in the case with the ball. However, again, when the moving objects are starting with the shedding of vortices, the sensors are reporting different values of the velocities and pressure. Further, it is observed that the onset of the vortex street caused by the ball takes place at an earlier moment in time than the onset of the vortex street originated by the cube.

In the three-dimensional simulations, however, barely any activity in the water was seen, let alone a vortex street. The absence of the shedding of vortices is partly caused by the coarsened grid used for these simulations. The coarser grid considers the tank in less detail, which leads to less accurate measurements. Also, the adding of a third dimension probably has an effect on the outcomes of the simulations as well. An extra dimension leads to more numerical diffusion such that the water is set in a lower motion and less differences in values of the velocities and pressure can be reported by the sensors.

Two different three-dimensional cases are considered and compared to each other: the case in which the sensors and walls are placed in the middle of the tank and the case in which the sensors and walls are located at the right side of the tank. For the U velocity we saw that the reported values by the sensors were quite similar. The only difference was that the minimum and maximum of the right side case were less extreme than the ones of the centered case. Probably, diffusion took place along the way to the right side of the tank. Similar observations could be made regarding to the pressure, where the effect of the approaching and passing object on the pressure reported by the sensors at the right side is smaller.

The movement of the ball in the centered case, barely has any effect on the V velocity reported by the sensors. In the right side case, however, a V velocity is reported from the start for the entire side. With the water having first a positive V value at the right side, which switches halfway the experiment in a negative V value. This is possibly caused by the returning of the flow that has clashed against the wall. This difference in direction of the flow is perhaps also the cause of the different obtained values of the W velocity at that side. For the W velocity, again in the first part of the

experiment, different values are seen than in the second part. Halfway, the water at the right side of the tank switched direction. In the centered case, the reported W values are only influenced by the approaching and passing of the moving object.

In the beginning of the study, the choice for the "most suitable" grid was partly based on the length of the computing time. There was not enough time in this research to use finer grids than the 515x1x280 grid, so this was the most suitable grid for this research. However, with more time one could have chosen a grid that needed more days to complete, but that would have given more accurate measurements as well. Also, with more time, the three-dimensional cases that now only have been simulated using the 172x50x94 grid, could also have been considered with a three-dimensional the 516x150x280 grid. Such that a better comparison could be made between the two-dimensional simulations and the three-dimensional simulations. A little more time could be achieved by, for example, using computers that are not turned off at night such that simulations can not be interrupted. Or by using computers that possess more processors, such that the computations can be spread over multiple cores and hence will go faster.

Bibliography

[1] Bleckmann, H. and Zelick, R. Lateral line system of fish. *Integrative Zoology*, 4:13–25, 2009.

[2] Herzog, H., Steltenkamp, S., Klein, A., Tätzner, S., Schulze, E. and Bleckmann, H. Micro-machined flow sensors mimicking lateral line canal neuromasts. *Micromachines*, 6:1189–1212, 2015.

[3] Barbier, C. and Humphrey, J.A.C. Drag force acting on a neuromast in the fish lateral line trunk canal. i. numerical modelling of external-internal flow coupling. *Journal of the royal society interface*, 6:627–640, 2008.

[4] Luppes, R., van der Plas, P., Iwanowski, B., Bunnik, B., Duz, B., van der Heiden, H., Wemmenhove, P., Wellens, S., Veldman, A., Helmolt-Kleefsman, T., Loots, E. and Helder, J. Manual comflow version 3.9.x/4.0. Technical Report ComFLOW manual, University of Groningen, 2015.

[5] Veldman, A.E.P. and Velická, A. Stromingsleer. Technical Report WISL-08, Institute of Mathematics and Computing Science, University of Groningen, 2010-2011.

[6] Veldman, A.E.P. Computational fluid dynamics. Technical Report WICFD-03, Institute of Mathematics and Computing Science, University of Groningen, 2012-2013.